Establishing the Physical Basis for Calcification by Amorphous Pathways

Christina R. Blue

Dissertation submitted to the faculty of the Virginia Polytechnic Institute and State University in partial fulfillment of the requirements for the degree of

Doctor of Philosophy
In
Geosciences

Patricia M. Dove, chair
J. Donald Rimstidt
Michael F. Hochella, Jr.
Shuhai Xiao

May 2, 2014
Blacksburg, Va

Keywords: ACC, magnesium, pH, partitioning, mixed flow reactor, calcite, polymorphs

ESTABLISHING THE PHYSICAL BASIS FOR CALCIFICATION BY AMORPHOUS PATHWAYS

Christina R. Blue

ABSTRACT

The scientific community is undergoing a paradigm shift with the realization that the formation of carbonate minerals with diverse compositions and textures can be understood within the framework of multiple pathways to mineralization. A variety of common minerals can form via an amorphous pathway, where molecules or clusters aggregate to form a metastable amorphous phase that later transforms to one or more crystalline polymorphs. Amorphous calcium carbonate (ACC) is now recognized in a wide variety of natural environments. Recent studies indicate the chemical signatures and properties of the carbonate polymorphs that transform from an ACC pathway may obey a different set of dependencies than those established for the "classical" step-growth process. The Mg content of ACC and calcite is of particular interest as a minor element that is frequently found in ACC and the final crystalline products of calcified skeletons or sediments at significant concentrations. Previous studies of ACC have provided important insights into ACC properties, but a quantitative understanding of the controls on ACC composition and the effect of mineralization pathway on Mg signatures in calcite has not been established.

This study utilized a new mixed-flow reactor (MFR) procedure to synthesize ACC from well-characterized solutions that maintain a constant supersaturation. The experimental design controlled the input solution Mg/Ca ratio, total carbonate concentration, and pH to produce ACC with systematic chemical compositions. Results show that ACC composition is regulated by the interplay of three factors at steady state conditions: 1) Mg/Ca ratio, 2) total carbonate concentration, and 3) solution pH. Findings from transformation experiments show a systematic and predictable chemical framework for understanding polymorph selection during ACC transformation. Furthermore, results suggest a chemical basis for a broad range of Mg contents in calcite, including high Mg calcite. We find that the final calcite produced from ACC is similar to the composition of the initial ACC phase, suggesting that calcite composition reflects local conditions of formation, regardless of the pathway to mineralization. The findings from this study provide a chemical road map to future studies on ACC composition, ACC transformation, polymorph selection, and impurities in calcite.

ACKNOWLEDGEMENTS

The work presented in this dissertation is truly a group effort, and I would be remiss if I did not mention the individuals who assisted in this project. I would like to thank undergraduates Lisa Scott and Morgan Distad for spending countless hours in the lab assisting in data collection. I would also like to thank Athena Tilley for analyzing all the ICP-AES samples collected for this study. A huge amount of thanks go to Nizhou Han for making my life a lot easier by keeping the lab in working order and making sure that I always had everything I needed for my research. Also, I would like to thank my committee members: Patricia Dove, Don Rimstidt, Mike Hochella, and Shuhai Xiao for their guidance throughout my project. I truly stood on the shoulders of giants.

Last, and certainly not least, I would like to thank my colleagues in the Geosciences Department and in the Biogeochemistry of Earth Processes research group, both past and present, for their helpful discussions, support, and general good company.

TABLE OF CONTENTS

LIST OF FIGURES

LIST OF TABLES

PREFACE

This dissertation is organized into four chapters. Chapter 1 is an introduction to the field of study and outlines the research objectives, but it is not a published manuscript. The subsequent three chapters are presented as manuscripts in various stages of publication or preparation. Chapter 2 is published in *Research Methods in Biomineralization* as Chapter 23, v. 532 of *Methods in Enzymology* published in 2013 (reproduced with permission by Elsevier). Chapter 3 is a peer-reviewed manuscript that is currently in press for *Geochimica et Cosmochimica Acta*. The final chapter is in preparation to be submitted for publication.

CHAPTER 1. INTRODUCTION

1.1 MOTIVATION FOR STUDY

The scientific community is undergoing a paradigm shift with the realization that the formation of carbonate minerals with diverse compositions and textures can be understood within the framework of multiple pathways to mineralization. Overwhelming evidence from structural biology shows that many calcifying organisms do not form their skeletons via the classical step-growth process of ion-by-ion attachment to step edges of crystal surfaces (Burton et al., 1951; Chernov, 1984), rather, mineralization occurs through a pathway that begins with the formation of an amorphous precursor (amorphous calcium carbonate), that subsequently transforms to calcite (Aizenberg et al., 1996; Nudelman et al., 2007; Politi et al., 2008). Little is known about the factors that regulate this type of calcification because the last 50 years of research have focused almost entirely on step-growth processes. Furthermore, recent work has shown that this alternate, aggregation-dominated pathway obeys a different set of dependencies upon chemical and environmental conditions from those established for classical growth (Bentov & Erez 2006; Loste et al., 2003; Rodriguez-Blanco et al., 2012).

An amorphous pathway may reconcile enigmas regarding carbonate formation and chemistry that cannot be explained by laboratory studies of classical growth. Advances in knowledge of amorphous-to-crystalline growth processes may reveal that the previously established principles of mineral formation are not applicable to many low temperature minerals. Therefore, understanding the physical and chemical controls on amorphous calcium carbonate (ACC) formation and transformation, and the resulting compositions and morphologies of the crystalline products that form from ACC, has the potential to change the current views of the nature of biogenic carbonates. The goal of this study to fill some of the major gaps in our

knowledge of ACC formation and transformation to crystalline products, through carefully designed and precisely controlled laboratory experiments, while focusing on the effects of Mg and carbonate chemistry on ACC and calcite mineralization and composition.

Meticulous experimentation is required to gain a quantitative understanding of ACC formation and its subsequent transformation: solution chemistry must be carefully controlled and synthesized products must be well characterized. Synthesis procedures, however, were unable to adequately control solution chemistry—significant changes in solution composition occur over the duration of the experiment (Koga et al., 1998; Wang et al., 2009)—and many studies have based findings upon interpretations of products that were not carefully characterized. As a result, previous studies of ACC provided important qualitative insights into ACC formation, but a quantitative understanding was not yet established. Therefore, the community needed a new ACC synthesis procedure that could control solution chemistry and produce a large amount of product with reproducible compositions. Developing and successfully employing a new method was the first objective in this study because this capability was vital to robust analysis of controls of ACC composition

Using this new method, this study on ACC formation and transformation is focused on the factors that control Mg signatures in the products. The magnesium content of ACC is of particular interest because this IIA ion: 1) is a strong inhibitor of calcite step growth (Berner, 1975; Davis et al., 2000), 2) has been shown to stabilize ACC, thus delaying time to transformation (Loste et al., 2003; Rodriguez-Blanco et al., 2012), and 3) is widely studied in biominerals as a proxy for paleotemperature (Dissard et al., 2010; Hastings et al., 1998; Morse et al., 1997; Rosenthal et al., 1997). Reports that biogenic calcite can contain up to 30 mole % $MgCO_3$ (Chave, 1954) and the occurrence of high-Mg carbonates in modern sedimentary

environments (Raz et al., 2000; Sánchez-Román et al., 2011; Wang et al., 2012) suggest an amorphous pathway to crystal growth could explain the anomalously high Mg content that is measured in some calcites. These levels cannot be achieved through classical step growth. Offsets in seawater temperature calibrations based on Mg/Ca ratios in biominerals may also be explained as mineralization by an alternate calcification pathway (Bentov & Erez, 2005). Previous work has shown the Mg content of ACC increases with the initial Mg/Ca ratio of a reactant solution (Loste et al., 2003; Wang et al., 2012; Han et al., 2013), but the control of carbonate chemistry on crystal Mg/Ca has been largely overlooked. Both carbonate concentration and pH and could play a much more important role in Mg signatures than previously thought. Thus, a detailed study is needed to determine the role of carbonate chemistry on the Mg content of ACC.

After establishing quantitative understanding of how carbonate chemistry affects the Mg content of ACC, the next step is to determine how carbonate chemistry affects the ACC transformation process and the Mg content of the final crystalline products. There are conflicting reports in the literature regarding the ACC transformation process because the phase transition is difficult to control and observe directly. Some argue for a dissolution/re-precipitation process (Lenders et al., 2011; Hu et al., 2012; Han et al., 2013), while others suggest a direct transformation mechanism (Long et al., 2011; Rodriguez-Blanco et al., 2012). There are few quantitative studies on the effect of mineralization pathway on Mg signatures in calcite (e.g. Loste et al., 2003; Wang et al., 2012; Han et al., 2013), and investigations into the role of carbonate chemistry on Mg signatures in calcite are completely lacking. Clearly, there are still many questions that need to be addressed regarding ACC transformation.

Although numerous qualitative studies have been reported, there is currently no clear or quantitative chemical framework for understanding polymorph formation from an ACC precursor. There is little agreement among these studies about the polymorphs of $CaCO_3$ (and their morphologies) that occur under similar solution conditions, and report multiple minerals phases transforming concurrently from ACC when Mg is present in solution (Loste et al., 2003; Sánchez-Román et al., 2011; Zhang et al., 2012; Rodriguez-Blanco et al., 2012). Only a few studies have focused on trace element signatures in calcites that form from ACC (e.g. Wang et al., 2012; Han et al., 2013; Angel, 2013) because of concurrent polymorph precipitation. By using the improved ACC synthesis method that controls carbonate chemistry in conjunction with carefully monitored transformation experiments, this study seeks to establish and quantify our understanding of crystals that form via an amorphous pathway. This approach is necessary to reconcile discrepancies reported in the literature and construct a broad based understanding of calcification processes.

1.2 STUDY OBJECTIVES

This dissertation quantified the chemical and physical controls on the Mg content of ACC and its transformed crystalline products. A systematic research plan was designed to obtain quantitative results to decipher the ACC formation and transformation processes. To approach this problem, I developed an experimental program that addressed three core objectives:

1. Develop new method for synthesizing ACC. To study the chemical controls on the Mg signatures in ACC, a new experimental design was needed to precisely control and maintain solution chemistry. The results of this work are described in Chapter 2, and are published as a research paper in *Research Methods in Biomineralization Science* (Blue et al., 2013).

2. Investigate the effect of carbonate chemistry on the Mg content of ACC. Due to inadequate synthesis methods, the factors that control the Mg content of ACC were not known. This study quantified the effect of total carbonate concentration and pH on ACC composition, and is described in Chapter 3. The corresponding manuscript is currently in press (*Geochimica et Cosmochimica Acta*) for this study.

3. Investigate the effect of carbonate chemistry and pH on ACC transformation rates and the Mg content of the crystalline phase. This study builds upon the previous study by quantifying the control of solution chemistry on ACC transformation and the Mg content of the resulting crystalline carbonate polymorphs. The experimental protocols, results of the transformation experiments, and the implications of the findings are described in Chapter 4. This manuscript is currently in preparation for publication.

1.3 REFERENCES

Aizenberg J., Addadi L., Weiner S. and Lambert G. (1996) Stabilization of amorphous calcium carbonate by specialized macromolecules in biological and synthetic precipitates. *Adv. Mater.* **8**, 222–226.

Angel A. M. (2013) Influence of solution composition and temperature on the strontium content of amorphous calcium carbonate and subsequent calcite. *Unpublished Thesis*, Virginia Polytechnic Institute and State University, Blacksburg, VA, U. S. A.

Bentov S. and Erez J. (2006) Impact of biomineralization processes on the Mg content of foraminiferal shells: A biological perspective. *Geochem. Geophys. Geosyst.* **7**, Q01P08.

Bentov S. and Erez J. (2005) Novel observations on biomineralization processes in foraminifera and implications for Mg/Ca ratio in the shells. *Geology* **33**, 841–844.

Berner R. A. (1975) The role of magnesium in the crystal growth of calcite and aragonite from sea water. *Geochim. et Cosmochim. Acta* **39**, 489–504.

Blue C. R., Rimstidt J. D. and Dove P. M. (2013) Chapter Twenty-Three - A mixed flow reactor method to synthesize amorphous calcium carbonate under controlled chemical conditions, in: James, J. D. Y. (Ed.), *Method. Enzymol*. Academic Press, 557–568.

Burton W. K., Cabrera N. and Frank F. C. (1951) The growth of crystals and the equilibrium structure of their surfaces. *Phil. Trans. Royal Soc. London. Series A, Math. & Phys. Sci.* **243**, 299–358.

Catherine H., Skinner W., Osbaldiston G. W. and Wilner A. N. (1977) Monohydrocalcite in a guinea pig bladder stone, a novel occurrence. *Amer. Mineral.* **62**, 273–277.

Chave K. E. (1954) Aspects of the biogeochemistry of magnesium 1. Calcareous marine organisms. *J. Geology* **62**, 266–283.

Chernov A. A. (1984) Modern crystallography III: Crystal growth. Springer-Verlag.

Davis K .J., Dove P. M. and De Yoreo J. J. (2000) The role of Mg^{2+} as an impurity in calcite growth. *Science* **290**, 1134–1137.

Dissard D., Nehrke G., Reichary G. J. and Bijma J. (2010) The impact of salinity on the Mg/Ca and Sr/Ca ratio in the benthic foraminifera *Ammonia tepida*: Results from culture experiments. *Geochim. et Cosmochim. Acta* **74**, 928–940.

Han N., Blue C. R., De Yoreo J. J. and Dove P. M. (2013) The effect of carboxylates on the Mg content of calcites that transform from ACC. *Proced. Earth Planet. Sci.* **7**, 223–227.

Hastings D. W., Russell A. D. and Emerson S. R. (1998) Foraminiferal magnesium in *Globeriginoides sacculifer* as a paleotemperature proxy. *Paleoceanography* **13**, 161–169.

Hu Q., Nielsen M. H., Freeman C. L., Hamm L. M., Tao J., Lee J. R. I., Han T. Y. J., Becker U., Harding J. H., Dove P. M. and De Yoreo J. J. (2012) The thermodynamics of calcite nucleation at organic interfaces: Classical vs. non-classical pathways. *Faraday Discuss.* **159**, 509–523.

Koga N., Nakagoe Y. and Tanaka H. (1998) Crystallization of amorphous calcium carbonate. *Thermochim. Acta* **318**, 239–244.

Lenders J. J. M., Dey A., Bomans P. H. H., Spielmann J., Hendrix M. M. R. M., de With G., Meldrum F. C., Harder S. and Sommerdijk N. A. J. M. (2011) High-magnesian calcite mesocrystals: A coordination chemistry approach. *J. Amer. Chem. Soc.* **134**, 1367–1373.

Long X., Ma Y. and Qi L. (2011) In vitro synthesis of high Mg calcite under ambient conditions and its implication for biomineralization process. *Cryst. Growth & Design* **11**, 2866–2873.

Loste E., Wilson R. M., Seshadri R. and Meldrum F. C. (2003) The role of magnesium in

stabilising amorphous calcium carbonate and controlling calcite morphologies. *J. Cryst. Growth* **254**, 206–218.
Morse J. W., Wang Q. and Tsio M. Y. (1997) Influences of temperature and Mg:Ca ratio on $CaCO_3$ precipitates from seawater. *Geology* **25**, 85–87.
Nishiyama R., Munemoto T. and Fukushi K. (2013) Formation condition of monohydrocalcite from $CaCl_2$–$MgCl_2$–$Na2CO_3$ solutions. *Geochim. et Cosmochim. Acta* **100**, 217–231.
Nudelman F., Chen H. H., Goldberg H. A., Weiner S. and Addadi L. (2007) Lessons from biomineralization: comparing the growth strategies of mollusc shell prismatic and nacreous layers in *Atrina rigida*. *Faraday Discuss.* **136**, 9–25.
Politi Y., Metzler R. A., Abrecht M., Gilbert B., Wilt F. H., Sagi I., Addadi L., Weiner S. and Gilbert P. U. P. A. (2008) Transformation mechanism of amorphous calcium carbonate into calcite in the sea urchin larval spicule *Proced. Natl. Acad. Sci. U. S. A.* **105**, 17362–17366.
Raz S., Hamilton P. C., Wilt F. H., Weiner S. and Addadi L. (2003) The transient phase of amorphous calcium carbonate in sea urchin larval spicules: The involvement of proteins and magnesium ions in its formation and stabilization. *Adv. Funct. Mater.* **13**, 480–486.
Raz S., Weiner S. and Addadi L. (2000) Formation of high-magnesium calcites via an amorphous precursor phase: Possible biological implications. *Adv. Mater.* **12**, 38–42.
Rodriguez-Blanco J. D., Shaw S., Bots P., Roncal-Herrero T. and Benning L. G. (2012) The role of pH and Mg on the stability and crystallization of amorphous calcium carbonate. *J. Alloy. Compound.* **536, Supplement 1**, S477–S479.
Rosenthal Y., Boyle E. A. and Slowey N. (1997) Temperature control on the incorporation of magnesium, strontium, fluorine, and cadmium into benthic foraminiferal shells from Little Bahama Bank: Prospects for thermocline paleoceanography. *Geochim. et Cosmochim. Acta* **61**, 3633–3643.
Sánchez-Román M., Romanek C. S., Fernández-Remolar D. C., Sánchez-Navas A., McKenzie J. A., Pibernat R. A. and Vasconcelos C. (2011) Aerobic biomineralization of Mg-rich carbonates: Implications for natural environments. *Chem. Geology* **281**, 143–150.
Wang D., Hamm L. M., Giuffre A. J., Echigo T., Rimstidt J. D., De Yoreo J. J., Grotzinger J. and Dove P. M. (2012) Revisiting geochemical controls on patterns of carbonate deposition through the lens of multiple pathways to mineralization. *Faraday Discuss.* **159**, 1–16.
Wang D., Wallace A. F., De Yoreo J. J. and Dove P. M. (2009) Carboxylated molecules regulate magnesium content of amorphous calcium carbonates during calcification. *Proced. Natl. Acad. Sci. U. S. A.* **106**, 21511–21516.
Zhang Z., Xie Y., Xu X., Pan H. and Tang R. (2012) Transformation of amorphous calcium carbonate into aragonite. *J. Cryst. Growth* **343**, 62–67.

CHAPTER 2. A MIXED FLOW REACTOR METHOD TO SYNTHESIZE AMORPHOUS CALCIUM CARBONATE UNDER CONTROLLED CHEMICAL CONDITIONS

Blue, C. R., Rimstidt, J. D. and Dove, P. M. (2013)*, in Research Methods in Biomineralization Science*, Jim De Yoreo Ed., Methods in Enzymology, **532***,* 557–568.

ABSTRACT: This study describes a new procedure to synthesize amorphous calcium carbonate (ACC) from well-characterized solutions that maintain a constant supersaturation. The method uses a mixed flow reactor (MFR) to prepare ACC in significant quantities with consistent compositions. The experimental design utilizes a high-precision solution pump that enables the reactant solution to continuously flow through the reactor under constant mixing, and allows the precipitation of ACC to reach steady state. As a proof of concept, we produced ACC with controlled Mg contents by regulating the Mg/Ca ratio of the input solution, as well as the carbonate concentration and pH. Our findings show that the Mg/Ca ratio of the reactant solution is the primary control for the Mg content in ACC, as shown in previous studies, but ACC composition is further regulated by the carbonate concentration and pH of the reactant solution. The method offers promise for quantitative studies of ACC composition and properties, and for investigating the role of this phase as a reactive precursor to biogenic minerals.

2.1 INTRODUCTION

Amorphous calcium carbonate (ACC) is now recognized in a wide variety of natural and engineered environments. ACC has been found in some soils and sediments (Jones & Peng, 2012; Sanchez-Roman et al., 2008) and its formation has applications for controlled synthesis in biomedicine and the materials sciences (Han & Aizenberg, 2008; Lee et al., 2012). Of particular interest is the ACC that forms during skeletal biomineralization of calcifying organisms (Politi et al., 2004; Addadi et al., 2006; Tao et al., 2009). Characterization studies show that ACC is a truly amorphous phase, with a typical composition of $CaCO_3 \bullet 1H_2O$, and it exhibits a unique short- and intermediate-range structure (Michel et al., 2008). The realization that ACC can be a reactive precursor to a number of crystalline polymorphs of $CaCO_3$ has motivated an extensive effort to understand the influence of the inorganic and organic factors on ACC composition. For example, the biomineralization community is interested in whether calcification by an ACC pathway affects the Mg content of calcitic biominerals that are used as proxies for seawater temperature (Dissard et al., 2010; Stanley, 2006).

Previous studies of ACC have provided important insights into ACC properties, but a quantitative understanding is not yet established. This is partially because current synthesis procedures are unable to control solution chemistry. For example, a widely used synthesis method involves "batch" mixing of Na_2CO_3 and $CaCl_2$ solutions, then filtering the precipitate (Koga et al., 1998). However, the closed configuration of this method inherently causes the solution composition to change significantly during synthesis, and the Na_2CO_3 salt raises solution pH to values that are much higher (pH 11–13.5) than most natural systems. Another popular approach diffuses $(NH_4)_2CO_3$ into $CaCl_2$ solutions to increase supersaturation and induce ACC formation (Aizenberg et al., 1996; Wang et al., 2009). This method produces ACC under

highly variable and uncontrolled supersaturation conditions, introduces significant amounts of NH_4^+ into the mineralizing solution, and yields a limited amount of ACC.

To overcome these limitations, we developed a new procedure for ACC synthesis (**Fig. 2.1**) that uses a mixed flow reactor (MFR) system to maintain constant and controlled solution chemistries. This new procedure for producing ACC is adapted from an earlier method that was used for kinetic studies of mineral growth (Saldi et al., 2009) and dissolution (Rimstidt & Dove, 1986). The MFR offers a number of advantages over batch and diffusion methods: 1) allows precise control on supersaturation; 2) produces ACC at steady state conditions, and 3) yields large amounts of ACC with reproducible compositions. We demonstrate this approach by quantifying the factors that influence the Mg content of ACC by producing Mg-ACC from well-characterized solutions under controlled conditions.

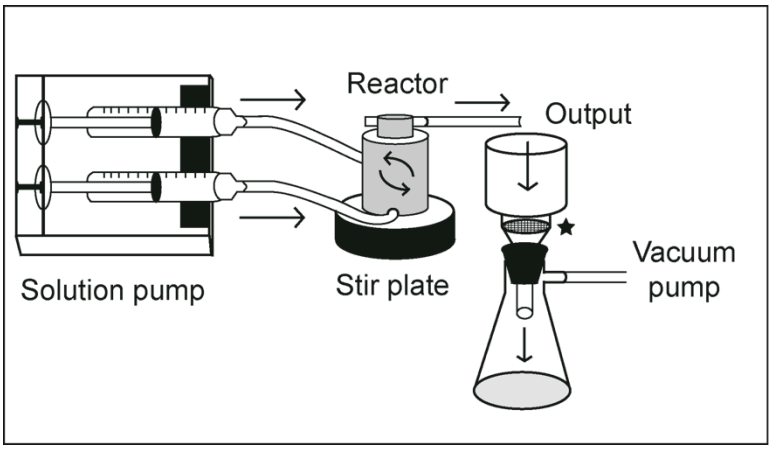

Figure 2.1. Schematic of the mixed flow reactor system. Arrows indicate the direction of flow. Black star denotes the location of the 0.20 μm nylon filter.

2.2 METHOD

The experimental design (**Fig. 2.1**) includes a high precision pump (Harvard Apparatus PHD 2000) fitted with two 100 ml syringes. For this study, one syringe contained Mg-doped $CaCl_2$ solutions with a prescribed Mg/Ca ratio (**Table 2.1**). A second syringe contained Na_2CO_3

or $NaHCO_3$ solution at a desired concentration (**Table 2.2**). The syringes were connected by Teflon tubing to opposite sides of the base of a 26 ml reactor unit. These solutions were continuously pumped into the reactor while mixing at a rate of 1000 rpm. As the solutions mixed, the contents of the MFR became supersaturated with respect to ACC, and ACC readily precipitated. The ACC-solution suspension exited the reactor through a single effluent tube located at the top of the reactor and the products were captured on a 0.20-micron nylon filter fitted on a vacuum flask (**Fig. 2.1**).

Table 2.1 Solution Chemistries for Variable Mg/Ca ratio Experiments

Mg:Ca	0.5:1	1:1	2:1	5:1	8:1
$CaCl_2$ (M)	0.025	0.025	0.01	0.01	0.01
$MgCl_2$ (M)	0.0125	0.025	0.02	0.05	0.08
$NaHCO_3$ (M)	0.10	0.10	0.10	0.10	0.10
Initial pH	9.50	9.50	9.75	9.75	9.75
Steady State pH	8.80	8.70	9.50	9.30	9.10
$\sigma_{(ACC)}$	4.94	2.43	1.61	1.31	1.02

Table 2.2. Solution Chemistries for Constant Mg/Ca ratio (5:1) Experiments

Carb. Source	Carb. Conc. (M)	Initial pH	Steady State pH	$\sigma_{(ACC)}$
Na_2CO_3	0.03	10.95	10.03	1.11
Na_2CO_3	0.06	11.12	10.13	1.58
Na_2CO_3	0.10	11.24	10.34	1.81
$NaHCO_3$	0.10	9.79	9.31	1.36
$NaHCO_3$	0.10	10.25	9.89	1.70
$NaHCO_3$	0.20	9.14	8.83	1.11
$NaHCO_3$	0.20	9.96	9.75	1.80

The average hydraulic residence time (τ) of solution in the reactor was held constant at 2 minutes for all experiments, where

$$\tau = \text{volume of reactor (ml) / flow rate (ml/hr).} \quad (2.1)$$

For each experiment, the reactor operated for a minimum of three hydraulic residence times to allow the input solutions and ACC products within the reactor to reach steady state conditions (Jensen, 2001). All ACC samples were rinsed thoroughly with ethanol and dried under in a class II biological safety cabinet for 30 minutes before storing overnight in a vacuum desiccator. Each sample was weighed the next day to obtain the mass of dry ACC and samples were immediately prepared for their respective mode of analysis. Samples that could not be analyzed immediately were stored at 4°C for no longer than 3 days.

As a proof of concept, ACC was synthesized from solutions with variable Mg/Ca ratios (**Table 2.1**) and solutions with different $NaHCO_3$ or Na_2CO_3 concentrations (**Table 2.2**). The initial pH of the $NaHCO_3$ solutions was adjusted using NaOH, so that the resulting pH was 8.7–9.5 upon mixing with the variable Mg/Ca solutions **(Table 2.1**). For the variable saturation experiments (**Table 2.2**), the initial Mg/Ca ratio was maintained at 5:1 and the saturation state (σ_{ACC}) was varied by adjusting carbonate concentration and pH (using NaOH). The saturation state of a solution (σ) with respect to ACC is expressed by the relationship:

$$\sigma_{\mathrm{ACC}} = \ln\left(\frac{a\mathrm{Ca}^{2+} \times a\mathrm{CO}_3^{2-}}{K_{\mathrm{sp\ (Pure\ ACC)}}}\right) \quad (2.2)$$

where a_i is the activity of an ion, and the $K_{sp\ (Pure\ ACC)} = 10^{-6.39}$ (25°C) (Brečević & Nielsen, 1986). (We note that there is some uncertainty in this K_{sp} value—given that recent studies suggest the solubility of ACC is considerably lower than the reported value (Gebauer et al., 2008; Hu et al., 2012)—but there have been no further studies on the solubility of ACC, so the Brečević and Nielsen (1989) value is used here.) Activities of ions in solution were calculated

using The Geochemist's Workbench© for each solution condition. In this study, saturation states were varied from 1.11–1.81, and all experiments were performed at ambient conditions.

The proposed mechanism for ACC particle formation in inorganic environments is the aggregation of aqueous ion pairs into prenucleation clusters (Gebauer et al., 2008), with a stability defined by thermodynamic equilibrium among the solvent, individual ions, and hydrated clusters. This is simplified by the general reaction

$$z\mathrm{Ca}^{2+} + z\mathrm{CO_3}^{2-} = z(\mathrm{CaCO_3})_{\mathrm{aq}}, \quad (2.3)$$

where z is the number of $CaCO_3$ units in a cluster. In the presence of Mg ion, we assume the reaction that is equivalent for the formation of amorphous calcium magnesium carbonate (Wang et al., 2009)

$$y\mathrm{Mg}^{2+} + z\mathrm{Ca}^{2+} + (y+z)(\mathrm{CO_3}^{2-}) = (\mathrm{Ca}_z\mathrm{Mg}_y(\mathrm{CO_3})_{y+z})_{\mathrm{aq}}, \quad (2.4)$$

where y is the number of $MgCO_3$ units in a cluster and the resulting solid solution has y plus z units in the cluster that forms. The equilibrium constant of reaction 2 and absolute values of y and z is unknown, but the ratio of y/z gives the fraction of Mg/Ca in the resulting ACC.

2.3 CHARACTERIZATION

The synthetic ACC was characterized using a combination of SEM, ICP-OES, Raman Spectroscopy, FTIR, and TGA methods.

2.3.1 Scanning Electron Microscopy (SEM)

Analyses were performed on an FEI Quanta 600 FEG ESEM. Images of the ACC were acquired using secondary electron (SE) microscopy. All samples were coated with approximately 10 nm of gold-palladium using a sputter coater before analysis. Optimal viewing parameters included 10 kv and a 3.5 spot size. Higher voltages destroyed the ACC samples and could not be used. All samples were examined for consistent morphology and particle size variations. SEM

analyses showed that all ACC samples exhibited a characteristic spherical morphology, and a similar particle size distribution, despite changes in Mg content (**Fig. 2.2**).

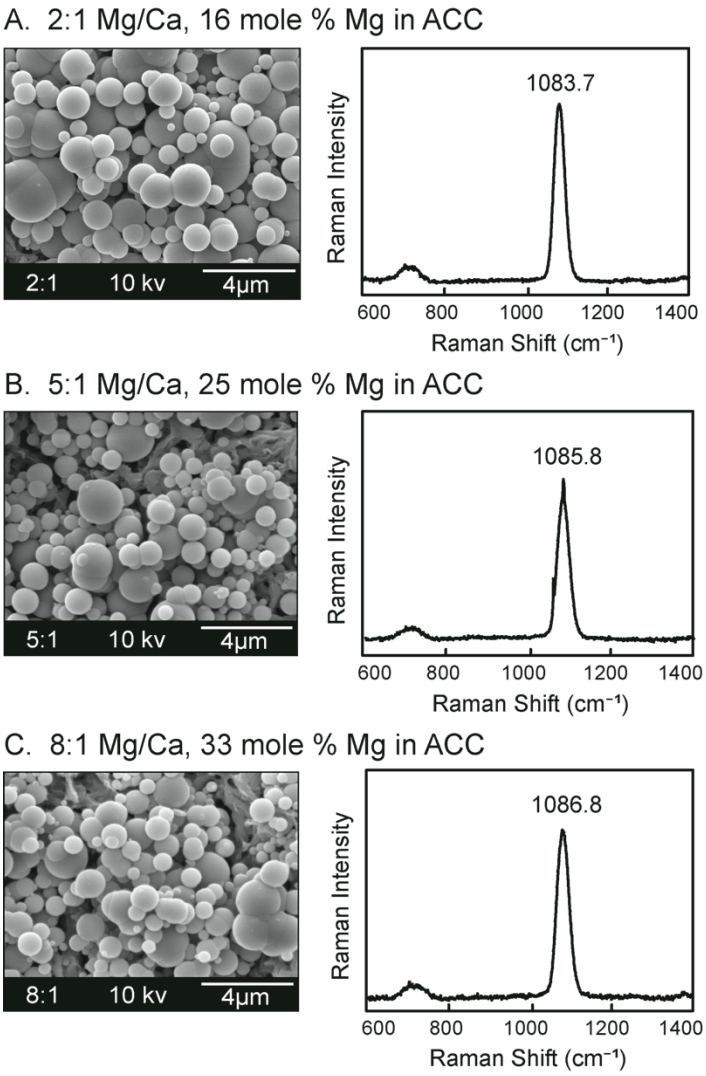

Figure 2.2. SEM images and corresponding Raman spectra of ACC synthesized from (A) 2:1, (B) 5:1, and (C) 8:1 Mg/Ca solutions using the new MFR method. The ACC morphology and particle sizes are similar for all Mg contents. The presence of a broadened carbonate symmetric stretch peak (ν_1) in the Raman spectra confirms all products are amorphous. The ν_1 peak shifts to higher wave numbers with increases in Mg content.

2.3.2 Inductively Coupled Plasma Optical Emission Spectrometry (ICP-OES)

Inductively Coupled Plasma – Optical Emission Spectrometry was performed using a Spectro CirOS VISION. The magnesium and calcium concentrations were determined from

calibration curves that were prepared from plasma-grade single element standards (SPEX CertiPreps). Samples were dissolved in 0.5 N nitric acid for 20 minutes. Total concentrations of magnesium and calcium (ppm) were corrected for absorbance of excess salt solution by the nylon membrane. A separate experiment was conducted to obtain the levels of calcium and magnesium absorbed by the filter based upon the amount of time the solution was in contact with the membrane, and a calibration table was constructed. Calcium and magnesium standards were analyzed in conjunction with ACC samples to verify the accuracy of the results. Measurements of Mg and Ca content in the ACC samples using ICP-OES showed the method is capable of producing ACC with Mg concentrations of 8–70 mole %.

2.3.3 Raman Spectroscopy

Raman spectra were obtained on a JY Horiba (800 mm) LabRam HR spectrometer equipped with a 632.81 nm He-Ne laser emitting 15 mW power and focused through an Olympus 50x objective. A small amount of ACC was removed from the nylon filter and placed on a clean glass slide for analysis. Three 180-second spectra accumulations were collected and averaged for each of the samples analyzed and reported in this study. The carbonate peak positions and widths were estimated using a summed Gaussian/Lorentzian peak-fitting routine after baseline corrections were made using Jobin Yvon Labspec version 4 software. Raman spectroscopy confirmed that all samples products were amorphous; only a broadened ν_1 (carbonate symmetric stretch) peak was present in all samples (**Fig. 2.2**). The peak position shifts to higher wavenumbers with Mg content, as reported previously (Wang et al., 2011).

2.3.4 Fourier-Transform Infrared Spectroscopy (FTIR)

Fourier-Transform Infrared Spectroscopy was performed on a Varian 670-IR with a Pike GladiATR attachment with a 4 cm^{-1} resolution. Samples were analyzed at a standard 32 scan

rate. All results were background ATR corrected using the instrument's software program. Characterization by FTIR (**Fig. A1, Appendix A**) corroborated the trend of higher ν_1 peak positions with higher Mg concentrations in the ACC for all samples, including those with Mg/Ca ratios in ACC as high as 2.5 (**Fig. A2**, **Appendix A**).

2.3.5 Thermogravimetric Analysis (TGA)

Thermogravimetric analysis was performed on a TA Instruments Hi-Res TGA Q5000 Thermogravimetic Analyzer. Samples were heated from 25°C to 700°C at a rate of 10°C per minute. The percentage of water lost during heating was calculated from the difference in the weight percent of the sample between 25°C and 250°C. TGA indicated that all ACC products contained approximately one water molecule per calcium, magnesium carbonate (**Fig. A3**, **Appendix A**). There was no correlation found between the water content and the Mg content of ACC for the conditions of this study.

2.4 RESULTS

The MFR method produces ACC with systematic and consistent compositions that systematically correlate with the solution chemistry conditions without evidence of secondary crystalline phases. At high supersaturation conditions, gram quantities of ACC were produced within one hour of run time, which makes the MFR method ideal for producing a large quantity of samples that can be used for numerous analyses. Experiments conducted with $NaHCO_3$ and regulated input solution Mg/Ca ratios (**Table 2.1**) produced synthetic ACC with 8–33 mole % Mg (**Fig. 2.3**). A key feature of this experimental design is that it allows precise control of the distribution of minor elements between the solution and the ACC. Assuming that kinetic effects are negligible, the distribution of Mg between the ACC and the solution is expressed by a distribution coefficient (K_D), defined as

$$K_D = \left(\frac{X_{Mg}}{X_{Ca}}\right) / \left(\frac{m_{Mg}}{m_{Ca}}\right) \quad (2.5)$$

where $\left(\frac{X_{Mg}}{X_{Ca}}\right)$ is the measured Mg/Ca ratio in ACC and $\left(\frac{m_{Mg}}{m_{Ca}}\right)$ is the Mg/Ca ratio in the steady state effluent solution. Equation 2.5 predicts the Mg content of ACC is linearly correlated with solution Mg/Ca, and previous studies (Radha et al., 2012; Wang et al., 2012) have reported a linear correlation when the initial Mg/Ca ratio in solution is >1. Indeed, when the *initial* solution Mg/Ca ratios are plotted versus the Mg/Ca ratio of ACC products (**Fig. 2.3**) we also find the linear dependence predicted by Equation 2.5.

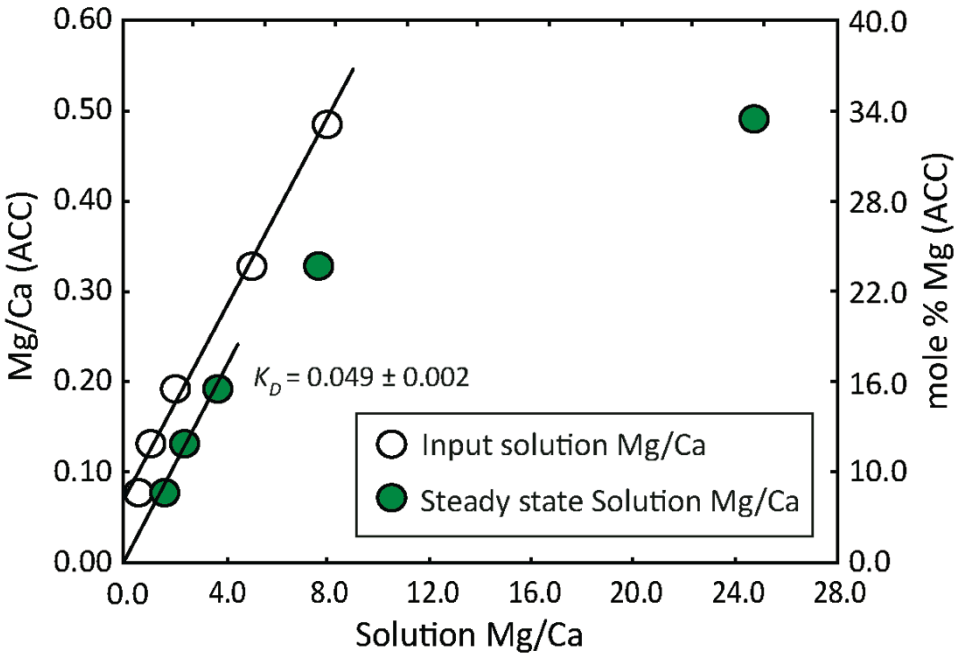

Figure 2.3. ACC compositions are dependent upon the Mg/Ca ratio of the reactant solution. The total amount of Mg in ACC increases as the solution Mg/Ca ratio increases, but two different K_D trends exist depending on how the data is plotted (see text for K_D equation). If input solution values are used (open circles), the trend is linear, but if effluent solution values are used (closed circles) the trend is linear only at low Mg/Ca values. Solution Mg/Ca values evolve to higher steady state values as ACC precipitates in the reactor, and therefore steady state Mg/Ca values should be used when calculating K_D. Each data point is an average of 3 experiments.

To obtain the true partition coefficient, we correlate ACC compositions with their corresponding steady state solution compositions. **Figure 2.3** shows two trends with increasing values of solution Mg/Ca that suggest the partitioning of Mg in ACC is more complex than previously assumed. Estimates of K_D obtain 0.049 ± 0.002x for steady state Mg/Ca ratios of 0–4, but above a solution Mg/Ca ratio of 6, the linear relationship breaks down (**Fig. 2.3**). This suggests there may be a departure from equilibrium at higher solution Mg/Ca values, and that kinetic effects, such as the precipitation rate, may control Mg signatures in ACC. It should be noted that the K_D values reported here are significantly lower than previous estimates based upon the initial solution Mg/Ca ratio (Wang et al., 2009; Radha et al., 2012), because solution Mg/Ca ratios evolve to higher values at steady state as ACC precipitates.

An additional series of ACC materials were produced using solutions with a constant Mg/Ca ratio of 5:1 while varying saturation state and carbonate source ($NaHCO_3$ and Na_2CO_3). By regulating carbonate solution chemistry, the method produced ACC with 33–70 mole % Mg (**Fig. 2.4**). **Figure 2.4** shows that higher pH and higher carbonate concentrations produce ACC with greater Mg content. Anecdotal evidence suggests these trends are caused in part by the effects of pH and carbonate concentration on precipitation rates. For example, faster precipitation rates cause the Mg/Ca ratio of the steady state solution to become higher because a larger fraction of Ca^{2+} is consumed during ACC precipitation than Mg^{2+}.

Results from these proof of concept experiments reiterate the primary control of solution Mg/Ca ratio on ACC composition (Radha et al., 2012; Wang et al., 2012). By having the ability to independently vary each component of the solution chemistry, we also show that ACC composition is further regulated by carbonate concentration and pH of the reactant solution.

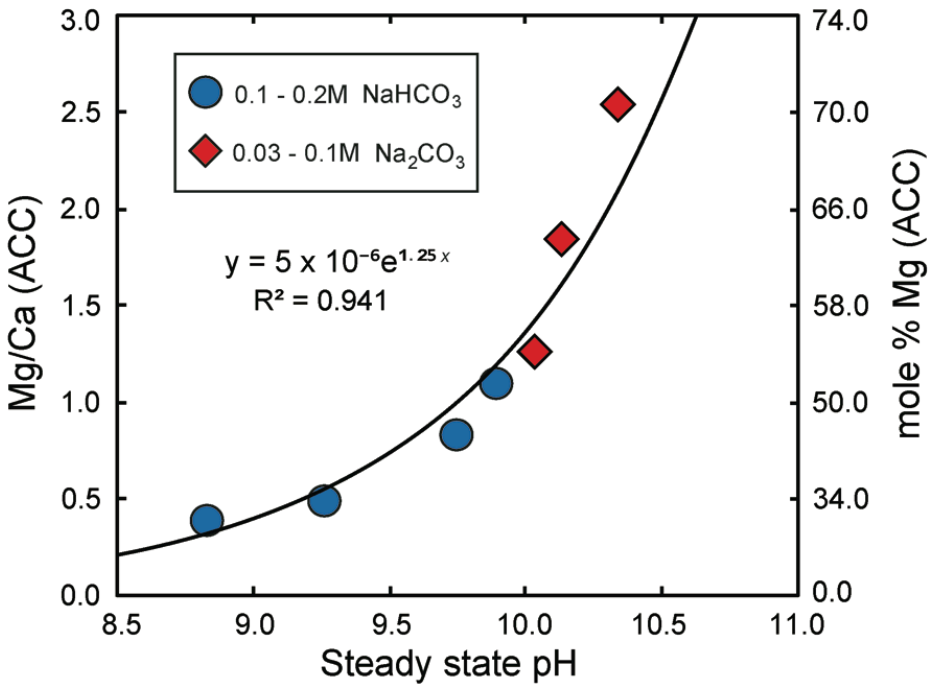

Figure 2.4. ACC synthesized at a constant Mg/Ca ratio (5:1) but with different carbonate concentrations and pH contain variable amounts of Mg, where higher carbonate concentrations and pH promote greater Mg uptake in ACC. The compositions show that carbonate concentrations, and largely pH, provide an additional means of tuning ACC composition. Each data point is an average of 3 experiments.

The demonstrated ability of the MFR method to produce ACC with a broad range of desired compositions presents opportunities to study other aspects of ACC formation. These include kinetic versus thermodynamic controls on composition, the incorporation of other trace elements, the factors that regulate isotopic signatures, and the nature of the transformation process from amorphous to crystalline phases. By this approach, it may become possible to decipher and quantify the roles of this phase as a reactive precursor to biogenic minerals.

2.5 REFERENCES

Addadi L., Joester D., Nudelman F. and Weiner S. (2006) Mollusk shell formation: A source of new concepts for understanding biomineralization processes. *Chem. A Euro. Journal* **12**, 980–987.

Aizenberg J., Addadi L., Weiner S. and Lambert G. (1996) Stabilization of amorphous calcium carbonate by specialized macromolecules in biological and synthetic precipitates. *Adv. Mater.* **8**, 222–226.

Brečević L. and Nielsen A. E. (1989) Solubility of amorphous calcium carbonate. *J. Cryst. Growth **98**, 504–510.*

Dissard D., Nehrke G., Reichary G. J. and Bijma J. (2010) The impact of salinity on the Mg/Ca and Sr/Ca ratio in the benthic foraminifera *Ammonia tepida*: Results from culture experiments. *Geochim. et Cosmochim. Acta* **74**, 928–940.

Gebauer D., Volkel A. and Cölfen H. (2008) Stable prenucleation calcium carbonate clusters. *Science* **322**, 1819–1822.

Han T. Y.-J. and Aizenberg J. (2008) Calcium carbonate storage in amorphous form and its template-induced nucleation. *Chem. Mater.* **20**, 1064–1068.

Hu Q., Nielsen M. H., Freeman C. L., Hamm L. M., Tao J., Lee J. R. I., Han T. Y. J., Becker U., Harding J. H., Dove P. M. and De Yoreo J. J. (2012) The thermodynamics of calcite nucleation at organic interfaces: Classical vs. non-classical pathways. *Faraday Discuss.* **159**, 509–523.

Jensen J. N. (2001) Approach to steady state in completely mixed flow reactors. *J. Environ. Engineer.* **127**, 13–18.

Jones B. and Peng X. (2012) Amorphous calcium carbonate associated with biofilms in hot spring deposits. *Sed. Geology* **269–270**, 58–68.

Koga N., Nakagoe Y. and Tanaka H. (1998) Crystallization of amorphous calcium carbonate. *Thermochim. Acta* **318**, 239–244.

Lee K., Wagermaier W., Masic A., Kommareddy K. P., Bennet M., Manjubala I., Lee S.-W., Park S. B., Cölfen H. and Fratzl P. (2012) Self-assembly of amorphous calcium carbonate microlens arrays. *Nature Comm.* **3**, 725.

Michel F. M., MacDonald J., Feng J., Phillips B. L., Ehm L., Tarabrella C., Parise J. B. and Reeder, R. J. (2008) Structural characteristics of synthetic amorphous calcium carbonate. *Chem. Mater.* **20**, 4720–4728.

Politi Y., Arad T., Klein E., Weiner S. and Addadi L. (2004) Sea urchin spine calcite forms via a transient amorphous calcium carbonate phase. *Science* **306**, 1161–1164.

Radha A. V., Fernandez-Martinez A., Hu Y., Jun Y.-S., Waychunas G. A. and Navrotsky A. (2012) Energetic and structural studies of amorphous $Ca_{1-x}Mg_xCaCO_3 \bullet nH_2O$ ($0 \leq x \leq 1$). *Geochim. et Cosmochim. Acta* **90**, 83–95.

Rimstidt J. D. and Dove P. M. (1986) Mineral/solution reaction rates in a mixed flow reactor: Wollastonite hydrolysis. *Geochim. et Cosmochim. Acta* **50**, 2509–2516.

Saldi G. D., Jordan G., Schott J. and Oelkers E. H. (2009) Magnesite growth rates as a function of temperature and saturation state. *Geochim. et Cosmochim. Acta* **73**, 5646–5657.

Sanchez-Roman M., Vasconcelos C., Schmid T., Dittrich M., McKenzie J. A., Zenobi R. and Rivadeneyra M. A. (2008) Aerobic microbial dolomite at the nanometer scale: Implications for the geologic record. *Geology* **36**, 879–882.

Stanley S. M. (2006) Influence of seawater chemistry on biomineralization throughout Phanerozoic time: Paleontological and experimental evidence. *Palaeogeo., Palaeoclim., Palaeoeco.* **232**, 214–236.

Tao J., Zhou D., Zhang Z., Xu X. and Tang R. (2009) Magnesium-aspartate-based crystallization switch inspired from shell molt of crustacean. *Proced. Natl. Acad. Sci. U. S. A.* **106**, 22096–22101.

Wang D., Hamm L. M., Bodnar R. J. and Dove P. M. (2011) Raman spectroscopic characterization of the magnesium content in amorphous calcium carbonate. *J. Raman Spec.* **43**, 543–548.

Wang D., Hamm L. M., Giuffre A. J., Echigo T., Rimstidt J. D., De Yoreo J. J., Grotzinger J. and Dove P. M. (2012) Revisiting geochemical controls on patterns of carbonate deposition through the lens of multiple pathways to mineralization. *Faraday Discuss.* **159**, 1–16.

Wang D., Wallace A. F., De Yoreo J. J. and Dove P. M. (2009) Carboxylated molecules regulate magnesium content of amorphous calcium carbonate. *Proced. Natl. Acad. Sci. U. S. A.* **106**, 21511–21516.

CHAPTER 3. CHEMICAL CONTROLS ON THE MAGNESIUM CONTENT OF AMORPHOUS CALCIUM CARBONATE

Blue C. R. and Dove P. M. (in press) Geochimica et Cosmochimica Acta.

ABSTRACT: Some calcifying organisms produce an amorphous calcium, magnesium carbonate (ACMC) as a reactive intermediate during skeleton formation, but the biogeochemical conditions that determine the composition of this phase are not established. This study uses a mixed flow reactor method to synthesize ACMC under controlled chemical conditions and establish the relationship between composition and inorganic solution chemistry. The experimental design used input solutions with a constant initial Mg/Ca ratio of 5/1 while regulating supersaturation through total carbonate concentration and pH. At steady state conditions, the Mg content of the resulting ACMC varies from 24 to >70 mole %. The corresponding input solution chemistry evolves in proportion to the extent of precipitation with a shift in the initial Mg/Ca ratio of 5 to values as high as 14.

We find the steady state solution composition that develops in the reactor during precipitation has a primary control on ACMC composition. Analysis of the data shows ACMC composition is regulated by the interplay of three factors at steady state conditions: 1) Mg/Ca ratio, 2) total carbonate concentration, and 3) solution pH. Using the Henderson-Kracek model to estimate the distribution coefficients (K_D) for the Mg content of ACMC, we find K_D is approximately constant when steady state pH is less than 9.5, but K_D triples as the steady state pH is increased from 9.5 to 10.3. The K_D values reported in this study are lower than previous estimates that were calculated from initial solution composition. This is because our estimates of K_D are based upon the solution chemistry at steady state and pH conditions that were lower than previous studies. We suggest the approach of using steady state composition to estimate K_D gives a more accurate representation of relationships between ACMC composition and local conditions during formation. The findings demonstrate that regulating local pH and total carbonate concentration at the time of formation can produce very high Mg amorphous carbonates.

3.1 INTRODUCTION

For the last 40 years, the "classical" terrace-ledge-kink (TLK) model for crystal growth (Burton et al., 1951; Chernov, 1984) has been adopted by the geological community to explain most types of mineralization (Berner, 1980). The process occurs via the ion-by-ion attachment of solutes to the step edges of mineral surfaces, and has provided a foundation for interpreting many studies of calcium carbonate formation. However, the inability of the step growth process to explain a number of observations in biological settings presents long-standing obstacles to fully understanding carbonate mineralization. For example, the ion-by-ion attachment process is too slow to explain the rapid development of skeletal structures that is observed in many calcifying organisms (Politi et al., 2004; Tao et al., 2009). In addition, laboratory studies show the "classical" crystal growth process is unable to produce calcite with >10–15% Mg (Bischoff et al., 1987), which contrasts with reports of up to 30% Mg in some biogenic calcite (Chave, 1954a). Calcification is further complicated in marine organisms by observations that step growth is fully inhibited at Mg levels far below seawater concentrations (Davis et al., 2000; Stephenson et al., 2008).

Evidence from structural biology shows the limitations imposed by the "classical" step growth process can be overcome by employing an alternative pathway to skeletal formation. The process begins by accumulating an amorphous calcium carbonate (ACC) that is stored until later transformation to a final crystalline phase (Aizenberg et al., 1996; Nudelman et al., 2007; Politi et al., 2008). For example, sea urchin larvae spicules are reported to form via an ACC precursor (Politi et al., 2004), and ACC is associated with calcite and aragonite in the nacreous layer of some mollusk species (Weiss et al., 2002; Addadi et al., 2006). It has been suggested that the

formation and storage of ACC is useful during biomineralization because this reactive precursor gives organisms greater energetic control over mineralization (Navrotsky, 2004).

Although ACC was recognized over 40 years ago (Towe & Malone, 1970), the local biogeochemical conditions that control the composition of the amorphous phase are not yet understood. Recent characterization studies show this material has a typical composition of $CaCO_3 \bullet H_2O$ and a unique short- and intermediate-range structure (Michel et al., 2008). In the absence of impurities, ACC formation is described by the balanced reaction

$$Ca^{2+} + CO_3^{2-} + H_2O = (CaCO_3) \bullet H_2O \quad (3.1)$$

where the solubility product, K_{sp}, equals $10^{-6.39}$ at 25°C (Brečević & Nielsen, 1989). ACC is metastable with respect to calcite with a K_{sp} that is approximately 100 times larger. Anecdotal evidence from recent studies suggests ACC solubility may be considerably lower (Gebauer et al., 2008; Hu et al., 2012)—but to our knowledge Brečević & Nielsen (1989) is the only published value. In the absence of impurities ACC is stable for only short periods, but its lifetime increases significantly with the addition of Mg (Loste et al., 2003; Radha et al., 2010) and in the presence of charged organic molecules (Han & Aizenberg, 2008; Wang et al., 2009).

The Mg content of ACC is of particular interest as a minor element that is frequently found in ACC and the final crystalline products of calcified skeletons at significant concentrations (Raz et al., 2000). For example, the ACC of sea urchin larvae spicules can contain up to 5 mole % Mg (Raz et al., 2003) and the shells of benthic foraminifera can contain greater than 12 mole % Mg (Bentov & Erez, 2005). The Mg content of ACC is also reported to regulate the ACC-to-calcite transformation process in terrestrial crustaceans during molting (Tao et al., 2009). Given that diverse organisms incorporate Mg into their skeletons by a pathway involving ACC formation, an understanding of inorganic and biochemical chemical controls on the

composition of this precursor phase is useful to developing a physical picture for biomineralization processes.

The formation of amorphous calcium, magnesium carbonate (ACMC) can be described by the reaction

$$(1 - x)\ Ca^{2+} + x\ Mg^{2+} + (CO_3^{2-}) + nH_2O = Ca_{1-x}Mg_x(CO_3) \bullet nH_2O \qquad (3.2)$$

where the values of x can exceed 0.88 and n can reach 1.80 (Radha et al., 2012). To our knowledge, the K_{sp} of ACMC has not been quantified. New findings indicate the chemical signatures and properties of the carbonate polymorphs that transform from an ACC or ACMC pathway may obey a different set of dependencies than those established for growth by the "classical" process (Bentov & Erez, 2006; Loste et al., 2003; Rodriguez-Blanco et al., 2012). This has particular significance for paleoclimate studies that use the Mg content of skeletal calcite as a proxy for seawater temperature (Dissard et al., 2010; Hastings et al., 1998; Morse et al., 1997; Rosenthal et al., 1997). Moreover, reports of biogenic calcite containing up to 30 mole % $MgCO_3$ (Chave, 1954a) and high-Mg carbonates in modern sedimentary environments (Raz et al., 2000; Sánchez-Román et al., 2011; Wang et al., 2012) suggest an amorphous intermediate could also explain the anomalously high amount of Mg incorporation which cannot be achieved through classical step growth.

This study establishes the influence of inorganic chemistry on the Mg content of ACC, hereafter referred to as ACMC. To quantify the relationships, we designed a series of experiments that synthesize ACMC under conditions of constant solution chemistry using a mixed flow reactor (MFR) method. The approach allowed us to produce the amorphous products at steady state conditions in sufficient quantities that can be characterized by multiple methodologies. Advantages of using the MFR method for conducting quantitative studies of

ACMC include 1) maintaining constant and controlled supersaturation; 2) synthesizing ACMC at known steady state conditions with reproducible compositions; 3) precipitating ACMC at pH values (8.9–10.4) that approximate natural environments better than the previous investigations that synthesized ACC at very high pH conditions. By using this method for ACMC synthesis, we find that ACMC composition is tuned by the interplay of Mg/Ca ratio of the initial solution, total carbonate concentration, and local pH.

3.2 EXPERIMENTAL METHODS

3.2.1 Sample Synthesis

ACMC was synthesized for a series of controlled chemical conditions using a mixed flow reactor (MFR) (Blue et al., 2013). The method utilizes a high-precision pump fitted with two syringes. One contains 100 ml of a $MgCl_2$ and $CaCl_2$ solution fixed at a 5:1 ratio, while the other contains 100 ml of $NaHCO_3$ or Na_2CO_3 solution of variable concentration and initial pH (**Table 3.1**). The reactant solutions were continuously pumped into the reactor while maintaining a constant stirring rate of 1000 rpm to ensure that precipitation was controlled by surface-reactions with minimal mass transport (Rimstidt & Dove, 1986). Previous studies of crystal precipitation show that impurity levels in carbonate and sulfate minerals can exhibit complex relationships between structural constraints and solution composition (Preito et al., 1993; Astilleros et al., 2003). Calcite compositions can also reflect a continuum of mass transport and surface-limited growth processes when rates are varied over many orders of magnitude (DePaolo, 2010; Nielsen et al., 2013). Although our study maintained the rate of ACMC precipitation within a factor of approximately 10X, analysis of the available data did not suggest a relationship between composition and precipitation rate (**Fig. B5, Appendix B**).

Table 3.1. Solution and ACMC compositions for all experiments (25±1°C)

All solutions mixed in reactor with 0.01 M $CaCl_2 \bullet 2H_2O$ and 0.05 M $MgCl_2 \bullet 6H_2O$

Experiments with $NaHCO_3$								
Input			Output			ACMC Composition		
$[CO_3^{2-}]_{Tot}$ (M)	pH	$\Omega_{(Pure\ ACC)}$	pH	$[CO_3^{2-}]$ (m)	I. S. (m)	X_{Mg}/X_{Ca}	mole % Mg	K_D (Eq. 5)
0.06	9.93	4.55	9.34	0.00056	0.0420	0.360	26.48	0.054
0.06	10.00	4.67	9.39	0.00058	0.0414	0.351	25.97	0.049
0.06	10.11	4.84	9.59	0.00078	0.0409	0.474	32.16	0.056
0.06	10.19	4.95	9.62	0.00080	0.0406	0.450	30.97	0.055
0.06	10.27	5.05	9.75	0.00098	0.0407	0.569	36.25	0.063
0.06	10.38	5.16	9.80	0.00098	0.0399	0.611	37.94	0.067
0.06	10.78	5.43	10.05	0.00121	0.0390	1.185	54.24	0.115
0.10	9.65	4.94	9.10	0.00068	0.0625	0.332	24.93	0.047
0.10	9.75	5.19	9.22	0.00201	0.0762	0.336	25.17	0.043
0.10	9.79	5.28	9.31	0.00089	0.0608	0.393	28.24	0.046
0.10	9.90	5.50	9.49	0.00117	0.0603	0.455	31.27	0.049
0.10	9.98	5.64	9.56	0.00127	0.0510	0.561	35.95	0.055
0.10	10.12	5.85	9.75	0.00163	0.0596	0.804	44.57	0.068
0.10	10.25	6.05	9.89	0.00370	0.0667	1.098	52.33	0.080
0.20	9.32	4.91	8.98	0.00106	0.1102	0.340	25.39	0.044
0.20	9.43	5.26	9.12	0.00133	0.1097	0.379	27.49	0.044
0.20	9.46	5.35	9.14	0.00140	0.1098	0.401	28.62	0.046
0.20	9.59	5.69	9.33	0.00201	0.1099	0.474	32.15	0.047
0.20	9.72	5.98	9.50	0.00256	0.1096	0.664	39.90	0.056
0.20	9.96	6.33	9.75	0.00721	0.1169	0.836	45.54	0.057
Experiments with Na_2CO_3								
Input			Output			ACMC Composition		
$[CO_3^{2-}]_{Tot}$ (M)	pH	$\Omega_{(Pure\ ACC)}$	pH	$[CO_3^{2-}]$ (m)	I. S. (m)	X_{Mg}/X_{Ca}	mole % Mg	K_D (Eq. 5)
0.06	11.12	5.28	10.13	0.00235	0.0752	1.844	64.84	0.160
0.10	11.24	6.10	10.34	0.00421	0.1130	2.545	71.79	0.178

As the solution in the reactor vessel became supersaturated with respect to ACMC, precipitation proceeded continuously. The average hydraulic residence time (τ) of solution in the reactor was 2 minutes for all experiments, where

$$\tau = \frac{\text{volume of reactor (ml)}}{\text{flow rate (ml/hr)}}. \qquad (3.3)$$

For each experimental condition, the input solutions flowed through the reactor for a minimum of three hydraulic residence times to allow the ACMC products and solutions to reach steady state conditions within the reactor vessel (Jensen, 2001). The pH of the effluent solution was also

monitored to determine the pH at steady state conditions for each experiment (**Table 3.1**). The time elapsed to steady state and sample collection varied with solution chemistry.

The ACMC-solution suspension exited the reactor through a single effluent tube located at the top of the reactor. At steady state conditions, the exiting solution and solid products were separated by filtration through a 0.20-micron nylon filter fitted on a vacuum flask. We assume this solution records the solution chemistry inside the reactor at steady state conditions. All ACMC samples were rinsed thoroughly with ethanol and dried in a class II biological safety cabinet for 30 minutes before being stored overnight in a vacuum desiccator. Each sample was weighed the next day to obtain the mass of the dry ACMC and was immediately prepared for the respective mode of analyses. Samples that could not be analyzed were stored at 4°C for no longer than 3 days. Effluent solution samples were immediately prepared for chemical analysis after collection.

This study used three $NaHCO_3$ concentrations (60 mM, 100 mM, and 200 mM), and two Na_2CO_3 concentrations (60 mM and 100 mM), each with variable pH levels (**Table 3.1**). The pH of the $NaHCO_3$ solutions was adjusted by adding small amounts of NaOH immediately before mixing in order to obtain a range of saturation states. The saturation state of a solution (Ω) with respect to pure ACC is expressed by

$$\Omega = \frac{\left(a_{Ca^{2+}}\right)\left(a_{CO_3^{2-}}\right)}{K_{sp\ (ACC)}} \tag{3.4}$$

where a_i is the activity of species i and $K_{sp} = 10^{-6.39}$ at 25°C (Brečević & Nielsen, 1989). The solubility product of pure ACC was used to calculate Ω because the K_{sp} of an ACMC solid solution has not been quantified. Ion activities were calculated using The Geochemist's Workbench© for each solution condition in order to quantify saturation state. All experiments were performed at 25±1°C.

3.2.2 Sample Characterization

The composition and morphology of ACMC products were characterized using a combination of SEM, Raman Spectroscopy, TGA, ICP-OES, and FTIR. A summary of all experimental conditions is given in **Table B1 (Appendix B)**.

SEM. All ACMC samples were sputter-coated with approximately 10 nm of gold-palladium. Analyses were performed on an FEI Quanta 600 FEG ESEM. Images of the ACMC were acquired using secondary electron (SE) microscopy. Optimal viewing parameters included 10 kV and a 3.5 spot size (instrument specific value). Higher voltages destroyed the samples and could not be used. All samples were examined to characterize their morphology and particle size.

Raman Spectroscopy. A small amount of ACMC sample was removed from the nylon filter and placed on a clean glass slide for analysis by Raman spectroscopy. Raman spectra were obtained on a JY Horiba (800 mm) LabRam HR spectrometer equipped with a 632.81 nm He-Ne laser emitting 15 mW power and focused through an Olympus 50x objective. Three 180-second spectra accumulations were collected and averaged for each of the samples analyzed. The carbonate peak positions were estimated using a summed Gaussian/Lorentzian peak-fitting routine after baseline corrections were made using Jobin Yvon Labspec version 4 software.

Thermogravimetric Analysis (TGA). Approximately 5 mg of an ACMC sample was collected from the nylon filter and placed into an aluminum pan for Thermogravimetric analysis. Analyses were performed on a TA Instruments Hi-Res TGA Q5000 Thermogravimetic Analyzer. Samples were heated in air from 25°C to 700°C at a rate of 10°C per minute. The percentage of water lost during heating was calculated from the difference in the weight percent of the sample between 25°C and 250°C.

Inductively Coupled Plasma – Optical Emission Spectrometry (ICP-OES). ACMC samples on the nylon filters were dissolved in 0.5 N nitric acid for 20 minutes. Analyses were performed using a Spectro CirOS VISION. The Mg and Ca concentrations were determined from calibration curves that were prepared from plasma-grade single element standards (SPEX CertiPreps). Ca and Mg standards were analyzed in conjunction with ACMC samples to verify the accuracy of the results. Total concentrations of Mg and Ca in the ACMC samples were corrected for absorbance of excess solution by the nylon filter.

Fourier-Transform Infrared Spectroscopy (FTIR). Approximately 2 mg of an ACMC sample was removed from the nylon filter and used for FTIR analysis. Fourier-Transform Infrared Spectroscopy was performed on a Varian 670-IR with a Pike GladiATR attachment with a 4 cm^{-1} resolution. Samples were analyzed at a standard 32 cm^{-1} scan rate. All results were background ATR corrected using the instrument's software.

3.3 RESULTS

3.3.1 Sample Characterization

Characterization of synthetic ACMC samples by multiple modes of analysis show the MFR method produces ACMC with reproducible compositions and morphology without evidence of secondary phases. For the conditions of this study, ICP-OES measurements found the ACMC had Mg concentrations of 24–70 mole % (**Table B1, Appendix B**). SEM analyses showed that all solution compositions produced ACMC with a characteristic spherical morphology and a similar particle size distribution of approximately 0.1 μm to 2 μm (average diameter of 1 μm) (**Fig. 3.1**). ACMC particles with the highest Mg content (**Fig. 3.1C, D**) are predominately comprised of coalesced particles. This texture is consistent with previous results (Ajikumar et al., 2005; Wang et al., 2011).

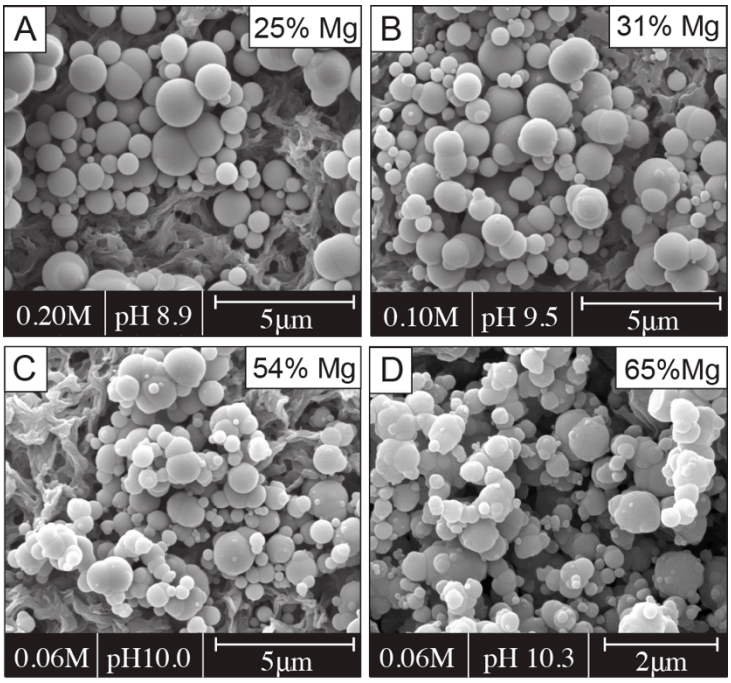

Figure. 3.1. SEM images show similar morphology and particle sizes of ACMC for all Mg contents (25–65 mole %) and reactant solution compositions. Particles become more amalgamated with increasing Mg content. (A) pH = 8.9, $NaHCO_3$ = 0.20M; (B) pH = 9.5, $NaHCO_3$ = 0.10M; (C) pH = 10.0, $NaHCO_3$ = 0.06M; (D) pH = 10.3, Na_2CO_3 = 0.06M.

Raman analyses of the products confirm that all materials are amorphous. In contrast with crystalline carbonates that typically exhibit six Raman vibrational modes, the ACMC produce only two modes as broadened ν_1 and ν_4 peaks (**Fig. B1a, Appendix B**), with the ν_1 peak having the strongest carbonate internal mode (Wang et al., 2011). The position of the ν_1 peak systematically shifts to higher wavenumbers (Wang et al., 2011) with increasing Mg content compared to pure ACC (1080 cm^{-1}). **Figure B1b** (**Appendix B)** shows a linear regression fit of the ν_1 peak positions to the measured Mg content (24–70 mole %) of synthetic samples with a slope (0.227±0.030) that is slightly higher than a previous calibration of 0.2017±0.0087 (Wang et al., 2011).

Additional characterization by Fourier-Transform Infrared Spectroscopy (FTIR) confirms that ACMC products are amorphous, including the samples that contain up to 70 mole % Mg.

Comparisons of FTIR spectra for the ACMS samples with baseline ACC prepared in the absence of Mg show peaks are present at 1406 cm^{-1} (ν_3), 1073 cm^{-1} (ν_1), 864 cm^{-1} (ν_2). Peaks due to vibrations of water molecules occur at 1644 cm^{-1} and around 3300 cm^{-1} (**Fig. B2, Appendix B**). These values are consistent with reports of 1455–1470/1396–1425 cm^{-1} (ν_3), 1065–1075 cm^{-1} (ν_1), and 863–873 cm^{-1} (ν_2) (Aizenberg et al., 1996; Brečević & Nielsen, 1989; Loste et al., 2003). These values shift when Mg is present (**Fig. B2, Appendix B**), but only the ν_1 peaks shift systematically with changes in Mg content (**Table B1, Appendix B**).

Thermogravimetric analyses indicate that all ACMC products contained slightly more than one water molecule per carbonate ion, resulting in compositions ranging from $Mg_{(0.24–0.72)}Ca_{(0.76–0.28)}CO_3 \bullet 1.37–1.63\ H_2O$ (**Fig. B3, Appendix B**). There is no correlation between the water content and the Mg content of ACMC for the conditions of this study.

3.3.2 Controls on Mg Content of ACMC

Apparent dependence upon alkalinity. A first group of experiments investigated the effect of alkalinity on the Mg content of ACMC using constant input Mg/Ca ratio of 5/1 and input solution pH of 9.75. **Figure 3.2** suggests a positive correlation between the solution alkalinity and the Mg content of ACMC, with a single trend that demonstrates an increase of 15 mole % Mg. However, the relationship is misleading because the composition space traverses multiple solution chemistry variables, with an increasing Ω (2.23–6.22), total carbonate concentration (60–400 mM), pH (9.1–9.7), and ionic strength (0.093–0.304 m). Previous studies show ionic strength can affect the precipitation kinetics of sparingly soluble salts, such as calcite (Zuddas & Mucci, 1998) and barite (Kowacz et al., 2010), but there is no relationship between the ionic strength of the precipitating solution and the Mg content of the ACMC (**Fig. B4, Appendix B**). However, a close look at the data suggest a positive correlation between the Mg content of

ACMC and both the pH and total carbonate concentration of the solution in the first group of experiments, which warranted further investigation discussed below.

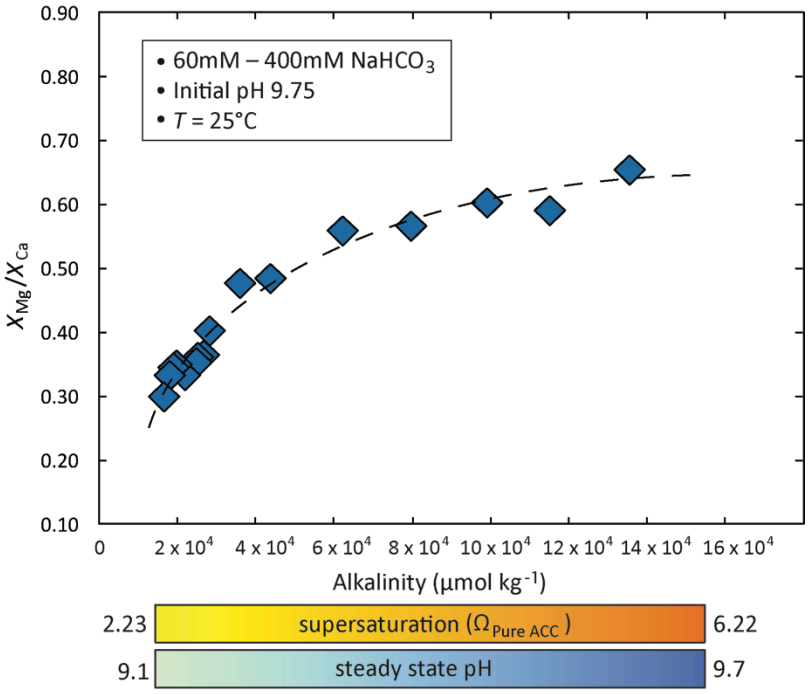

Figure. 3.2. Early experiments suggested the Mg content of ACMC correlates with solution alkalinity. The relationship is misleading, however, because of differences in pH (9.1–9.7) and supersaturation (2.23–6.22) occur across alkalinity as a result of the buffering capacity of the carbonate solution. The dashed line provides a visual guide and is not a quantitative fit.

Interplay of carbonate concentration, pH, and Mg/Ca ratio. To decipher the influence of total carbonate concentration and pH on ACMC composition, additional experiments were conducted to independently vary carbonate concentration and pH (**Table 3.1**). **Figure 3.3a** shows the dependence of ACMC composition on the *input* solution saturation state (Ω = 4.55–6.33). Recall the experimental design maintains a constant initial Ca concentration, thus, differences in Ω arise primarily from CO_3^{2-} concentration. Trends in **Fig. 3.3a**, however, do not show a simple relationship between input Ω and ACMC composition (**Fig. 3.3a**). Rather, composition follows contours of the input carbonate concentration. Indeed, the relationship between ACMC composition and the output carbonate ion concentration (**Fig. 3.3b**) is similar to

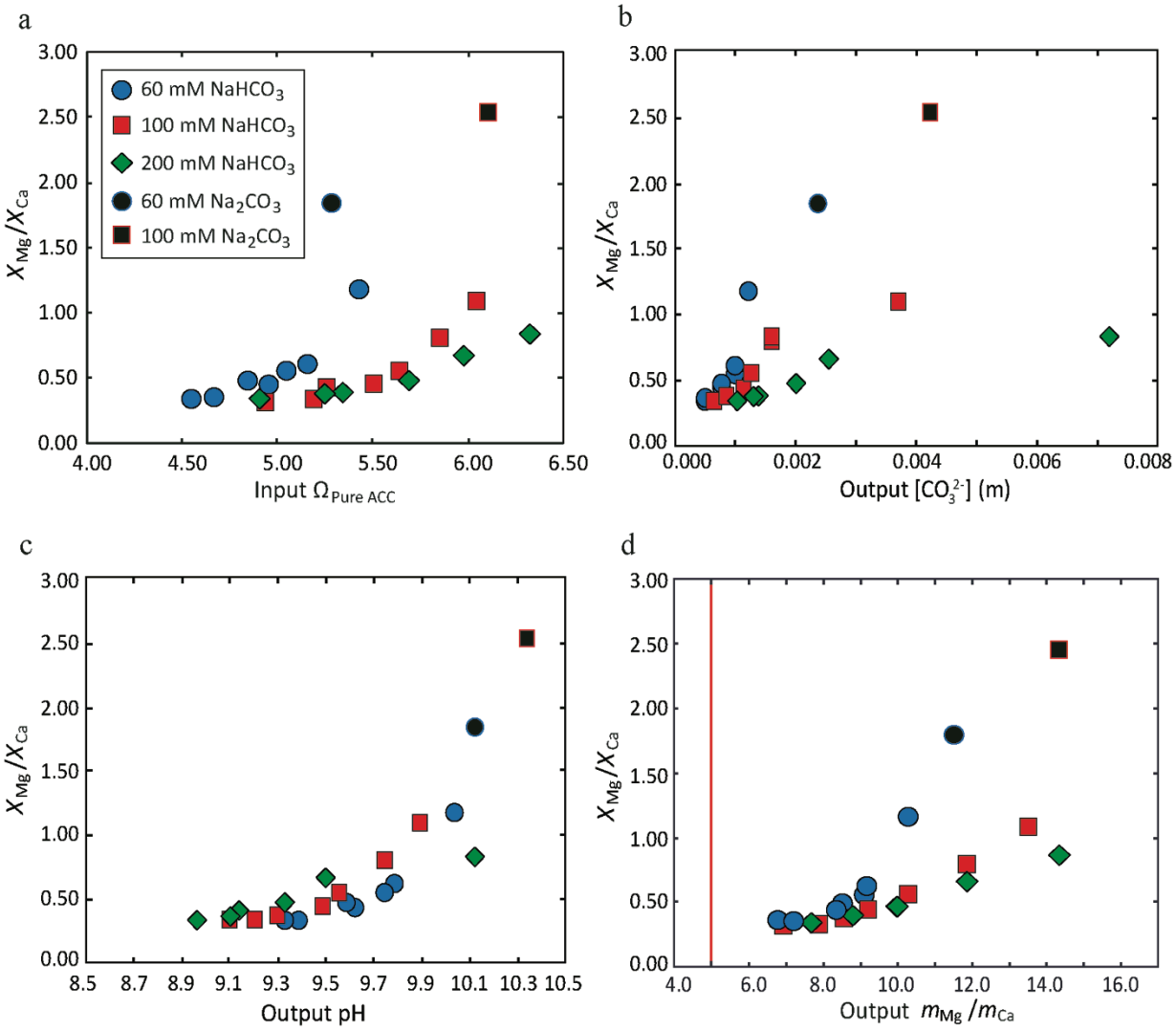

Figure 3.3 The interplay of carbonate concentration, pH, and solution Mg/Ca ratio on Mg content in ACMC. (a) The mole fraction of Mg in ACMC does not show a simple dependence on the initial supersaturation of the reactant solution (Ω, Eq. 4). The individual trends for each total carbonate solution concentration reflect differences in Ω. (b) The output CO_3^{2-} concentration of the reactant solution has a similar relationship to Mg content, with trends existing for each total carbonate solution concentration. The largest offsets are measured for the higher pH conditions of the Na_2CO_3 solutions. (c) The Mg content of ACMC increases with a combination of higher output pH and total carbonate concentration. (d) In this study, input solutions began with an initial Mg/Ca ratio 5 (red line). As ACMC precipitates, the Mg/Ca ratio evolves to higher values depending upon Ω. The output (steady state) solution Mg/Ca values (m_{Mg}/m_{Ca}) shown here do not correlate with the Mg/Ca ratios in ACMC (X_{Mg}/X_{Ca}), thus reiterating our conclusion that additional factors control the partitioning of Mg into ACMC.

Fig. 3.3a; reiterating the primary control of CO_3^{2-} concentration on Ω in these experiments. The relationships also show offsets that indicate the greatest Mg contents are associated with the higher pH of the Na_2CO_3 solutions (e.g. **Table 3.1**).

By re-plotting the ACMC compositions versus pH of the output solution (**Fig. 3.3c**), we find the data largely collapse onto one trend whereby higher pH solutions promote a greater Mg content in ACMC. Further inspection shows that for a constant output pH, small offsets to higher Mg levels are correlated with the higher total carbonate concentrations. Thus, the data demonstrate that solution pH, as regulated by the total carbonate concentration at steady state conditions, has a primary control on ACMC composition. These connections can be understood by recalling that the input pH of the initial carbonate solutions was varied across each of the total carbonate conditions used in this study (**Table 3.1**). For a given total carbonate concentration, differences in pH account for the variations in Ω. Thus, the trends seen in **Figs. 3.3a** and **3.3b** are primarily determined by differences in solution pH at steady state conditions. This also explains the relationship between alkalinity and ACMC composition seen in **Fig. 3.2**.

It is important to remember that the molal Mg/Ca ratio of the output solution (m_{Mg}/m_{Ca}) has an overarching control on these composition relations. Although all synthesis experiments began with an initial Mg/Ca ratio of 5/1, experiments with the higher chemical driving forces produced greater extents of reaction within the reactor. Because a greater extent of reaction consumes a larger fraction of Ca^{2+} than Mg^{2+} during ACMC precipitation, each initial solution composition evolves to a condition-specific Mg/Ca ratio (**Fig. 3.3d**). For examples, solutions with the greater total carbonate concentrations and pH levels acquired Mg/Ca ratios as high as 14.

Partitioning relationships. The dependence of ACMC composition on the interplay of solution variables discussed in **Fig. 3.3** can be quantified by evaluating the composition data with the corresponding conditions during formation. Assuming that precipitation conditions are in a regime where rates are reaction-limited and mass transport effects are negligible (see **Section 2.1**), the distribution coefficient for Mg partitioning between ACMC precipitates and the reactant solution is expressed by:

$$K_D = \frac{\left(\frac{X_{Mg}}{X_{Ca}}\right)}{\left(\frac{m_{Mg}}{m_{Ca}}\right)} \tag{3.5}$$

where $\left(\frac{X_{Mg}}{X_{Ca}}\right)$ is the ratio of the Mg/Ca concentration in the ACMC product and $\left(\frac{m_{Mg}}{m_{Ca}}\right)$ is the ratio of the total concentration of cations in the corresponding effluent solutions at steady state conditions. Note that K_D is a consequence of growth and hence, does not reflect equilibrium conditions. This parameter, therefore, normalizes the steady state chemistry of the solution during precipitation with the corresponding composition of the resulting solid. Equation (3.5), also known as the Henderson-Kracek or homogeneous distribution coefficient (Henderson & Kracek, 1927), is used because the composition of the solution was maintained constant within the reactor at steady state conditions. **Figure 3.4** shows that when calculated K_D values are compared to the output pH of the corresponding experiment, the data collapse onto one trend. The value of K_D is approximately constant when steady state pH is less than approximately 9.5, but then triples between pH 9.5 and 10.3.

It is notable that our study finds much lower K_D values than reported values (0.44±0.02) for ACMC with similar Mg contents (Radha et al., 2012). There are two probable explanations for this difference. First, our estimates of K_D are based upon the values of Mg/Ca at steady state conditions in contrast with the standard practice of using initial solution Mg/Ca values. **Figure**

3.3d shows the mole fractions of Mg/Ca in output solutions evolve to significantly higher values in proportion to the extent of supersaturation. Thus, the larger denominator of Equation (3.5) inevitably leads to a lower K_D. One can see that, when the steady state solution information is available, the local Mg/Ca values are more representative of the chemical conditions during the time of formation.

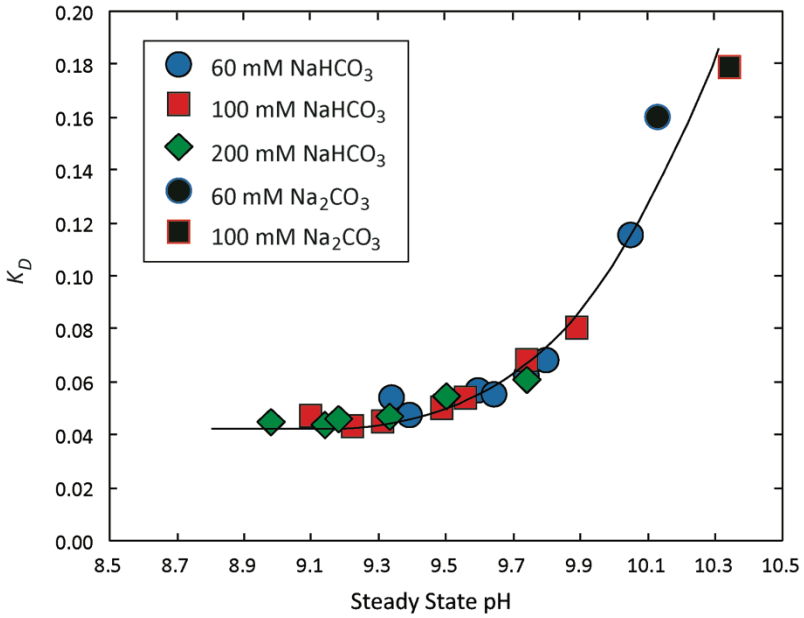

Figure. 3.4. Mg partitioning into ACMC correlates with the steady state pH of the local precipitation environment. Below pH 9.5, K_D is independent of pH, and is primarily controlled by steady state solution Mg/Ca ratio. Above approximately pH 9.5, solution pH exerts a strong control on the K_D values of ACMC, with values tripling between 9.5 and 10.3.

A second explanation for our lower K_D values is likely found in the lower pH conditions of this study. To better approximate natural environments, this study was designed to produce output pH values of 8.9 to 10.4 (e.g. **Fig. 3.3c** and **Fig. 3.4**). In contrast, previous studies used reagents of Na_2CO_3 (Koga et al., 1998; Radha et al., 2012; Rodriguez-Blanco et al., 2012) and $(NH_4)_2CO_3$ (Aizenberg et al., 1996; Raz et al., 2000; Wang et al., 2009, 2012). Although the in situ pH during mineralization is unknown, their conditions are qualitatively associated with very high pH. We attempted additional experiments to extend the pH range upward and make direct

comparisons with these higher pH studies, but we encountered an experimental limitation with the formation of a different phase, possibly brucite ($MgOH_2$), precipitated at very high pH. We confirmed the presence of this new phase by SEM observations of rosette features that are morphologically similar to those reported by Hsu and Nacu (2005), the presence of a sharp O-H peak around 3700cm^{-1} in the FTIR spectra, and a unique TGA weight loss curve that did not resemble those produced by ACMC. Indeed, our experimental conditions that led to $Mg(OH)_2$ formation are in agreement with previous reports (Hsu & Nacu, 2005).

3.4 DISCUSSION

By using a synthesis method that allows us to quantify the relationship between ACMC composition and steady state solution chemistry, we find that three inorganic "levers" regulate the Mg content of ACMC. The primary control on composition is the Mg/Ca ratio of the input solution, a conclusion shown previously (Loste et al., 2003; Radha et al., 2012; Wang et al., 2009). A higher initial concentration of Mg^{2+} ions in solution establishes the minimum baseline for total Mg in the resulting ACMC. However, we have shown the Mg content of ACMC for a *fixed* solution Mg/Ca ratio is regulated by total carbonate concentration, in proportion to the extent of precipitation due to its principal control on supersaturation. Local solution pH also influences the amount of Mg in ACMC. This dependence of Mg content on pH is not fully understood, but could be due to the increasing the proportion of CO_3^{2-} and the progressive formation of ion pairs and additional Mg-carbonate stoichiometries that become incorporated into ACMC.

As noted earlier, kinetic effects are known to influence composition under some conditions (Section 2.1), and a kinetic explanation is also given in an experimental study of abiogenic aragonite that shows elemental partitioning with similar departures from a

thermodynamic model based upon the K_D values of trace elements (Gaetani & Cohen, 2006). In our study, however, precipitation rates were similar within a factor of 10X, suggesting the chemical 'levers' proposed herein are more significant in regulating composition for the conditions used in this study (e.g. **Fig. B5, Appendix B**).

The quantitative relationships presented in this study raise the point that the controls on ACMC composition are most accurately interpreted in conjunction with the local solution composition at the time of formation. As ACMC precipitates, solution Mg/Ca ratios evolve to higher values in proportion to the extent of reaction. Thus, conventional estimates of K_D that use the (lower) initial solution Mg/Ca values produce erroneously high values. We show the Mg/Ca ratios of steady state solutions almost triple (from 5 to 14) for some conditions despite the flow through conditions. Previous investigations that used batch (closed) methods, either through mixing of $NaHCO_3/Na_2CO_3$ or ammonium carbonate diffusion, show that extreme shifts in Mg/Ca ratios are possible over the course of precipitation with values that can easily exceed 60-100 (Wang et al., 2012).

Our findings suggest the conventional practice of estimating K_D from initial solution chemistry may need to be revisited because this approach does not give meaningful representations of solution conditions at the time of formation. Moreover, the concept of K_D assumes Mg content of ACMC is linearly correlated with solution Mg/Ca (Equation 3.5). **Figure 3.4** shows this is not the case when K_D is determined by using solution conditions *at the time of formation*, with observations of a nonlinear relationship between ACMC composition and steady state solution chemistry. Although the conventional approach indeed gives a linear relationship between *initial* solution Mg/Ca ratios and ACMC composition (Blue et al., 2013; Radha et al., 2012; Wang et al., 2012), this is not an accurate representation of solution-solid relationships.

This insight has particular significance for the formation of ACMC and perhaps other carbonates in closed and semi-closed biogeochemical environments. As precipitation proceeds, the Mg/Ca ratio of the local chemical environment increases to significantly higher values. Sites of rapid calcification within tissues of organisms that produce ACMC provide a natural setting for large increases in local Mg/Ca ratio, but similar processes can be at work in closed basin lakes and some marine porewaters where supersaturations can exceed ACC solubility (Chave, 1954b; Nishiyama et al., 2012; Katz & Nishri, 2013). In these settings, local Mg/Ca ratios are 1) driven to extremely high (and condition-specific) values and 2) evolve over the extent of reaction to complicate estimates of K_D.

It is notable that ACMC can be produced at pH conditions relevant to many geological and biogeochemical systems. This suggests ACMC formation is feasible in environmental settings where waters can become highly supersaturated with respect to the crystalline polymorphs for short periods of time. Previous studies that used extreme pH conditions propose that a nonclassical mineralization pathway involving an amorphous intermediate can explain the formation of very high Mg calcite (Long et al., 2011; Wang et al., 2012). Our ability to form ACMC at milder pH supports this idea and we suggest that the carbonate geologic record should be revisited for evidence of mineralization via this metastable phase.

Our findings are consistent with an earlier postulation that the Mg content of calcite minerals is dependent upon the alkalinity of a solution (Boyle & Erez, 2003; Given & Wilkinson, 1985). We show, however, this relationship is an apparent dependence that is rooted in the local pH of the precipitation environment (when total carbonate is held constant). Finally, our findings have implications for the question of how ocean acidification will affect carbonate biomineralization. This study observed that less ACMC is produced at lower pH values, with a

higher solubility than ACMC formed in higher pH environments. This suggests that it may become more difficult for organisms to produce ACMC, and less likely for ACMC to persist for longer periods of time, in lower pH environments.

3.5 REFERENCES

Addadi L., Joester D., Nudelman F. and Weiner S. (2006) Mollusk shell formation: A source of new concepts for understanding biomineralization processes. *Chem. Eur. J.* **12**, 980–987.

Aizenberg J., Addadi L., Weiner S. and Lambert G. (1996) Stabilization of amorphous calcium carbonate by specialized macromolecules in biological and synthetic precipitates. *Adv. Mater.* **8**, 222–226.

Ajikumar P. K., Wong L. G., Subramanyam G., Lakshminarayanan R. and Valiyaveettil S. (2005) Synthesis and characterization of monodispersed spheres of amorphous calcium carbonate and calcite spherules. *Cryst. Growth Des.* **5**, 1129–1134.

Astilleros J. M., Pina C. M., Fernández-Díaz L. and Putnis A. (2003) Supersaturation functions in binary solid solution–aqueous solution systems. *Geochim. et Cosmochim. Acta* **67**, 1601–1608.

Beniash E., Aizenberg J., Addadi L. and Weiner S. (1997) Amorphous calcium carbonate transforms into calcite during sea urchin larval spicule growth. *Proceed. Royal Soc. London Series B: Bio. Sci.* **264**, 461–465.

Bentov S. and Erez J. (2005) Novel observations on biomineralization processes in foraminifera and implications for Mg/Ca ratio in the shells. *Geology* **33**, 841–844.

Bentov S. and Erez J. (2006) Impact of biomineralization processes on the Mg content of foraminiferal shells: A biological perspective. *Geochem. Geophys. Geosyst.* **7**, Q01P08.

Berner R. A. (1980) Early diagenesis- A theoretical approach. Princeton University Press, Princeton, N. J.

Bischoff W. D., Mackenzie F. T. and Bishop F. C. (1987) Stabilities of synthetic magnesian calcites in aqueous solution: Comparison with biogenic materials. *Geochim. et Cosmochim. Acta* **51**, 1413–1423.

Blue C. R., Rimstidt J. D. and Dove P. M. (2013) Chapter Twenty-Three - A mixed flow reactor method to synthesize amorphous calcium carbonate under controlled chemical conditions, in: James, J. D. Y. (Ed.), *Method. Enzymol*. Academic Press, 557–568.

Boyle E. A. and Erez J. (2003) Does carbonate ion influence foraminiferal Mg/Ca, Ocean Sciences Meeting. *Eos Trans*. *AGU*.

Brečević L. and Nielsen A. E. (1989) Solubility of amorphous calcium carbonate. *J. Cryst. Growth* **98**, 504–510.

Burton W. K., Cabrera N. and Frank F. C. (1951) The growth of crystals and the equilibrium structure of their surfaces. *Phil. Tran. Royal Soc. London. Series A, Math. and Phys. Sci.* **243**, 299–358.

Chave K. E. (1954a) Aspects of the biogeochemistry of magnesium 1. Calcareous marine organisms. *J. Geology* **62**, 266–283.

Chave K. E. (1954b) Aspects of the biogeochemistry of magnesium 2. Calcareous sediments and rocks. *J. Geology* **62**, 587–599.

Chernov A. A. (1984) Modern Crystallography III: Crystal Growth. Springer-Verlag. 517 p.

Davis K. J., Dove P. M. and De Yoreo J. J. (2000) The role of Mg^{2+} as an impurity in calcite growth. *Science* **290**, 1134–1137.

DePaolo D. J. (2011) Surface kinetic model for isotopic and trace element fractionation during precipitation of calcite from aqueous solutions. *Geochim. et Cosmochim. Acta* **75**, 1039–1056.

Dissard D., Nehrke G., Reichary G. J. and Bijma J. (2010) The impact of salinity on the Mg/Ca and Sr/Ca ratio in the benthic foraminifera Ammonia tepida: Results from culture experiments. *Geochim. et Cosmochim. Acta* **74**, 928–940.

Gaetani G. A. and Cohen A.L. (2006) Element partitioning during precipitation of aragonite from seawater: A framework for understanding paleoproxies. *Geochim. et Cosmochim. Acta* **70**, 4617–4634.

Gebauer D., Volkel A. and Cölfen H. (2008) Stable prenucleation calcium carbonate clusters. *Science* **322**, 1819–1822.

Given R. K. and Wilkinson B. H. (1985) Kinetic control of morphology, composition, and mineralogy of abiotic sedimentary carbonates. *J. Sed. Petr.* **55**, 0109–0119.

Han N., Blue, C. R., De Yoreo J. J. and Dove P. M. (2013) The effect of carboxylates on the Mg content of calcites that transform from ACC. *Proced. Earth Planet. Sci*. **7**, 225–227.

Han T. Y.-J. and Aizenberg J. (2008) Calcium carbonate storage in amorphous form and its template-induced nucleation. *Chem. Mater.* **20**, 1064–1068.

Hastings D. W., Russell A. D. and Emerson S. R. (1998) Foraminiferal magnesium in Globeriginoides sacculifer as a paleotemperature proxy. *Paleoceanography* **13**, 161–169.

Henderson L. M. and Kracek F. C. (1927) The fractional precipitation of barium and radium chromates. *J. Amer. Chem. Soc.* **49**, 738–749.

Hsu J.-P. and Nacu A. (2005) Preparation of submicron-sized $Mg(OH)_2$ particles through precipitation. *Colloids and Surfaces A: Physicochem. Eng. Aspects* **262**, 220–231.

Hu Q., Nielsen M. H., Freeman C. L., Hamm L. M., Tao J., Lee J. R. I., Han T. Y. J., Becker U., Harding J. H., Dove P. M. and De Yoreo J. J. (2012) The thermodynamics of calcite nucleation at organic interfaces: Classical vs. non-classical pathways. *Faraday Discuss*. **159**, 509–523.

Jensen J. N. (2001) Approach to steady state in completely mixed flow reactors. *J. Environ. Engineer.* **127**, 13–18.

Katz A. and Nishri A. (2013) Calcium, magnesium and strontium cycling in stratified, hardwater lakes: Lake Kinneret (Sea of Galilee), Israel. *Geochim. et Cosmochim. Acta* **105**, 372–394.

Koga N., Nakagoe Y. and Tanaka H. (1998) Crystallization of amorphous calcium carbonate. *Thermochim. Acta* **318**, 239–244.

Kowacz M., Prieto M. and Putnis A. (2010) Kinetics of crystal nucleation in ionic solutions: Electrostatics and hydration forces. *Geochim. et Cosmochim. Acta* **74**, 469–481.

Long X., Ma Y. and Qi L. (2011) In Vitro Synthesis of High Mg Calcite under Ambient Conditions and Its Implication for Biomineralization Process. *Cryst. Growth & Design* **11**, 2866–2873.

Loste E., Wilson R. M., Seshadri R. and Meldrum F. C. (2003) The role of magnesium in stabilising amorphous calcium carbonate and controlling calcite morphologies. *J. Cryst. Growth* **254**, 206–218.

Michel F. M., MacDonald J., Feng J., Phillips B. L., Ehm L., Tarabrella C., Parise J. B. and Reeder R. J. (2008) Structural characteristics of synthetic amorphous calcium carbonate. *Chem. Mater.* **20**, 4720–4728.

Morse J. W., Wang Q. and Tsio M. Y. (1997) Influences of temperature and Mg:Ca ratio on $CaCO_3$ precipitates from seawater. *Geology* **25**, 85–87.

Navrotsky A. (2004) Energetic clues to pathways to biomineralization: Precursors, clusters, and nanoparticles. *Proc. Natl. Acad. Sci. U. S. A.* **101**, 12096–12101.

Nielsen L. C., De Yoreo J. J. and DePaolo D. J. (2013) General model for calcite growth kinetics in the presence of impurity ions. *Geochim. et Cosmochim. Acta* **115**, 100–114.
Nishiyama R., Munemoto T. and Fukushi K. (2013) Formation condition of monohydrocalcite from $CaCl_2$–$MgCl_2$–Na_2CO_3 solutions. *Geochim. et Cosmochim. Acta* **100**, 217–231.
Nudelman F., Chen H. H., Goldberg H. A., Weiner S. and Addadi L. (2007) Lessons from biomineralization: comparing the growth strategies of mollusc shell prismatic and nacreous layers in *Atrina rigida*. *Faraday Discuss.* **136**, 9–25.
Politi Y., Arad T., Klein E., Weiner S. and Addadi L. (2004) Sea urchin spine calcite forms via a transient amorphous calcium carbonate phase. *Science* **306**, 1161–1164.
Politi Y., Metzler R. A., Abrecht M., Gilbert B., Wilt F. H., Sagi I., Addadi L., Weiner S. and Gilbert P. U. P. A. (2008) Transformation mechanism of amorphous calcium carbonate into calcite in the sea urchin larval spicule *Proc. Natl. Acad. Sci. U. S. A.* **105**, 17362–17366.
Prieto M., Putnis A. and Fernández-Díaz L. (1993) Crystallization of solid solutions from aqueous solutions in a porous medium: zoning in (Ba, Sr)SO_4. *Geological Magazine* **130**, 289–299.
Radha A. V., Fernandez-Martinez A., Hu Y., Jun Y.-S., Waychunas G. A. and Navrotsky A. (2012) Energetic and structural studies of amorphous $Ca_{1-x}Mg_xCO_3 \bullet nH_2O$ ($0 \le x \le 1$). *Geochim. et Cosmochim. Acta* **90**, 83–95.
Radha A. V., Forbes T. Z., Killian C. E., Gilbert P. U. P. A. and Navrotsky A. (2010) Transformation and crystallization energetics of synthetic and biogenic amorphous calcium carbonate. *Proc. Natl. Acad. Sci. U. S. A.* **107**, 16438–16443.
Raz S., Hamilton P. C., Wilt F. H., Weiner S. and Addadi L. (2003) The transient phase of amorphous calcium carbonate in sea urchin larval spicules: The involvement of proteins and magnesium ions in its formation and stabilization. *Adv. Funct. Mater.* **13**, 480–486.
Raz S., Weiner S. and Addadi L. (2000) Formation of high-magnesium calcites via an amorphous precursor phase: Possible biological implications. *Adv. Mater.* **12**, 38–42.
Rimstidt J. D. and Dove P. M. (1986) Mineral/solution reaction rates in a mixed flow reactor: Wollastonite hydrolysis. *Geochim. et Cosmochim. Acta* **50**, 2509–2516.
Rodriguez-Blanco J. D., Shaw S., Bots P., Roncal-Herrero T. and Benning L. G. (2012) The role of pH and Mg on the stability and crystallization of amorphous calcium carbonate. *J. Alloys and Compounds* **536, Supplement 1**, S477–S479.
Rosenthal Y., Boyle E. A. and Slowey N. (1997) Temperature control on the incorporation of magnesium, strontium, fluorine, and cadmium into benthic foraminiferal shells from Little Bahama Bank: Prospects for thermocline paleoceanography. *Geochim. et Cosmochim. Acta* **61**, 3633–3643.
Sánchez-Román M., Romanek C. S., Fernández-Remolar D. C., Sánchez-Navas A., McKenzie J. A., Pibernat R. A. and Vasconcelos C. (2011) Aerobic biomineralization of Mg-rich carbonates: Implications for natural environments. *Chem. Geology* **281**, 143–150.
Stephenson A. E., DeYoreo J. J., Wu L., Wu K. J., Hoyer J. and Dove P. M. (2008) Peptides enhance magnesium signature in calcite: Insights into origins of vital effects. *Science* **322**, 724–727.
Tao J., Zhou D., Zhang Z., Xu X. and Tang R. (2009) Magnesium-aspartate-based crystallization switch inspired from shell molt of crustacean. *Proc. Natl. Acad. Sci. U. S. A.* **106**, 22096–22101.
Towe K. M. and Malone P. G. (1970) Precipitation of metastable carbonate phases from seawater. *Nature* **226**, 348–349.

Wang D., Hamm L. M., Bodnar R. J. and Dove P. M. (2011) Raman spectroscopic characterization of the magnesium content in amorphous calcium carbonates. *J. Raman Spec.* **43**, 543–548.

Wang D., Hamm L. M., Giuffre A. J., Echigo T., Rimstidt J. D., De Yoreo J. J., Grotzinger J. and Dove P. M. (2012) Revisiting geochemical controls on patterns of carbonate deposition through the lens of multiple pathways to mineralization. *Faraday Discuss.* **159**, 1–16.

Wang D., Wallace A. F., De Yoreo J. J. and Dove P. M. (2009) Carboxylated molecules regulate magnesium content of amorphous calcium carbonates during calcification. *Proc. Natl. Acad. Sci. U. S. A.* **106**, 21511–21516.

Weiss I. M., Tuross N., Addadi L. and Weiner S. (2002) Mollusc larval shell formation: amorphous calcium carbonate is a precursor phase for aragonite. *J. Exper. Zoology* **293**, 478–491.

Zhang Z., Xie Y., Xu X., Pan H. and Tang R. (2012) Transformation of amorphous calcium carbonate into aragonite. *J. Cryst. Growth* **343**, 62–67.

Zuddas P. and Mucci A. (1998) Kinetics of calcite precipitation from seawater: II. The influence of the ionic strength. *Geochim. et Cosmochim. Acta* **62**, 757–766.

CHAPTER 4. THE EFFECT OF SOLUTION CHEMISTRY ON THE TRANSFORMATION OF AMORPHOUS CALCIUM CARBONATE

Blue C. R., Han N. and Dove P. M. (in prep)

ABSTRACT: A number of studies have suggested that amorphous calcium carbonate (ACC) can form as a reactive intermediate to the carbonates produced in unique geological settings. Previous experimental work shows ACC can transform to one or more of the crystalline polymorphs of $CaCO_3$ (e.g. calcite, aragonite, vaterite). This pathway to mineralization may provide a missing link to explain long-standing enigmas regarding carbonate formation and chemistry in natural environments that are not readily interpreted by the classical growth process. The control of mineralization pathway on Mg content is particularly interesting because recent studies show the process can produce carbonates with compositions and textures that are significantly different from those grown by the classical step-growth mechanisms.

This study uses a mixed flow reactor method to prepare ACC in an inorganic environment under controlled chemical conditions and establish relationships between polymorph composition, solution chemistry, and environment of transformation. The experimental design controlled the input solution Mg/Ca ratio, total carbonate concentration, and pH to produce ACC with systematic chemical compositions. The resulting ACC was allowed to transform within the output suspension in a batch reactor under both mixed and unmixed conditions. Findings from transformation experiments provide a systematic and predictable chemical framework for understanding polymorph selection during ACC transformation: the first crystalline phase is controlled by the relative activities of Mg^{2+} and CO_3^{2-} to Ca^{2+} and solution mixing. Results suggest a chemical basis for a broad range of Mg contents in calcite, including high Mg calcite. We find that the final calcite produced from ACC is similar to the composition of the initial ACC phase, suggesting that calcite composition reflects local conditions of formation, regardless of the pathway to mineralization. The findings from this study provide a chemical road map to future studies on ACC transformation, polymorph selection, and impurities in calcite.

4.1 INTRODUCTION

Recent studies on nucleation and crystal growth have shown that there is more than one pathway to form a mineral. Fifty years of geochemical research on mineral growth has assumed the classical terrace-ledge-kink (TLK) model—where crystals grow via direct ion-by-ion attachment along the edge of a growing surface (Burton et al., 1951; Chernov, 1984)—is the mechanism that forms crystals in natural environments. However, there is mounting evidence that a variety of common minerals can form via an amorphous pathway (Cölfen & Antonietti, 2008), where molecules or clusters aggregate to form a metastable amorphous phase that later transforms to one or more crystalline polymorphs. This crystal growth process occurs under specific conditions where the free energy to forming a metastable amorphous phase is lower than the stable bulk crystal (Navrotsky, 2004; De Yoreo, 2013). Amorphous precursor phases have also been documented in diverse biomineralizing organisms (e.g. Weiss et al., 2002; Politi et al., 2008; Tao et al., 2009; Akiva-Tal et al., 2011). An amorphous pathway to mineralization is more common in natural environments than previously thought, but little is known about the mechanisms that control this type of mineralization and how the chemical signatures of the final crystal are affected. It is critical to understand how an amorphous pathway to carbonate mineralization differs from "classic" growth.

Amorphous calcium carbonate (ACC) is now widely recognized as a metastable intermediate to crystalline phases. Emerging studies indicate that the three anhydrous polymorphs of $CaCO_3$ (calcite, aragonite, and vaterite) and one hydrated polymorph (monohydrocalcite) can form from an amorphous precursor (Loste et al., 2003; Radha et al., 2010; Zhang et al., 2012; Rodriguez-Blanco et al., 2012). The transformation of ACC to crystalline carbonates is an important and widespread process. It is well documented that diverse

organisms produce amorphous carbonate phases during skeletal mineralization (Aizenberg et al., 1996; Beniash et al., 1997; Nudelman et al., 2007; Politi et al., 2008), and ACC can form in some earth environments (Dupraz et al., 2009; Jones & Peng, 2012) where supersaturation can become high. The amorphous-to-crystalline pathway is particularly significant for calcite because recent studies suggest the chemical compositions and textures of calcite that forms from an ACC precursor are significantly different from those that grow classically (Loste et al., 2003; Wang et al., 2012; Han et al., 2013). Specifically, an amorphous pathway could be the missing link to understand the formation of high Mg calcite.

The realization that ACC can be a reactive precursor to the crystalline polymorphs of $CaCO_3$ has motivated an extensive effort to understand the influence of the inorganic and organic factors on ACC composition and transformation. Table 4.1 shows a summary of results from recent ACC transformation experiments, and the diversity of experimental conditions, polymorphs produced, and crystal compositions are perplexing. The vast majority of studies have focused on reporting the mixtures of polymorphs that are produced in different solution conditions or synthesis methods because the transformation process is difficult to control and observe directly. Unfortunately, the procedures reported in the literature are so diverse that it becomes difficult to directly compare results. The most common methods range from batch mixed (Rodriguez-Blanco et al., 2012; Nishiyama et al., 2012) or unmixed (Loste et al., 2003; Han et al., 2013) solutions of $NaHCO_3$ or Na_2CO_3 with $CaCl_2$, to $(NH_4)_2CO_3$ diffusion into $CaCl_2$ solutions (Raz et al., 2000; Wang et al., 2012). None of these methods, however, have control over the evolution of the solution chemistry during ACC precipitation. Although previous studies have provided insights for ACC transformation, there is no established systematic framework for understanding polymorph formation or calcite composition.

Table 4.1
Summary of published results of ACC transformation experiments.

Study	Synthesis method	Stirring (Y/N)	Temp (°C)	Initial [Mg]/[Ca]	Initial $[CO_3^{2-}]$ (M)	Phases reported*	%Mg in Calcite
Sand et al., 2011	Batch reactor with Na_2CO_3	Y; gentle vs. vigorous	24	n/a	0.025	ACC; Calc.; Arag.; Vat.	n/a
Nishiyama et al., 2012	Batch reactor with Na_2CO_3	Y	25	0–2:1	0.03-1.0	ACC; MHC; Calc.; Vat.	0–8
Rodriguez-Blanco et al., 2012	Batch reactor with Na_2CO_3	Y	10-25	0; 9:1	1.0	ACC; Calc.; Vat.	10
Zhang et al., 2012	Batch reactor with Dimethyl carbonate	Y (shaken)	30	0–5:1	0.06	ACC; MHC; Calc.; Arag.	not reported
Niedermayr et al., 2013	CO_2 diffusion	Y	6-40	0–5:1	variable	ACC; Vat.; Arag.; Calc.	0–4
Rodriguez-Blanco et al., 2014	Batch reactor with Na_2CO_3	Y	21	7:3	1.0	ACC; MHC; Calc.	3–7
This study	*Mixed flow reactor with $NaHCO_3$*	*Y*	*25*	*0.4:1–6:1*	*0.05–0.20*	*ACC; Vat.; Calc.; Arag.; MHC*	*4–13*
Towe and Malone, 1970	$(NH_4)_2CO_3$ diffusion	N	23–25	5:1	not reported	ACC; MHC; Nesq.; Arag.; **H-Mg calc.**	3–32
Raz et al., 2000	$(NH_4)_2CO_3$ diffusion	N	25	4:1	not reported	ACC; Arag.; **H-Mg calc**.	11–14
Loste et al., 2003	Batch reactor with $NaHCO_3$ (open to air)	N	25	0–10:1	0.54	ACC; MHC; Arag.; Vat.; **H-Mg calc**.	0–22 (top & bottom samples)
Ajikumar et al., 2005	$(NH_4)_2CO_3$ diffusion	N	4; 25	1:9–1:3	not reported	ACC; Calc.	"low Mg"
Lam et al., 2007	$(NH_4)_2CO_3$ diffusion	N	25	2:1–9:1	not reported	ACC; Nesq.; MHC	n/a
Wang et al., 2012	$(NH_4)_2CO_3$ diffusion	N	25	0-6:1	5.2	ACC; **H-Mg calc.**	0–40
Han et al., 2013	Batch reactor with $NaHCO_3$	N	25	0.5:1–10:1	0.20	ACC; **H-Mg calc.**	10–30
This study	*Mixed flow reactor with $NaHCO_3$*	*N*	*25*	*0.4:1–6.5:1*	*0.07–0.20*	*ACC; MHC; **H-Mg calc**.*	*7–28*

* Calc = Calcite; Arag. = Aragonite; Vat. = Vaterite; MHC = Monohydrocalcite; H-Mg = High-Mg; Nesq. = Nesquehonite ($MgCO_3 \bullet 3H_2O$)

The recent advent of the mixed flow reactor (MFR) for ACC synthesis (Blue et al., 2013) offers a new approach to construct a quantitative framework for ACC composition and subsequent crystalline transformation. The MFR offers a number of advantages over previous synthesis methods: 1) allows precise control on supersaturation; 2) produces ACC at steady state conditions, and 3) yields large amounts of ACC with reproducible compositions. Blue et al., (*in press*) demonstrated that the Mg content of ACMC is regulated by the interplay three inorganic factors: the initial solution Mg/Ca ratio, total carbonate concentration, and solution pH. The study also showed that the Mg content of ACC could be tuned to remarkably high levels (70 mole %) by using the MFR method. Recent work by Han et al. (2013) also shows that ACC compositions can reach Mg/Ca ratios as high as 0.60 by adjusting the initial solution Mg/Ca ratio. These quantitative insights into the controls on ACC composition in a wide range of conditions raise the question of the consequences of transformation on the final crystal composition.

Here, we use the MFR approach to synthesize ACC under carefully controlled conditions and then conduct experiments to transform the ACC to crystalline products. This study quantifies 1) the control of solution chemistry on the polymorph that transforms from ACC, 2) the effect of Mg on ACC transformation time, and 3) the chemical basis for a broad range of Mg contents in calcite that forms from ACC. We show a systematic and predictable chemical framework for understanding polymorph selection during ACC transformation, in which the first crystalline phase is controlled by the relative activities of Mg^{2+} and CO_3^{2-} to Ca^{2+} and solution mixing. Results from carefully monitored transformation experiments show that higher solution Mg/Ca ratios slow the time to transformation for all polymorphs. Findings from calcite transformation experiments suggest a chemical basis for a broad range of Mg contents in calcite, including high

Mg calcite, where composition is controlled by the interplay of the solution Mg/Ca ratio, carbonate level, and mixing. We also find that the final calcite produced from ACC is similar to the composition of the initial ACC phase, suggesting that calcite composition reflects local conditions of formation, regardless of the pathway to mineralization.

4.2 METHODOLOGY

4.2.1 ACC Synthesis

ACC was synthesized at 25°C (±1°C) with variable solution conditions using a mixed flow reactor (MFR). The MFR method used in this study was adapted from Blue et al. (2013). A 100 mL solution of variable $MgCl_2$ and $CaCl_2$ concentrations and a 100 mL solution of variable $NaHCO_3$ concentrations were prepared transferred into syringes that were placed on a high precision pump. Small amounts of NaOH were added to the $NaHCO_3$ solution to adjust the initial pH to the desired value. A full summary of all MFR input solution conditions is given in **Table C1** in **Appendix C.** A range of saturation states was prepared for ACC synthesis as a result of varying the carbonate concentrations and pH. The saturation state of a solution ($\Omega_{calcite}$) with respect to pure calcite is expressed by

$$\Omega_{\text{calcite}} = \frac{\left(a_{Ca^{2+}}\right)\left(a_{CO_3^{2-}}\right)}{K_{sp\ \text{calcite}}} \tag{4.1}$$

where a_i is the activity of species i and $K_{sp} = 10^{-8.48}$ at 25°C. Initial solution $\Omega_{calcite}$ values are high because ACC is approximately 100 times more soluble than calcite (Brečević & Nielsen, 1989) and requires very high supersaturations. Recent studies suggest the solubility of pure ACC is considerably lower than the reported value (Gebauer et al., 2008; Hu et al., 2012), but there are no updated values for the solubility of ACC. Ion activities were calculated using The Geochemist's Workbench for each solution condition in order to quantify saturation state.

The high precision pump continuously pumped the $MgCl_2$ and $CaCl_2$ solution and the $NaHCO_3$ solution into the reactor, where the solutions mixed at approximately 800 rpm. As the solutions mixed, the contents of the MFR became supersaturated with respect to ACC, and ACC readily precipitated. A 1 minute hydraulic residence time (τ), defined as

$$\tau = \frac{\text{volume of reactor (mL)}}{\text{flow rate } \left(\frac{\text{mL}}{\text{min}}\right)} \tag{4.2}$$

was used for all experiments. For each experiment, the reactor operated for a minimum of three hydraulic residence times to allow input solutions and ACC products within the reactor to reach steady state conditions (Jensen, 2001). The time elapsed to steady state and the sample collection varied with solution chemistry. The output suspension from the top of the reactor unit was sampled using vacuum filtration, where the ACC was collected on a 0.2μm nylon filter and the effluent solution was retained in a flask. The steady state pH was measured from the effluent solution for each experiment (**Table C1, Appendix C**). The ACC products were rinsed with ethanol and dried in a Class II Biological Safety Cabinet for 20 minutes, then dried for an additional 10 minutes in a vacuum desiccator. Samples were then weighed and placed in a 4°C refrigerator overnight prior to analysis.

4.2.2 ACC Transformation

After the initial ACC suspension was prepared and sampled in the MFR, the output slurry from the MFR was aged in a batch reactor (i.e. transformation of the ACC took place within the MFR output solution). The output suspension from the MFR was collected in a 100 mL glass vessel with a constant stir rate of 250 rpm, with a 1-minute rest interval every hour before switching the stirring direction of the stir bar (e.g. clockwise to counterclockwise). All vessels were maintained at 25°C in a temperature controlled room or incubator throughout the transformation process. Sample collection time varied with solution conditions depending upon

the transformation rate. Samples were collected at intervals ranging from 30 minutes, to 12 hours until complete transformation was reached. The slurry was sampled while it was being stirred to sample solid and solution together. The pH of the solution was measured before every sample time point and the pH electrode was calibrated approximately every 2 hours using a pH 7 and a pH 10.1 buffer solution. Samples were prepared by extracting 6.0 mL of the suspension from the stirred vessel and then the solid was separated using vacuum filtration fitted with a 0.2 μm nylon filter. The filtered solution was analyzed separately, and the precipitates were rinsed from the filter with ethanol into a petri dish and then prepared for their respective modes of analysis. The same transformation protocol was used for unmixed experiments, except they were not stirred after they were collected from the MFR.

The solution chemistry was monitored throughout the transformation process by measuring $[Mg]_{tot}$, $[Ca]_{tot}$, and solution pH at each sample time. The total carbonate concentration of a solution at a given time point was determined by assuming that all Ca and Mg removed from solution was precipitated as Ca,Mg carbonate. Using the stoichiometry of

$$(1 - x)Ca^{2+} + xMg^{2+} + (CO_3^{2-}) + nH_2O = Ca_{1-x}Mg_x(CO_3) \bullet nH_2O \qquad (4.3)$$

the moles of Ca + Mg removed from solution must equal the moles of carbonate removed from solution. The difference between the initial concentration and the amount removed at each time point was then used to calculate the total carbonate concentration. From these solution data the activities of ions at a given sample time were calculated using The Geochemist's Workbench (**Table C1, Appendix C**).

4.2.3 Sample Characterization

SEM. All dried precipitate samples were placed on ultra smooth carbon tape and sputter-coated with approximately 10 nm of gold-palladium. Analyses were performed on an FEI Quanta

600 FEG ESEM. Images of the ACC and crystalline products were acquired using secondary electron (SE) microscopy. Optimal viewing parameters included 10 kV and a 3.5 spot size (instrument specific value). Higher voltages destroyed the samples and could not be used. All samples were examined to characterize their morphology and particle size. An image compilation of typical product morphologies and sizes is shown in **Fig. 4.1**.

XRD. X-ray diffraction was used to identify the mineralogy of each sample. Samples were prepared by pipetting 0.30 mL of an ethanol smear containing the filtered precipitate onto a zero background holder. The samples were allowed to dry completely before analysis. A Rigaku MiniFlex II was used for all analyses. Data was collected from 10°–60° 2θ using a step width of 0.05° with a 5 second count time. Calcite (var. Iceland Spar) and aragonite standards were acquired from Ward's Science and run prior to sample analyses. A representative XRD pattern for each phase identified in this study is shown in **Fig. 4.2**.

Inductively Coupled Plasma – Atomic Emission Spectrometry (ICP-AES). After being rinsed in ethanol and dried, ACC samples from the MFR were dissolved in 0.5 N nitric acid for 20 minutes on the nylon filters. Timed samples collected from the batch reactor were rinsed off the nylon filter with ethanol, dried in air in a Class II Biological Safety Cabinet for 20 minutes, and dissolved in 0.5 N nitric acid a petri dish. Analyses were performed using a Spectro ARCOS SOP. An yttrium internal standard was added to each sample in an internal standard mixing chamber (Glass Expansion, Inc.). Each sample then passed through a cross-flow nebulizer into a modified Scott-style spray chamber. The sample uptake rate was 2 mL/min, with each sample analysis using 5 mL. Calibration standards for Ca and Mg were from Environmental Express, Inc., and the second source check standards were from Spex, Inc.

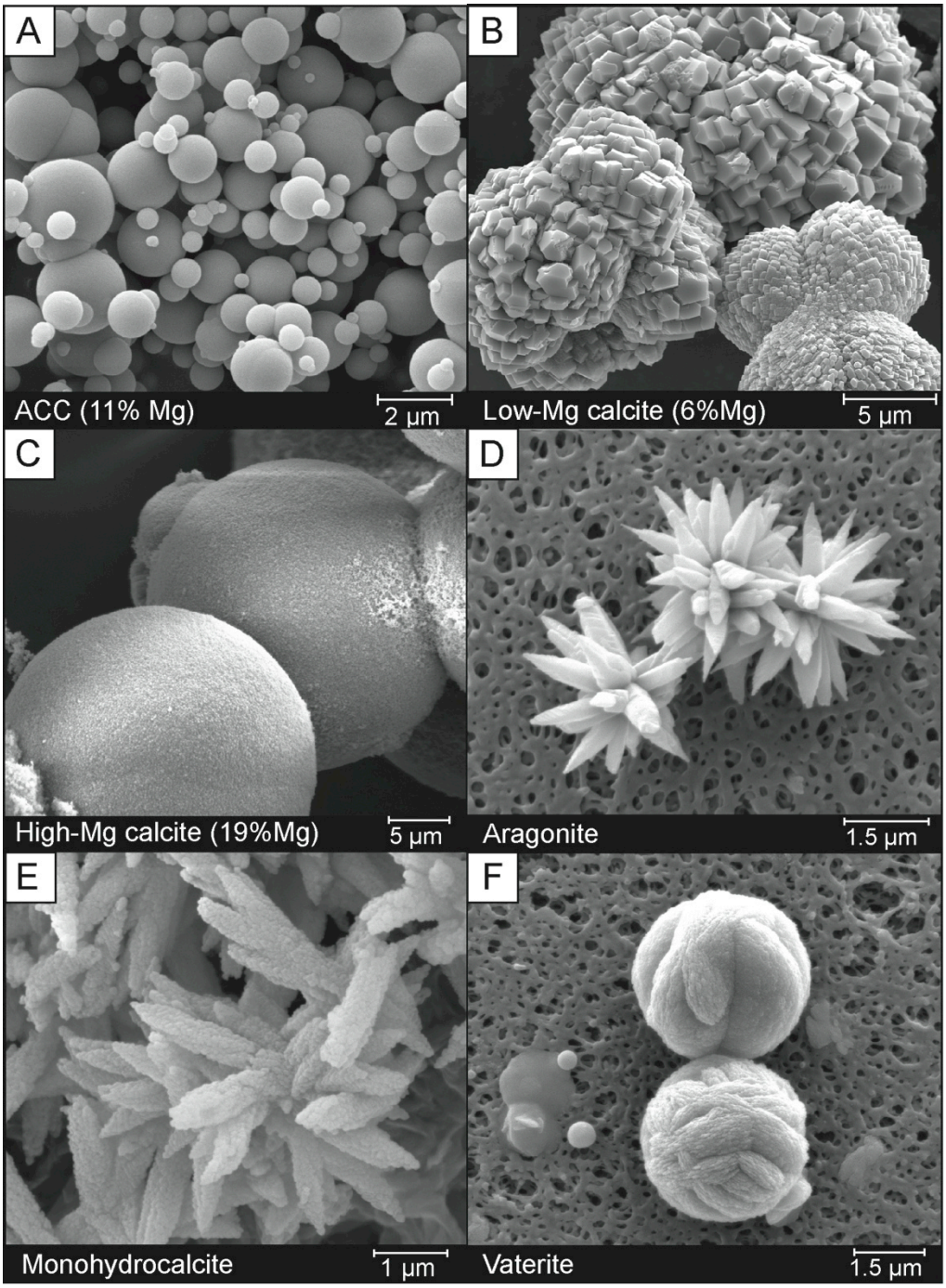

Figure 4.1. SEM images show the morphologies and sizes of the synthesized products. A representative SEM image of each polymorph observed in this study is shown. (A) ACC; (B) Low-Mg calcite with 6% Mg; (C) High-Mg calcite with 20% Mg; (D) Aragonite; (E) Monohydrocalcite; (F) Vaterite.

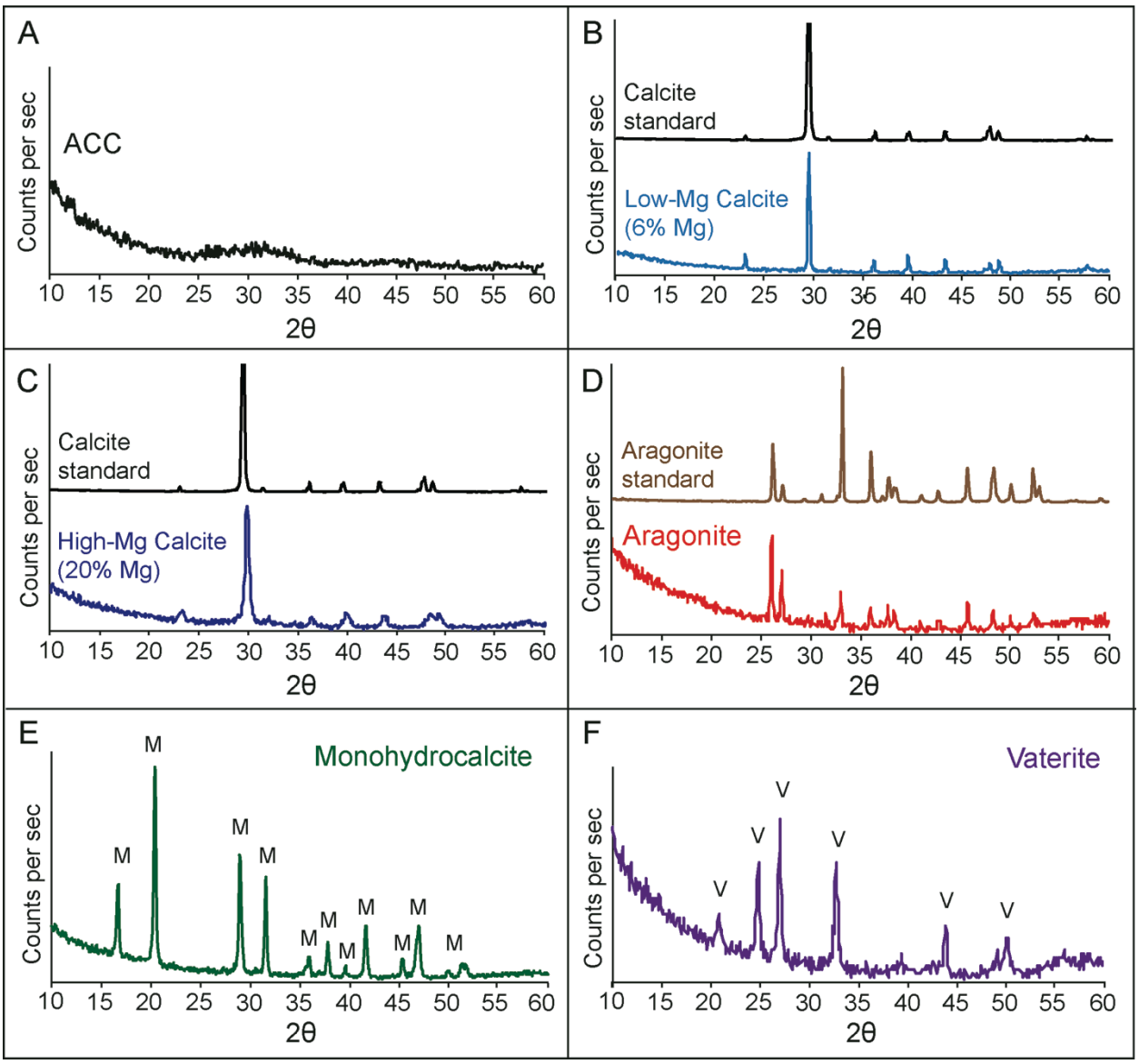

Figure 4.2. XRD confirms the mineralogy of synthesized products. A measured XRD pattern of each polymorph observed in this study is shown. (A) ACC; (B) low-Mg calcite with a pure calcite standard (Iceland Spar*, Ward's Science*) shown for reference; (C) high-Mg calcite with a pure calcite standard (Iceland Spar, *Ward's Science*) shown for reference; (D) aragonite with a standard (*Ward's Science*) shown for reference; (E) monohydrocalcite; (F) vaterite.

4.3 RESULTS

4.3.1 Polymorph Characterization

Characterization of the initial precipitates formed in the MFR show that all initial products are amorphous, with no Bragg peaks and only a broad hump displayed from 25°–35° 2θ on the XRD pattern (**Fig. 4.2A**) and SEM images showing a characteristic spherical morphology with a particle size distribution of approximately 0.1 μm to 2.0 μm (**Fig 4.1A**). The data from the transformation experiments show that all three anhydrous polymorphs of $CaCO_3$ (calcite, aragonite, and vaterite) and one hydrated polymorph (monohydrocalcite: $CaCO_3 \bullet 1H_2O$) form from an ACC precursor at 25°C. The SEM images (**Fig. 4.1B–F**) and The XRD patterns (**Fig. 4.2B–F**) confirm the occurrence of each of these polymorphs.

SEM imaging shows that all polymorphs form as polycrystalline clusters with distinct morphologies: vaterite forms spherical rosettes (**Fig. 4.1F**), monohydrocalcite generally forms twisted, branching structures (**Fig. 4.1E**), aragonite forms clusters of needles (**Fig. 4.1D**), and calcite occurs as notched spherulites with facets that become more curved with increasing amounts of Mg (i.e. **Fig. 4.1B,C**). The XRD patterns for vaterite (**Fig. 4.2F**) and monohydrocalcite (**Fig. 4.2E**) are in good agreement with other synthesis studies (e.g. Sand et al., 2012; Hu et al., 2012; Kimura & Koga, 2011; Rodriguez-Blanco et al., 2014), and all aragonite patterns (**Fig. 4.2D**) match the standard (*Ward's science*). The XRD patterns for low-Mg calcite (**Fig. 4.2B**) line up well with the pure calcite standard (v. Iceland Spar, *Ward's Science*), but the peaks become broader and shift with increasing Mg content (**Fig. 4.2C**). Peak broadenings may indicate the presence of small Mg-enhanced crystal domains (Lenders et al., 2011). **Fig. 4.2C** shows there are d-spacing reductions for all the reflecting faces compared to the pure calcite standard. For instance, 2θ of the (104) reflection increases from 29.583 for pure

calcite to 29.727 for calcite with 20 mole % Mg, corresponding to a d-spacing reduction from 3.017 Å to 3.003 Å. Both peak broadening and d-spacing reduction are the consequence of Mg incorporation into the crystallites (Bischoff et al., 1983; Mackenzie et al., 1983), indicating that Mg^{2+} ions are located within the crystal lattice rather than adsorbed on surfaces as free ions (Vegard, 1921; Denton & Ashcroft, 1991).

4.3.2 Control of Solution Chemistry on Polymorph Selection

In order to constrain polymorph formation after ACC transforms, the solution chemistry (at the time of ACC precipitation) must be well characterized and controlled. Utilizing a MFR system provided the necessary control for a wide range of solution compositions that were precisely maintained, during ACC precipitation. Data from the mixed transformation experiments show that the initial formation of a particular polymorph after ACC transformation is controlled by the activity ratio of Mg^{2+}/Ca^{2+} and CO_3^{2-}/Ca^{2+} in the MFR output solution (**Fig. 4.3**). The data shown in **Fig. 4.3** illustrate that the *initial* polymorph that forms from ACC transformation can be predicted from the MFR output solution chemistry. The relative activities of Mg^{2+} and CO_3^{2-} compared to Ca^{2+} outline "stability fields" for different polymorphs. Monohydrocalcite forms when the Mg^{2+} activity is high and/or the CO_3^{2-} activity is very high. Calcite forms at more moderate Mg^{2+} and CO_3^{2-} activities (**Fig. 4.3**). Vaterite only forms at low Mg^{2+}/Ca^{2+} ratios (<1.0), which is in agreement with previous reports (e.g. Loste et al., 2003; Nishiyama et al., 2012; Niedermayr et al., 2013).

Notably, just one experiment produced only aragonite after ACC—the other experiments produced a mixture of both aragonite and calcite immediately after ACC transformation—showing that aragonite formation from an ACC precursor is more difficult to control. Given more time in solution, other polymorphs precipitated after the formation of the initial crystals

(**Fig. C1**, **Appendix C**), and aragonite eventually appeared in almost all experiments over time (**Table C1**, **Appendix C**). Other minerals that formed included nesquehonite ($MgCO_3 \bullet 3H_2O$) and possibly hydromagnesite ($Mg_5(CO_3)_4(OH)_2 \bullet 4H_2O$) at high Mg levels (**Fig. C2**, **Appendix C**).

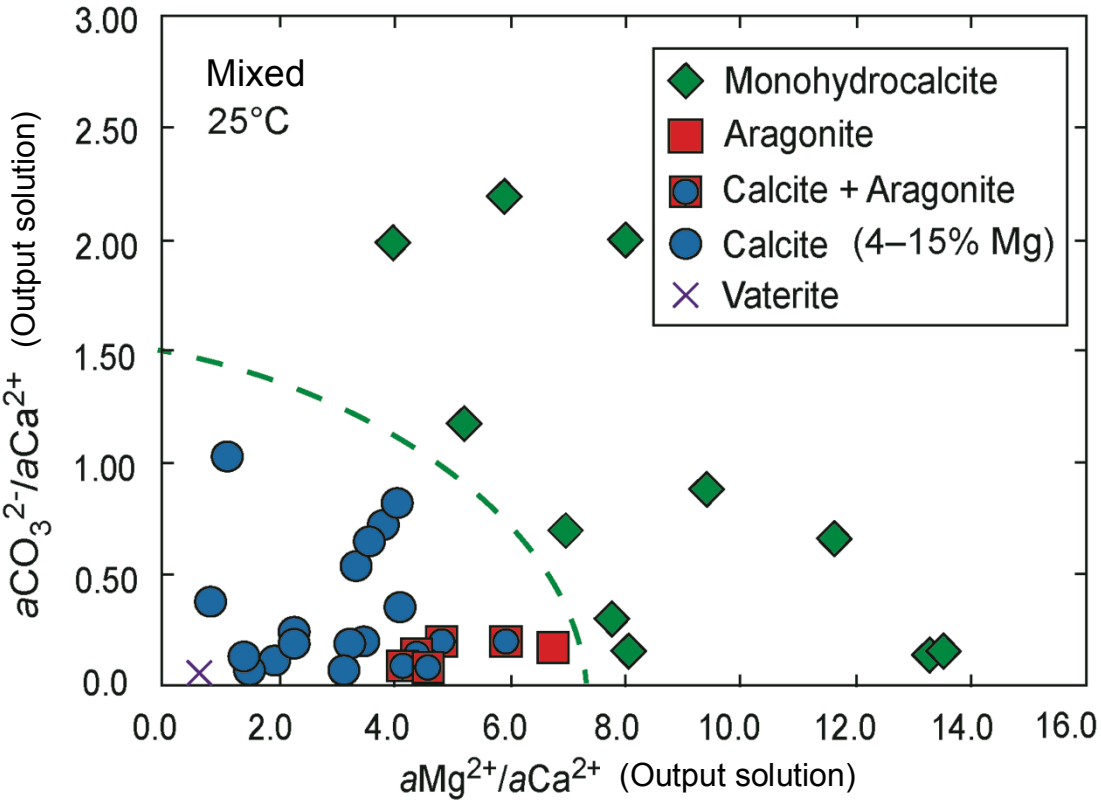

Figure 4.3. Plotting the solution activity ratios of Mg^{2+}/Ca^{2+} and CO_3^{2-}/Ca^{2+} during steady state precipitation of ACC gives a stability diagram for initial polymorph formation from ACC transformation. The MFR output solution chemistry thus provides a predictive map of the first polymorph to form from ACC under mixed conditions. The time to transformation for these polymorphs varies with solution chemistry. Over time, other phases precipitate from solution (Table C1, Appendix C), including aragonite (for all conditions) and nesquehonite and possibly hydromagnesite (at high Mg levels).

4.3.3 Solution Chemistry and an Indicator of Transformation Process

The data gathered by monitoring the changes in solution chemistry over time revealed some interesting trends in how polymorphs affect the solution chemistry evolution. Specifically, monohydrocalcite affects the solution chemistry differently from the anhydrous polymorphs

(calcite, aragonite, and vaterite). The main differences in the formation of these polymorphs can be seen in the changes in solution pH and Mg/Ca ratio over time (**Fig. 4.4**). The trends in the data for calcite, aragonite, and vaterite are similar (**Table C1**, **Appendix C**), and since there are more data available from calcite transformation experiments, the calcite data will be used as a comparison to monohydrocalcite.

When ACC transforms to calcite, the pH drops significantly from its initial, output solution value (**Fig. 4.4A**). After initial calcite formation, aragonite precipitates later at a similar solution pH. Given longer periods of time, the pH rises slightly, which may be due to the removal of CO_3^{2-} by the growing crystal or the precipitation of a new carbonate phase. When ACC transforms to monohydrocalcite, however, the pH remains relatively unchanged (**Fig. 4.4B**). Monohydrocalcite can exist in solution for very long periods of time at a consistent pH, depending upon the solution chemistry. If monohydrocalcite remains stable in solution for a long time, the pH remains relatively unchanged, but if an anhydrous polymorph forms after monohydrocalcite, the pH drops significantly.

There are several possible explanations for these pH trends. During ACC transformation to calcite, the release and the dissociation of water could result in the adsorption of hydroxyl ions on the surface of calcite, or possibly the integration of hydroxyl ions in the calcite lattice. It has been demonstrated that hydroxyl ions can be incorporated as interstitial defects in the calcite lattice, where a carbonate ion is replaced by one hydroxyl ion and one bicarbonate ion (Kuriyavar et al., 2000). Additionally, it is possible that when ACC forms it incorporates a small amount of bicarbonate in the structure (Michel et al., 2008). During the transformation to calcite, these bicarbonate ions would be released to solution, and the growing calcite crystal would consume the carbonate ions that are produced from the dissociation of bicarbonate, causing a

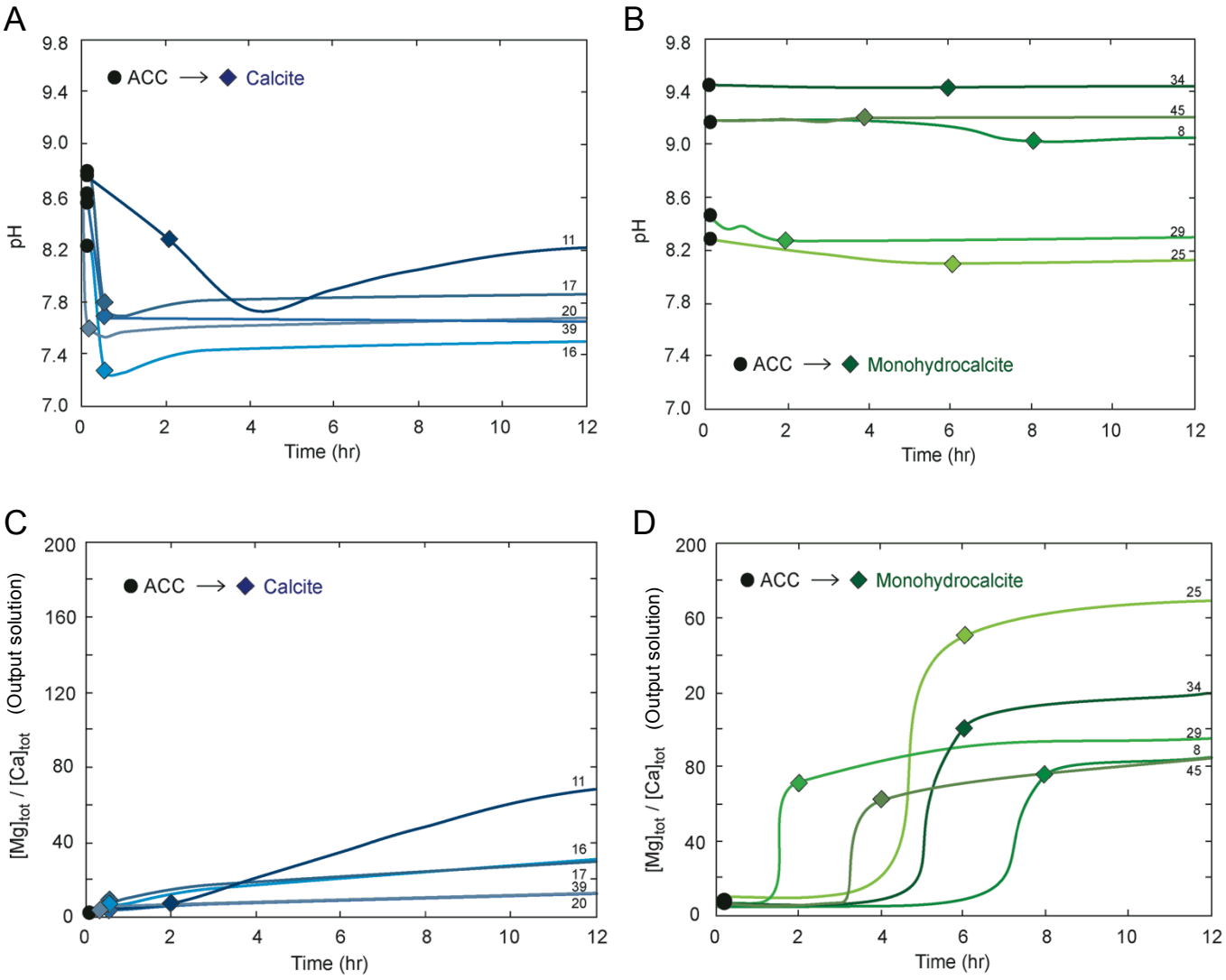

Figure 4.4. The evolution of solution chemistry differs between calcite and monohydrocalcite transformation. Five experimental conditions for calcite and monohydrocalcite are shown, with the numbers on the right side of the graph corresponding to the experiment number in Table C1 (In Appendix C). Black dots show the formation conditions of ACC, and the diamonds represent the time point where the ACC transformed to either calcite (blue) or monohydrocalcite (green). (A) The pH drops significantly when ACC transforms to calcite. (B) There is very little change in pH when ACC transforms to monohydrocalcite, and the pH remains stable after monohydrocalcite formation. (C) The solution Mg/Ca ratio increases slightly during transformation to calcite, and then slowly rises after initial calcite formation, with Mg/Ca ratios remaining fairly low. (D) Upon monohydrocalcite formation, the solution Mg/Ca ratio increases abruptly and continues to rise slowly after initial formation, resulting in Mg/Ca ratios over 100.

significant drop in pH. Other possible explanations for this occurrence may exist, and the actual mechanism for the pH drop cannot be deduced from the data collected in this study.

Another difference in the solution chemistry between calcite and monohydrocalcite is the evolution of the solution Mg/Ca ratio (**Fig. 4.4C,D**). When calcite transforms from ACC, there is a slow, consistent rise in the solution Mg/Ca ratio over time (**Fig. 4.4C**). The largest jump occurs during the initial formation of calcite, and as the calcite grows and other polymorphs precipitate, the Mg/Ca ratio slowly rises as Ca^{2+} is preferentially consumed. The total solution Mg/Ca ratio remains fairly low, and rarely rises above 20 when calcite is the only mineral in solution (**Fig. 4.4C**)—this ratio can increase significantly, however, if aragonite forms because Mg is not incorporated into the aragonite lattice. Conversely, there is a huge jump in the Mg/Ca ratio upon initial monohydrocalcite formation, with ratios commonly reaching above 50 (**Fig. 4.4D**). After initial monohydrocalcite formation, the solution Mg/Ca ratio continues to increase steadily as the crystals grow and other polymorphs form, and solution Mg/Ca ratios commonly reach above 100. Because monohydrocalcite formation is favored in solutions with higher Mg/Ca ratios (**Fig. 4.3**), it is expected that the resulting Mg/Ca ratios after transformation would be higher than calcite.

There are a couple of explanations for why the Mg/Ca ratio in solutions containing monohydrocalcite is so much higher than in solutions containing calcite. Firstly, monohydrocalcite can incorporate significant amounts of Mg^{2+}, but at high Mg^{2+} levels it is unstable and quickly releases the Mg^{2+} in favor of a more stable, low Mg crystal (Nishiyama et al., 2012; Rodriquez-Blanco et al., 2014). In addition, monohydrocalcite forms at higher $a CO_3^{2-}/a Ca^{2+}$ than calcite at a similar $a Mg^{2+}/a Ca^{2+}$ ratio (**Fig. 4.3**) due to its higher solubility (Hull &

Turnbull, 1973; Kralj & Brečević, 1995). The higher supersaturations from increased CO_3^{2-} activities consume more Ca^{2+} during monohydrocalcite crystal growth.

Because the Mg/Ca ratios in solution evolve as the transformation proceeds, calculating the partition coefficient (λ) can determine the partitioning of Mg into a solid by determining the initial solution chemistry and the solution chemistry at a given time point. The Doerner-Hoskins model is expressed as:

$$\lambda = \frac{\ln\left(\frac{m_{\mathrm{Mg}}}{m^{\circ}_{\mathrm{Mg}}}\right)}{\ln\left(\frac{m_{\mathrm{Ca}}}{m^{\circ}_{\mathrm{Ca}}}\right)} \tag{4.4}$$

where m is the total concentration (in moles) of an element in solution at a given time point and m° is the total concentration (in moles) of an element in the initial solution. For λ greater than unity the solid is enriched in the trace element, and for λ less than unity the solid is depleted in the trace element. The Doerner-Hoskins law assumes there is no mass exchange between the interior of the precipitating solid and the solution, therefore, the content of the tracer in the solid is heterogeneous (Doerner & Hoskins, 1925). The Doerner-Hoskins model was used to quantify partition coefficients because the amount of time elapsed during transformation experiments, and the corresponding changes in solution chemistry, were significant. A summary of λ values for all experiments and time points is given in **Table C1 (Appendix C)**.

The changes in Mg partition coefficient values (λ) over time agree well with the changes in solution chemistry and corresponding crystal growth (**Fig. C3**, **Appendix C**). Values start high initially, and are generally fairly close to 1.0 during ACC precipitation, unless the initial solution Mg/Ca ratios are very high (**Table C1, Appendix C**). Over time, λ values drop significantly as Mg^{2+} is excluded from, and Ca^{2+} is preferentially included in, the growing crystal (for all polymorphs) (**Fig. C3**, **Appendix C**). While ACC is stable in solution λ values stay fairly

constant, but a sudden drop occurs upon crystallization (**Fig. C3**, **Appendix C**). Over time the values continue to decrease, as a result of Ostwald ripening, until the crystals reach equilibrium with the solution. For this study, the solutions were not sampled over time scales long enough to reach the equilibrium condition. The final phases in solution were most commonly a mixture of calcite and aragonite, and the final partition coefficient values averaged 0.284±0.058, which are significantly higher than those reported by Angel (2013) (0.094±0.0011). The discrepancy between the two reported values are likely due to the difference in synthesis methods, solution chemistries, and total transformation time used for the synthesis experiments.

4.3.4 ACC Transformation Time and Polymorph Formation

Analysis of the solution chemistry data (section 4.3.2 and 4.3.3) and corresponding XRD data over sampled time intervals revealed trends in ACC transformation times. **Figure 4.4** illustrates that there is a much greater induction time for monohydrocalcite than calcite, where calcite takes no more than 2 hours (and commonly less than 1 hour) to form but monohydrocalcite takes at least 2 hours (and commonly more than 4 hours) to form. The solution conditions in which monohydrocalcite forms corresponds to high levels of Mg in the amorphous precursor (>15 mole % Mg) (Blue et al., *in press*), whereas calcite forms from ACC precursors with significantly less Mg. Therefore, it is expected to take longer for ACC to transform to monohydrocalcite than calcite because of the stabilizing effect Mg^{2+} has on ACC (Loste et al., 2003; Han et al., 2013).

Furthermore, the transformation to vaterite occurred very quickly, taking less than 10 minutes. The solution chemistry data show this is largely due to the Mg/Ca ratio in solution before transformation. The polymorph "stability fields" in **Fig. 4.3** shows that vaterite only forms at very low Mg/Ca ratios (<1), calcite (and aragonite) forms when solution Mg/Ca ratios are low

to moderate (0–5), and monohydrocalcite forms in solutions with moderate to high Mg/Ca ratios (>5). When the solution chemistry data is combined with the XRD data that shows time to transformation (e.g. **Fig. C1**, **Appendix** C), the results show that the solution Mg/Ca ratio is a proxy for ACC transformation time and polymorph selection (**Fig 4.5**). Increasing the solution Mg/Ca ratio results in longer transformation times and a progression from vaterite, to calcite, to aragonite, to monohydrocalcite formation. There is more scatter in the monohydrocalcite transformation time data because the inclusion of Mg^{2+} in monohydrocalcite is complex and highly variable (Nishiyama et al., 2012; Rodriquez-Blanco et al., 2014), and the activity of CO_3^{2-} is also a controlling factor for transformation due to the tendency for monohydrocalcite to form in conjunction with various Mg-carbonates (Kimura & Koga, 2011; Nishiyama et al., 2012).

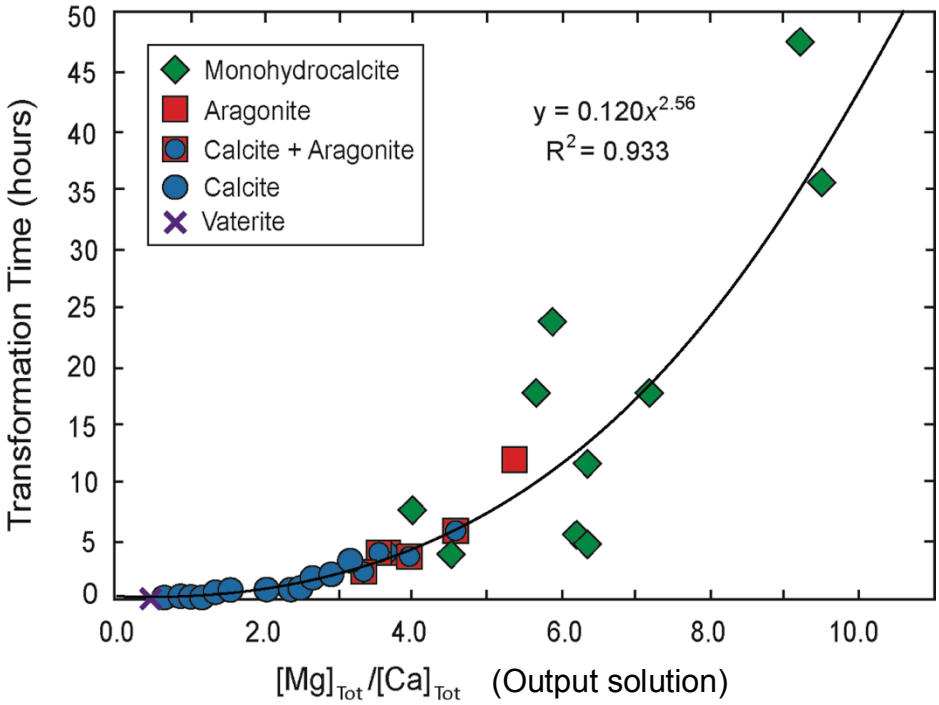

Figure 4.5. Higher solution Mg/Ca ratios result in longer transformation times and a transition to different polymorphs for mixed conditions. Vaterite forms only at very low Mg/Ca ratios (<1) and transforms quickly (<10 minutes). Calcite forms in low to moderate Mg/Ca ratios (0–4) and takes between 10 minutes to 3 hours to transform. Aragonite occurs when Mg/Ca ratios are moderately high (~5) and transformation takes up to 10 hours. Monohydrocalcite only forms at high solution Mg/Ca ratios (>4) and takes at least 4 hours, but up to 45 hours, to transform.

4.3.5 Influence of Mixing vs. Non-mixing

ACC that transformed in solution that was not mixed resulted in a shift of the "stability fields" for initial polymorphs. **Figure 4.6** shows the *initial* polymorph that formed after ACC transformation in unmixed conditions as a function of the output solution activity ratio of Mg^{2+}/Ca^{2+} and CO_3^{2-}/Ca^{2+}. The results are significantly different from those shown in **Fig. 4.3**. The most notable difference in **Fig. 4.6** is the extension of the calcite stability field at higher aMg^{2+}/aCa^{2+} ratios. Furthermore, monohydrocalcite is only forms in unmixed conditions when the CO_3^{2-}/Ca^{2+} activity ratio is high. Interestingly, high-Mg calcite formed in the solutions with higher Mg^{2+}/Ca^{2+} activity ratios in unmixed conditions, but was not observed to form in any of the mixed solution conditions.

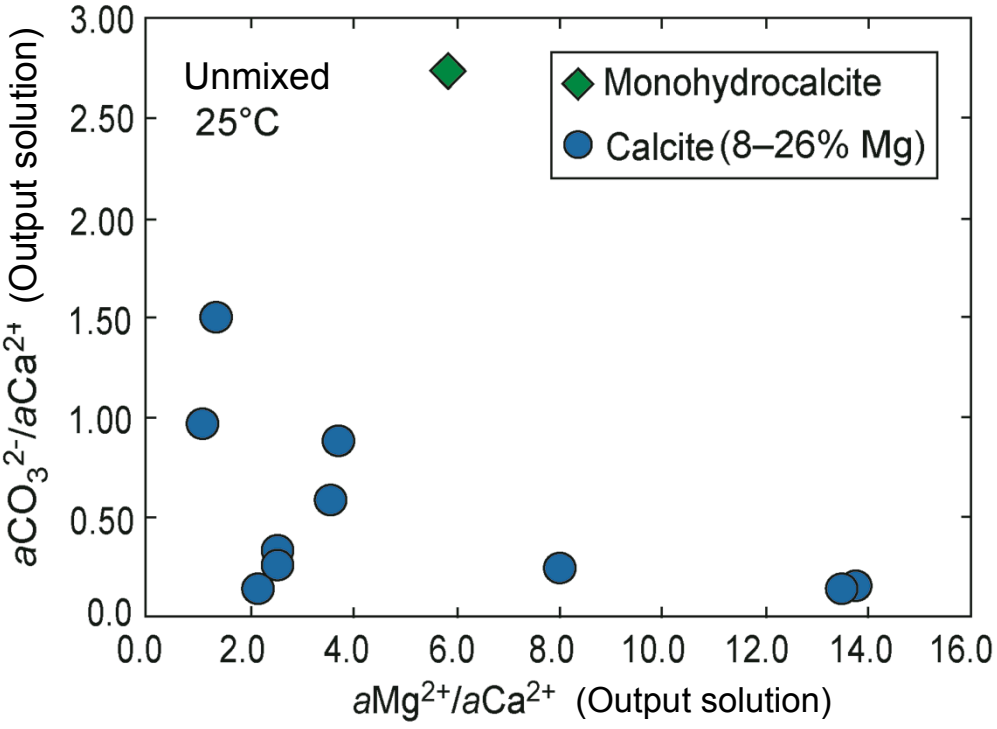

Figure 4.6. The stability diagram for initial polymorph formation after ACC transformation is different for unmixed conditions**.** The calcite stability field extends into much higher $Mg^{2+/}Ca^{2+}$ activity ratios when the output solution remains unmixed. The calcite formed in the higher $Mg^{2+/}Ca^{2+}$ activity ratio solutions is high Mg calcite, containing up to 26 mole % Mg in this study.

In the case of calcite, it is known that Mg^{2+} inhibits the step-growth of calcite (Davis et al., 2000; Stephenson et al., 2011) and the strong hydration shell of Mg^{2+} makes it more difficult to dehydrate and form Mg-rich $CaCO_3$ (Di Tommaso & Leeuw, 2010; Hamm et al., 2010). Therefore, it is not surprising that higher solution Mg/Ca ratios during ACC precipitation would result in longer transformation times, as reported previously (Loste et al., 2003; Han et al., 2013). In this study, the solution Mg/Ca ratio correlates well to transformation time to calcite in both mixed and unmixed conditions (**Fig. 4.7).** In mixed conditions (**Fig. 4.7A**), the transformation time took up to 3 hours when output solution Mg/Ca ratios reached above 3:1, and higher solution Mg/Ca ratios could not be reached because it crossed into other polymorph "stability fields." For unmixed conditions (**Fig. 4.7B**), the transformation time reached up to 30 hours when the output solution Mg/Ca ratio approached 10:1. Even at lower Mg/Ca ratios (~ 2:1) unmixed solutions resulted in longer transformation times than those that were mixed.

In addition to longer transformation times, higher solution Mg/Ca ratios also produced calcite with greater Mg contents: up to 15 mole % $MgCO_3$ in mixed conditions and 26 mole % $MgCO_3$ in unmixed conditions (**Fig. 4.7**). Previous studies show that calcite becomes more soluble with increasing amounts of Mg (Berner, 1975; Bischoff et al., 1987; Davis et al., 2000), and above approximately 8.5 mole % $MgCO_3$ it is more soluble than aragonite (Berner, 1975). When Mg^{2+} is incorporated in calcite, there is an effective decrease in supersaturation due to the higher solubility of the mineral. Lower supersaturations also result in slower growth rates; therefore, the longer transformation times may also be the result of the higher solubility of the Mg-calcites.

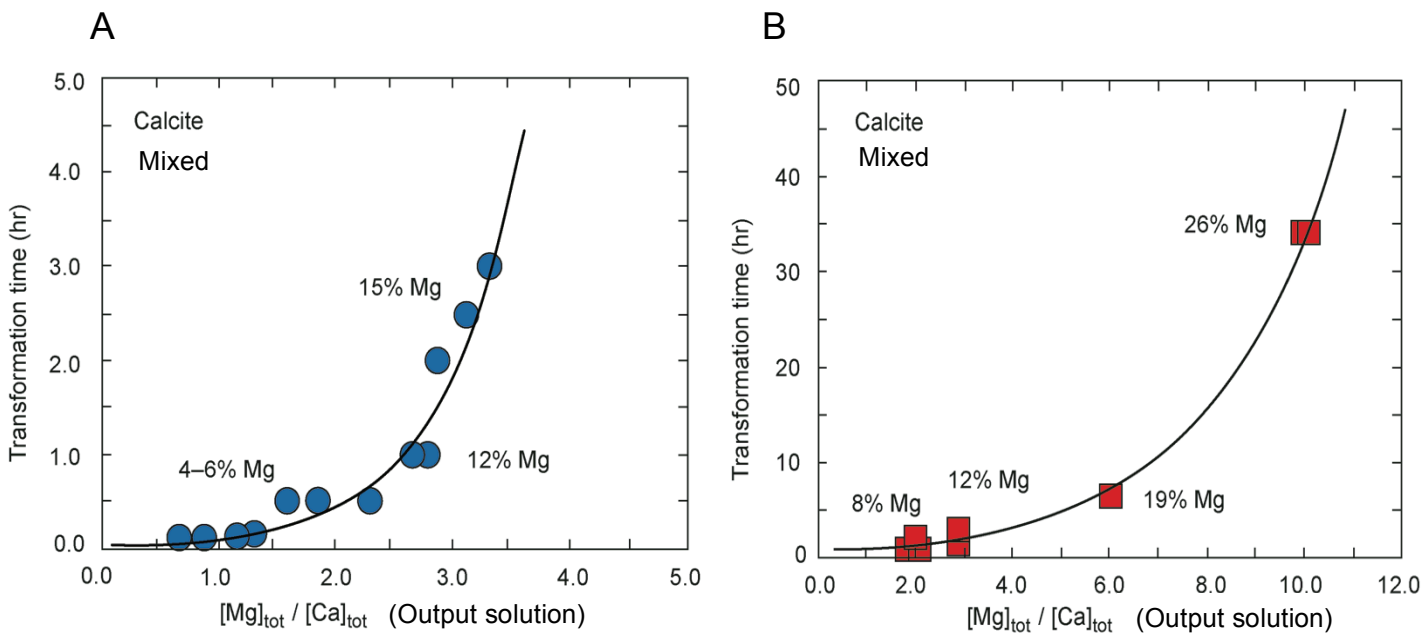

Figure 4.7. The transformation time for calcite increases with the output solution Mg/Ca ratio. Higher solution Mg/Ca ratios and longer transformation times also result in greater Mg content in calcite. (A) For mixed conditions, the transformation time increases from 10 minutes to 3 hours by increasing the output Mg/Ca ratio from ~0.75 to 3.0, and the Mg content of calcite increases from 4 to 15 mole percent. (B) For unmixed conditions, the transformation time increases from 1 hour to 34 hours by increasing the output Mg/Ca ratio from ~2 to 10, and the Mg content of calcite increase from 8 mole % to 26 mole %.

4.3.6 Consequence of ACC Transformation for Calcite Composition

Recent studies have shown that the solution Mg/Ca ratio exerts primary control on the Mg content of ACC and subsequent calcite (Han et al., 2013; Blue et al., 2013). The relationship between solution Mg/Ca ratio (from the output solution in this study) and crystal composition was also observed in our experimental data (**Fig. 4.8**). Results show that for both mixed and unmixed conditions, the output solution Mg/Ca ratio (i.e., during ACC precipitation) controls the amount of $MgCO_3$ incorporated into subsequent calcite (**Fig. 4.8**). There is an offset in the data between mixed and unmixed conditions, reiterating the differences discussed in Section 4.3.5. The mole % of $MgCO_3$ in ACC and subsequent calcite is linearly dependent upon the output

solution Mg/Ca ratio, suggesting that the partitioning of Mg in ACC and calcite is governed by equilibrium thermodynamics for the conditions of this study. Recent studies, however, have suggested that the Mg content of ACC and calcite is controlled by a combination of thermodynamic and kinetic factors (Wang et al., 2012; Hu et al., 2012; Blue et al., *in press*).

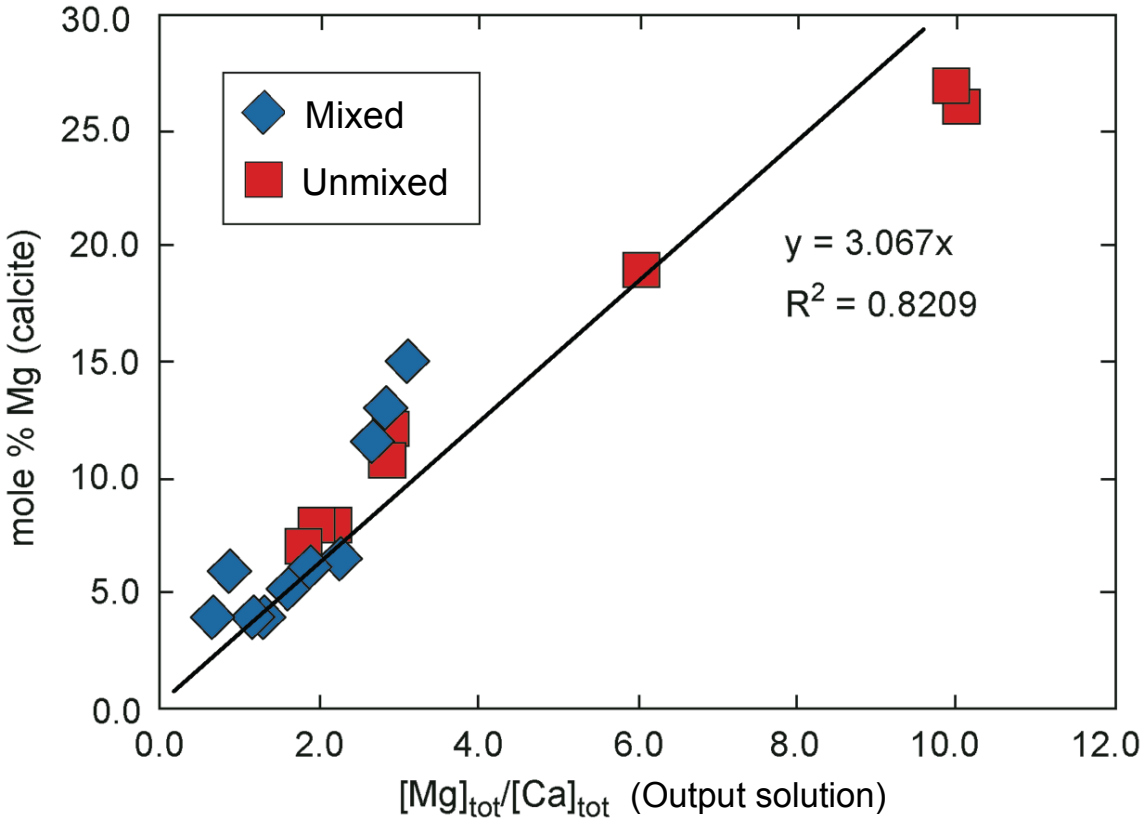

Figure 4.8. The output solution Mg/Ca ratio during ACC precipitation controls the Mg content of transformed calcite. There is a slight offset in the data for mixed and unmixed conditions.

Additionally, the Mg content in ACC is similar to the subsequently formed calcite (**Fig. 4.9**). Typically, there was only a difference of approximately 1–3 mole % $MgCO_3$ between ACC and transformed calcite (**Table 4.2**), suggesting that Mg signatures are essentially "set" at the time of ACC precipitation. Strikingly, the relationship between the Mg content of ACC and subsequent calcite occurs in both mixed and unmixed conditions for the conditions of this study. These results suggest that the composition of calcite reflects the local conditions of formation,

whether it grows via a "classical" pathway or forms from an amorphous intermediate. It should be noted that the partition coefficients (λ, Equation 4.4) for individual experiments decrease between the time of initial ACC formation and calcite growth (**Fig. C3**). Due to the evolution of the solution chemistry during crystal growth, the distribution of Mg^{2+} in the crystals is likely heterogeneous; the initial calcite crystals formed with $MgCO_3$ concentrations close to that of the ACC, however, over time Mg^{2+} is excluded from the growing crystal.

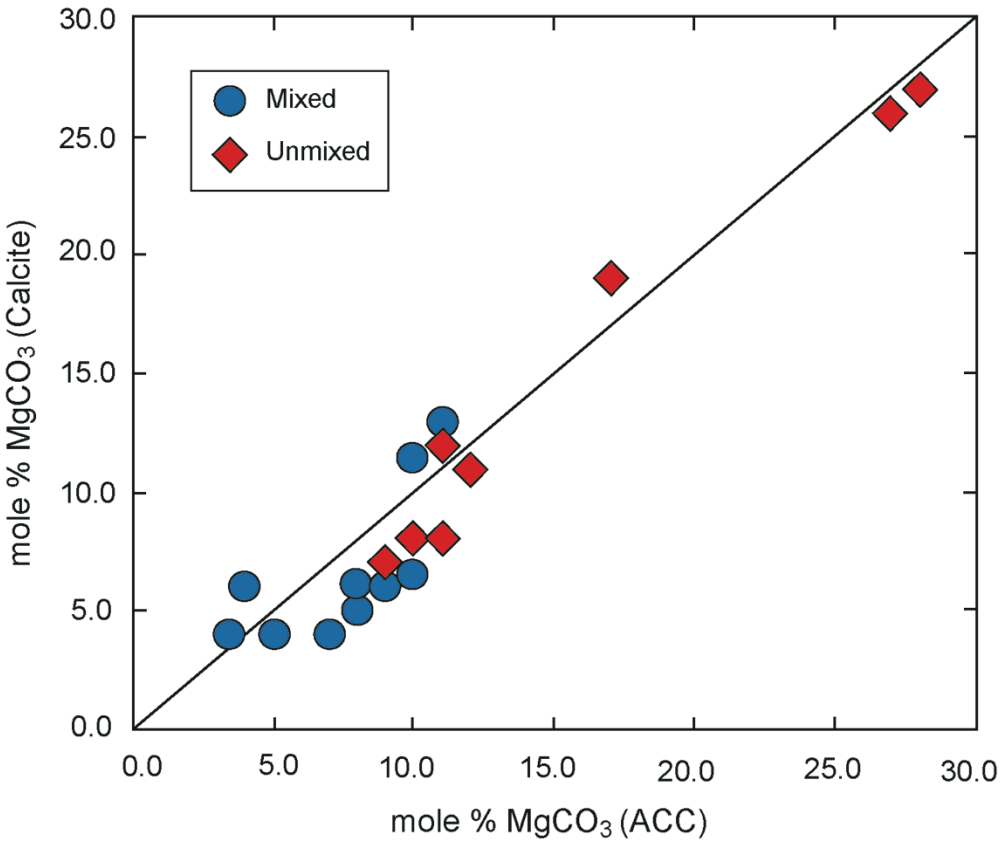

Figure 4.9. The Mg content of ACC and subsequent calcite are similar. The black line represents no change in Mg content between ACC and calcite, and the data from both mixed and unmixed experiments fall close to the line. The maximum value for mixed experiments is limited by the transformation to monohydrocalcite (see Fig. 4.3).

Table 4.2
Summary of mole % $MgCO_3$ measured in ACC and the subsequent calcite crystals

Exp. #*	Mixing (Y/N)	Initial [Mg]/[Ca]	Initial $[CO_3^{2-}]$ (M)	Steady state pH	mole % $MgCO_3$#	
					ACC	Calcite
16	Y	1.6	0.120	8.22	10	6.5
17	Y	1.4	0.072	8.76	9	6
19	Y	1.1	0.066	8.53	7	4
20	Y	0.77	0.070	8.62	5	4
22	Y	0.38	0.068	8.95	3.5	4
23	Y	0.38	0.090	9.18	4	6
31	Y	1.4	0.140	8.71	11	13
32	Y	1.4	0.140	8.75	11.5	13
37	Y	1.4	0.075	8.69	8	6
39	Y	1.4	0.075	8.53	8	5
40	Y	1.4	0.140	8.68	10	11.5
38	Y	1.4	0.140	8.81	11	15
26	N	5.0	0.200	8.28	28	27
27	N	5.0	0.200	8.31	27	26
30	N	2.0	0.200	8.37	17	19
46	N	1.4	0.075	8.60	9	7
47	N	1.4	0.140	8.54	11	8
48	N	1.4	0.750	8.79	10	8
49	N	1.4	0.140	8.85	12	11
50	N	1.4	0.75	9.06	11	12

*Exp. numbers correspond to those in Table C1 (Appendix C)
% $MgCO_3$ = 100 x ($[MgCO_3]$ / $[CaCO_3]$ + $[MgCO_3]$)

4.4 DISCUSSION

A surprising result of the transformation experiments was the repeated appearance of monohydrocalcite across a wide range of conditions (**Table C1**, **Appendix C**). Monohydrocalcite is carbonate mineral that is less common in nature because it is metastable at Earth surface temperatures and pressures relative to calcite and aragonite. The oldest known example of monohydrocalcite (800 ka) is in the deep sediments of Lake Hovsgol, Mongolia (Solotchina, 2009), so it does not persist for long on the Earth's surface. The most common depositional setting of the mineral is in sediments of saline alkaline lakes around the world (Stoffers & Fischbeck, 1974; Taylor, 1975; Swainson, 2008; Last et al., 2010; Nishiyama et al.,

2013) and saline spring waters (Ito, 1993), but it has also been documented in speleothems of limestone (Fischbeck & Müller, 1971) and basaltic (Léveillé et al., 2000) caves, as well as in polar systems (Bird et al., 1991; Dahl & Buchardt, 2006). In nature, monohydrocalcite is typically associated with other carbonates: such as calcite, aragonite, dolomite ($Ca,Mg(CO_3)_2$), hydromagnesite ($Mg_3(CO_3)_4(OH)_2 \bullet 4H_2O$), and nesquehonite ($MgCO_3 \bullet 3H_2O$) (Fischbeck & Müller, 1971; Nishiyama et al., 2013). As a biomineral, monohydrocalcite is rare but diverse—it has been reported as a constituent of the calcareous corpuscles of tapeworms (Señorale-Pose et al., 2008), in a guinea pig bladder stone (Catherine et al., 1977), in bacterial cultures (Rivadeneyra et al., 2004), as a biomineralization product in some mollusks (Lowenstam, 1981), in vertebrate otoliths (Carlström, 1963), and as a decay product of the Saguaro cactus (Garvie, 2003).

Recent studies on monohydrocalcite show that the formation of the mineral requires the initial solution CO_3^{2-}/Ca^{2+} ratio to be >1 with a moderate amount of Mg in solution (>0.01 M) (Kimura & Koga, 2011; Nishiyama et al., 2013). Monohydrocalcite can also form in conjunction with hydrous Mg carbonates, which helps stabilize the mineral on short time scales (Kimura & Koga, 2011; Nishiyama et al., 2013). Recently, it has been demonstrated that monohydrocalcite can incorporate significant amounts of Mg (up to 26 mole percent), and that the Mg content is proportional to the saturation index of the precipitating solution (Rodriguez-Blanco et al., 2014). Studies of monohydrocalcite synthesis show that it forms from an amorphous precursor and transforms to aragonite over time (Fukushi et al., 2011; Zhang et al., 2012;), which was also corroborated in this study (**Fig. C1**, **Appendix C**). Therefore, monohydrocalcite can also be an intermediate phase.

Data from this study, combined with previous reports, suggest monohydrocalcite is an important intermediate for a wide range of conditions. Generally speaking, monohydrocalcite can be considered as a "forgotten" polymorph because it can persist on the order of only hours before it dissolves at the expense of aragonite. The solution chemistry data from this study also suggests that the presence of monohydrocalcite as an intermediate phase also has consequences for the pH evolution of calcification environments, which could be relatively unnoticed over large spans of time.

An important result of this study is a systematic and predictable chemical framework for understanding polymorph selection during ACC transformation. The results presented in **Figs. 4.3** and **4.6** show that the baseline solution conditions from the MFR output during ACC precipitation fundamentally predicts the first polymorph that will form in solution upon transformation. It is also notable that all polymorph assemblages changed over time in this study: confirming that careful monitoring and timely sampling of the solutions over time is crucial for obtaining accurate transformation data. The findings of this study, therefore, help make sense of the polymorph variability reported in other studies (**Table 4.1**) by providing a framework based upon solution chemistry (i.e. Mg^{2+} and CO_3^{2-} activity) and physical mixing.

Using the framework presented in this study, there are some similarities and apparent trends in the diverse experimental results reported in the literature. Vaterite forms from ACC in a variety of saturation conditions and in both mixed and unmixed environments, but only when there is little to no Mg in solution and it generally forms quickly (Sand et a., 2011; Rodriguez-Blanco et al., 2012). Monohydrocalcite formation, on the other hand, is favored in solutions with high alkalinity and high levels of Mg and can also form in mixed or unmixed conditions (Loste et al., 2003; Nishiyama et al., 2012). Generally, aragonite forms from ACC via another

intermediate phase like monohydrocalcite (Munemoto & Fukushi, 2008; Zhang et al., 2012) or it is a secondary mineralogy (i.e. in addition to calcite), and the formation of aragonite is triggered when there is moderate levels of Mg in solution (Niedermayr et al., 2013).

The information presented in **Table 4.1** also outlines the importance of the carefully choosing the method of ACC synthesis and transformation, and the necessity of controlling and characterizing the solution chemistry. The variability of results for similar initial solution conditions show that the final products of ACC transformation are method-dependent. The reason for this variability is because the solution conditions evolve differently over time for different transformation methods (e.g., batch mixing vs. $(NH_4)_2CO_3$ diffusion), and without proper control and characterization, the transformation results cannot be fully understood within a predictive framework. The MFR method used for ACC synthesis in this study is ideal because it allows precise control over supersaturation and produces ACC at steady-state conditions (Blue et al., 2013), providing a baseline for solution conditions before ACC transformation.

It has been documented that higher initial solution Mg/Ca ratios produce calcite with greater Mg content (Berner, 1975; Mucci & Morse, 1983; Bischoff et al., 1987). In addition, ACC synthesis studies have shown that high levels of Mg (up to 80 mole percent) can be reached by increasing the initial solution Mg/Ca ratio (Loste et al., 2003; Radha et al., 2012; Han et al., 2013). These reports generated interest that the very high Mg ACC formed in those studies could be the pathway to forming very high-Mg calcite and dolomite (Wang et al., 2012). However, the results from this study have shown that high initial solution Mg/Ca ratios used to synthesize very high Mg ACC can result in the formation of other polymorphs, and not necessarily high Mg-calcite. Previous work has suggested the final Mg content of natural calcites is a function of both the Mg/Ca ratio and the CO_3^{2-} concentration of the precipitating solution (Given & Wilkinson,

1985). Recently it has been demonstrated that the Mg content of ACC is also regulated by total carbonate concentration and pH, in addition to the initial Mg/Ca ratio (Blue & Dove, *in press*). Results from this study establish a chemical basis for a broad range of Mg contents in ACC and calcite, in which the Mg content of ACC and subsequent calcite is the result of the interplay between solution Mg/Ca ratio, carbonate level (or supersaturation), and physical mixing.

An intriguing trend seen in the literature is the control of physical mixing on the Mg content of calcite. Other studies have shown that the energy added to the precipitation environment, either through stirring or shaking, affects mineral precipitation and morphology (Sand et al., 2012; Given & Wilkinson, 1985). Reports from the literature show calcite forms from ACC in a wide variety of solution conditions and energy settings, but high-Mg calcite formation is restricted to studies where solutions were not stirred during transformation (**Table 4.1**). The results from this study also corroborate this trend: for nearly identical solution chemistries, monohydrocalcite formed in mixed solution conditions and high-Mg calcite formed in unmixed conditions (**Figs. 4.3, 4.6**; **Table C1**, **Appendix C**). Furthermore, the calcite that formed after ACC in mixed conditions only included up to about 10 mole percent Mg on average (**Fig. 4.7A**). The results from this study, combined with previous reports (**Table 4.1**), make a strong argument that high-Mg calcite can only form in low energy settings.

An additional finding of the transformation experiments is the similarity between the composition of the initial ACC phase and subsequent calcite. Results show that the calcites produced from ACC contain nearly identical amounts of Mg as the initial ACC phase, suggesting that calcite composition reflects local conditions of formation regardless of mineralization pathway. The insights gained from this study have particular significance for closed and semi-closed calcification environments. The sites of rapid calcification in organisms that use ACC are

an example of a natural setting where similar trends in the solution chemistry may develop in the calcifying fluid. Some organisms incorporate high amounts of Mg in various parts of their bodies (Chave, 1954; Raz et al., 2003; Woodcock et al., 2012), and several studies have reported that organic molecules, such as self-assembled monolayers with biologically relevant functional groups or carboxylated molecules, enhance the Mg content of ACC or calcite (Han & Aizenberg, 2008; Wang et al., 2009; Han et al., 2013). However, results from this study show that higher Mg content in ACC or calcite can be achieved by adjusting the carbonate concentration and/or pH of the solution, and does not necessarily require adding more Mg or organic additives. Studies have shown that organisms can precisely control alkalinity and/or pH conditions during calcification (Dupraz et al., 2009; Gagnon et al., 2013), so this gives organisms that use Mg another way of using the chemistry of the calcifying fluid to their advantage.

The solution conditions necessary to precipitate and transform ACC, as reported in this study, may also exist in a variety of closed system environments on the Earth. Saline environments where supersaturations can exceed ACC solubility—such as marine porewaters, sabkhas, and closed basin lakes—are ideal for polymorph formation via an ACC precursor. It has been reported that ACC can occur in hot spring deposits (Jones & Peng, 2012) and microbial mats (Dupraz et al., 2009) as well. $CaCO_3$ crystallization via an amorphous precursor is likely more prevalent in natural environments than previously thought. Many saline, alkaline lakes display a variety of $CaCO_3$ polymorphs, morphologies, and elemental and isotopic signatures (Thompson, 1990; Solotchina, et al., 2009; Katz & Nishri, 2013; Nielsen & DePaolo, 2013). The findings from this study suggest that is may be possible to put the occurrence of different carbonate minerals into context by understanding the framework solution chemistry that produces different polymorphs from an amorphous precursor.

4.5 CONCLUSIONS

The findings from this study show ACC can form in solutions with a broad range of Mg^{2+} concentrations, CO_3^{2-} concentrations, and pH conditions for short (for low Mg^{2+} concentrations) to very long (for high Mg^{2+} concentrations) periods of time. This suggests that the formation of carbonate minerals by an amorphous pathway is likely much more common than currently thought. ACC transforms to a crystalline polymorph that is controlled by a systematic relationship to the relative activities of Mg^{2+} and CO_3^{2-}, forming a conceptual "stability field" for a particular polymorph. According to the "stability fields" documented in this study, calcite will only form from ACC when the aCO_3^{2-}/aCa^{2+} ratio is ≤ 1.0 and the aMg^{2+}/aCa^{2+} ratio is <5.0 for mixed conditions. In unmixed conditions, calcite can form at much higher aMg^{2+}/aCa^{2+} ratios (up to 14.0).

The stability field for monohydrocalcite is much larger than the three anhydrous forms of $CaCO_3$, but the phase is less stable over time due to its higher solubility. Therefore, it is likely that MHC is commonly another intermediate phase that occurs along the path of crystallization via an amorphous precursor. The physical mixing of the growth environment also controls polymorph formation and morphology. High-Mg calcite was only documented form from ACC in unmixed conditions, and this trend is corroborated in the literature. For the conditions of this study, the Mg content of ACC and subsequent calcite is similar, suggesting that calcite composition reflects local conditions of formation, regardless of the pathway to mineralization. The results of this study have implications for understanding biomineralization processes and calcification in diverse Earth environments. Fundamentally, the findings presented in this study provide a chemical road map to future studies of ACC composition, ACC transformation, polymorph selection, and impurities in calcite.

4.6 REFERENCES

Aizenberg J., Addadi L., Weiner S. and Lambert G. (1996) Stabilization of amorphous calcium carbonate by specialized macromolecules in biological and synthetic precipitates. *Adv. Mater.* **8**, 222–226.

Akiva-Tal A., Kababya S., Balazs Y. S., Glazer L., Berman A., Sagi A. and Schmidt A. (2011) In situ molecular NMR picture of bioavailable calcium stabilized as amorphous $CaCO_3$ biomineral in crayfish gastroliths. *Proceed. Natl. Acad. Sci. U. S. A.* **108**, 14763–14768.

Angel A. M. (2013) Influence of solution composition and temperature on the strontium content of amorphous calcium carbonate and subsequent calcite. *Unpublished Thesis*, Virginia Polytechnic Institute and State University, Blacksburg, VA, U. S. A.

Beniash E., Aizenberg J., Addadi L. and Weiner S. (1997) Amorphous calcium carbonate transforms into calcite during sea urchin larval spicule growth. *Proceed. Royal Soc. London B: Bio. Sci*. **264**, 461–465.

Berner R.A. (1975) The role of magnesium in the crystal growth of calcite and aragonite from sea water. *Geochim. et Cosmochim. Acta* **39**, 489–504.

Bird M. I., Chivas A. R., Radnell C. J. and Burton H. R. (1991) Sedimentological and stable-isotope evolution of lakes in the Vestfold Hills, Antarctica. *Palaeogeo., Palaeoclim., Palaeoeco*. **84**, 109–130.

Bischoff W. D., Bishop F .C., and Mackenzie F. T. (1983) Biogenically produced magnesian calcite: Inhomogeneities in chemical and physical properties; comparison with synthetic phases. *Amer. Mineral.***, 68,** 1183–1188.

Bischoff W. D., Mackenzie F. T. and Bishop F. C. (1987) Stabilities of synthetic magnesian calcites in aqueous solution: Comparison with biogenic materials. *Geochim. et Cosmochim. Acta* **51**, 1413–1423.

Blue C. R. and Dove P. M. (*in press*) Chemical controls on the magnesium content of amorphous calcium carbonate. *Geochim. et Cosmochim. Acta*.

Blue C. R., Rimstidt J. D. and Dove P. M. (2013) Chapter twenty-three - A mixed flow reactor method to synthesize amorphous calcium carbonate under controlled chemical conditions, in: James, J. D. Y. (Ed.), *Method. Enzymol.*, Academic Press, 557–568.

Brečević L. and Nielsen A. E. (1989) Solubility of amorphous calcium carbonate. *J. Cryst. Growth* **98**, 504–510.

Burton W. K., Cabrera N. and Frank F. C. (1951) The growth of crystals and the equilibrium structure of their surfaces. *Phil. Trans. Royal Soc. London. Series A, Math. & Phys. Sci.* **243**, 299–358.

Carlström D. (1963) A crystallographic study of vertebrate otoliths. *Bio. Bulletin* **125**, 441–463.

Catherine H., Skinner W., Osbaldiston G. W. and Wilner A. N. (1977) Monohydrocalcite in a guinea pig bladder stone, a novel occurrence. *Amer. Mineral.* **62**, 273–277.

Chave K. E. (1954) Aspects of the biogeochemistry of magnesium 1. Calcareous marine organisms. *J. Geology* **62**, 266–283.

Chernov A. A. (1984) Modern crystallography III: Crystal growth. Springer-Verlag.

Dahl K. and Buchardt B. (2006) Monohydrocalcite in the arctic Ikka Fjord, SW Greenland: First reported marine occurrence. *J. Sed. Research* **76**, 460–471.

Davis K .J., Dove P. M. and De Yoreo J. J. (2000) The role of Mg^{2+} as an impurity in calcite growth. *Science* **290**, 1134–1137.

Denton A. R. and Ashcroft N. W. (1991) Vegard's law. *Phys. Rev. A*, **43**, 3161–3164.

De Yoreo J. J. (2013) More than one pathway. *Nature Mater*. **12**, 284–285.
Di Tommaso D. and de Leeuw N. H. (2010) First principles simulations of the structural and dynamical properties of hydrated metal ions (Me^{2+}) and solvated metal carbonates (Me = Ca, Mg, and Sr). *Cryst. Growth & Design* **10**, 4292–4302.
Doerner H. A. and Hoskins W. M. (1925) Co-precipitation of radium and barium sulfates. *J. Amer. Chem. Soc*. **47**, 662–675.
Dupraz C., Reid P. R., Braissant O., Decho A. W., Norman R. S. and Visscher P. T. (2009) Processes of carbonate precipitation in modern microbial mats. *Earth-Sci. Reviews* **96**, 141–162.
Fernández-Díaz L., Putnis A., Prieto M. and Putnis C. V. (1996) The role of magnesium in the crystallization of calcite and aragonite in a porous medium. *J. Sed. Research* **66**, 482–491.
Fischbeck R. and Müller G. (1971) Monohydrocalcite, hydromagnesite, nesquehonite, dolomite, aragonite, and calcite in speleothems of the Fränkische Schweiz, Western Germany. *Contr. Mineral. and Petrol.* **33**, 87–92.
Fukushi K., Munemoto T., Sakai M. and Yagi S. (2011) Monohydrocalcite: A promising remediation material for hazardous anions. *Sci. Technol. Adv. Mater*. **12**, 1–12.
Gagnon A. C., Adkins J. F., Erez J., Eiler J. M. and Guan Y. (2013) Sr/Ca sensitivity to aragonite saturation state in cultured subsamples from a single colony of coral: Mechanism of biomineralization during ocean acidification. *Geochim. et Cosmochim. Acta* **105**, 240–254.
Garvie L. A .J. (2003) Decay-induced biomineralization of the saguaro cactus (*Carnegiea gigantea*). *Amer. Mineral*. **88**, 1879–1888.
Gebauer D., Volkel A. and Cölfen H. (2008) Stable prenucleation calcium carbonate clusters. *Science* **322**, 1819–1822.
Given R. K. and Wilkinson B. H. (1985) Kinetic control of morphology, composition, and mineralogy of abiotic sedimentary carbonates. *J. Sed. Petr.* **55**, 0109–0119.
Hamm L. M., Wallace A. F. and Dove P. M. (2010) Molecular dynamics of ion hydration in the presence of small carboxylated molecules and implications for calcification. *J. Phys. Chem. B* **114**, 10488–10495.
Han N., Blue C. R., De Yoreo J. J. and Dove P. M. (2013) The effect of carboxylates on the Mg content of calcites that transform from ACC. *Proced. Earth Planet. Sci*. **7**, 223–227.
Hu Q., Nielsen M. H., Freeman C. L., Hamm L. M., Tao J., Lee J. R. I., Han T. Y.J., Becker U., Harding J. H., Dove P. M. and De Yoreo J. J. (2012) The thermodynamics of calcite nucleation at organic interfaces: Classical vs. non-classical pathways. *Faraday Discuss*. **159**, 509–523.
Hu Q., Zhang J., Teng H. and Becker U. (2012) Growth process and crystallographic properties of ammonia-induced vaterite. *Amer. Mineral*. **97**, 1437–1445.
Hull H. and Turnbull A. G. (1973) A thermochemical study of monohydrocalcite. *Geochim. et Cosmochim. Acta* **37**, 685–694.
Ito T. (1993) The occurrence of monohydrocalcite from calcareous sinter of cold spring of Shiowakka, Asyoro, Hokkaido. *J. Min. Petr. Econ. Geol* **88**, 485–491.
Jensen J .N. (2001) Approach to steady state in completely mixed flow reactors. *J. Environ. Engineer.* **127**, 13–18.
Jones B. and Peng X. (2012) Amorphous calcium carbonate associated with biofilms in hot spring deposits. *Sed. Geology* **269–270**, 58–68.
Katz A. and Nishri A. (2013) Calcium, magnesium and strontium cycling in stratified, hardwater lakes: Lake Kinneret (Sea of Galilee), Israel. *Geochim. et Cosmochim. Acta* **105**, 372–394.

Kimura T. and Koga N. (2011) Monohydrocalcite in comparison with hydrated amorphous calcium carbonate: Precipitation condition and thermal behavior. *Cryst. Growth & Design* **11**, 3877–3884.

Kralj D. and Brečević L. (1995) Dissolution kinetics and solubility of calcium carbonate monohydrate. *Colloids & Surfaces A: Physicochem. & Engineer. Aspects* **96**, 287–293.

Kuriyavar S. I., Vetrivel R., Hegde S. G., Ramaswamy A. V., Chakrabarty D. and Mahapatra S. (2000) Insights into the formation of hydroxyl ions in calcium carbonate: temperature dependent FTIR and molecular modeling studies. *J. Mater. Chem*. **10**, 1835–1840.

Last F. M., Last W. M. and Halden N. M. (2010) Carbonate microbialites and hardgrounds from Manito Lake, an alkaline, hypersaline lake in the northern Great Plains of Canada. *Sed. Geol.* **225**, 34–49.

Lenders J. J. M., Dey A., Bomans P. H. H., Spielmann J., Hendrix M. M. R. M., de With G., Meldrum F. C., Harder S. and Sommerdijk N. A. J. M. (2011) High-magnesian calcite mesocrystals: A coordination chemistry approach. *J. Amer. Chem. Soc*. **134**, 1367–1373.

Léveillé R. J., Fyfe W. S. and Longstaffe F. J. (2000) Geomicrobiology of carbonate–silicate microbialites from Hawaiian basaltic sea caves. *Chem. Geol*. **169**, 339–355.

Loste E., Wilson R. M., Seshadri R. and Meldrum F. C. (2003) The role of magnesium in stabilising amorphous calcium carbonate and controlling calcite morphologies. *J. Cryst. Growth* **254**, 206–218.

Lowenstam H. A. (1981) Minerals Formed by Organisms. *Science* **211**, 1126–1131.

Mackenzie F. T., Bischoff W. D., Bishop F. C., Loijens M., Schoonmaker J. and Wollast R. (1983) Magnesian calcites: Low-temperature occurrence, solubility and solid-solution behavior. *Reviews in Mineralogy*, **11**, 96–144.

Michel F. M., MacDonald J., Feng J., Phillips B. L., Ehm L., Tarabrella C., Parise J. B. and Reeder R. J. (2008) Structural characteristics of synthetic amorphous calcium carbonate. *Chem. Mater*. **20**, 4720–4728.

Mucci A. and Morse J. W. (1983) The incorporation of Mg^{2+} and Sr^{2+} into calcite overgrowths: Influences of growth rate and solution composition. *Geochim. et Cosmochim. Acta* **47**, 217–233.

Munemoto T. and Fukushi K. (2008) Transformation kinetics of monohydrocalcite to aragonite in aqueous solutions. *J. Mineral. Petrol. Sci*. **103**, 345–349.

Navrotsky A. (2004) Energetic clues to pathways to biomineralization: Precursors, clusters, and nanoparticles. *Proceed. Natl. Acad. Sci. U. S. A*. **101**, 12096–12101.

Niedermayr A., Köhler S. J. and Dietzel M. (2013) Impacts of aqueous carbonate accumulation rate, magnesium and polyaspartic acid on calcium carbonate formation (6–40°C). *Chem. Geology* **340**, 105-120.

Nielsen L. C. and DePaolo D. J. (2013) Ca isotope fractionation in a high-alkalinity lake system: Mono Lake, California. *Geochim. et Cosmochim. Acta* **118**, 276–294.

Nishiyama R., Munemoto T. and Fukushi K. (2013) Formation condition of monohydrocalcite from $CaCl_2$–$MgCl_2$–Na_2CO_3 solutions. *Geochim. et Cosmochim. Acta* **100**, 217–231.

Nudelman F., Chen H. H., Goldberg H. A., Weiner S. and Addadi L. (2007) Lessons from biomineralization: comparing the growth strategies of mollusc shell prismatic and nacreous layers in *Atrina rigida*. *Faraday Discuss.* **136**, 9–25.

Politi Y., Metzler R. A., Abrecht M., Gilbert B., Wilt F. H., Sagi I., Addadi L., Weiner S. and Gilbert P. U. P. A. (2008) Transformation mechanism of amorphous calcium carbonate into calcite in the sea urchin larval spicule *Proceed. Natl. Acad. Sci. U. S. A*. **105**, 17362–17366.

Radha A. V., Fernandez-Martinez A., Hu Y., Jun Y.-S., Waychunas G. A. and Navrotsky A. (2012) Energetic and structural studies of amorphous $Ca_{1-x}Mg_xCO_3 \cdot nH_2O$ ($0 \leq x \leq 1$). *Geochim. et Cosmochim. Acta* **90**, 83–95.

Radha A. V., Forbes T. Z., Killian C. E., Gilbert P. U. P. A. and Navrotsky A. (2010) Transformation and crystallization energetics of synthetic and biogenic amorphous calcium carbonate. *Proceed. Natl. Acad. Sci. U. S. A.* **107**, 16438–16443.

Raz S., Hamilton P. C., Wilt F. H., Weiner S. and Addadi L. (2003) The transient phase of amorphous calcium carbonate in sea urchin larval spicules: The involvement of proteins and magnesium ions in its formation and stabilization. *Adv. Funct. Mater*. **13**, 480–486.

Raz S., Weiner S. and Addadi L. (2000) Formation of high-magnesium calcites via an amorphous precursor phase: Possible biological implications. *Adv. Mater.* **12**, 38–42.

Rivadeneyra M. A., Párraga J., Delgado R., Ramos-Cormenzana A. and Delgado G. (2004) Biomineralization of carbonates by *Halobacillus trueperi* in solid and liquid media with different salinities. *FEMS Microbio. Ecology* **48**, 39–46.

Rodriguez-Blanco J. D., Shaw S., Bots P., Roncal-Herrero T. and Benning L. G. (2012) The role of pH and Mg on the stability and crystallization of amorphous calcium carbonate. *J. Alloys & Compounds* **536**, **Supplement 1**, S477–S479.

Rodriguez-Blanco J. D., Shaw S., Bots P., Roncal-Herrero T. and Benning L. G. (2014) The role of Mg in the crystallization of monohydrocalcite. *Geochim. et Cosmochim. Acta* **127**, 204–220.

Sánchez-Román M., Romanek C. S., Fernández-Remolar D. C., Sánchez-Navas A., McKenzie J. A., Pibernat R. A. and Vasconcelos C. (2011) Aerobic biomineralization of Mg-rich carbonates: Implications for natural environments. *Chem. Geology* **281**, 143–150.

Sand K. K., Rodriguez-Blanco J. D., Makovicky E., Benning L. G. and Stipp S. L. S. (2011) Crystallization of $CaCO_3$ in water–alcohol mixtures: Spherulitic growth, polymorph stabilization, and morphology change. *Cryst. Growth & Design* **12**, 842–853.

Señorale-Pose M., Chalar C., Dauphin Y., Massard P., Pradel P. and MarÌn M. (2008) Monohydrocalcite in calcareous corpuscles of *Mesocestoides corti*. *Experiment. Parasit*. **118**, 54–58.

Solotchina E. P., Prokopenko A. A., Kuzmin M. I., Solotchin P. A. and Zhdanova A. N. (2009) Climate signals in sediment mineralogy of Lake Baikal and Lake Hovsgol during the LGM-Holocene transition and the 1-Ma carbonate record from the HDP-04 drill core. *Quat. Internat*. **205**, 38–52.

Stephenson A. E., Hunter J. L., Han N., De Yoreo J. J. and Dove P. M. (2011) Effect of ionic strength on the Mg content of calcite: Toward a physical basis for minor element uptake during step growth. *Geochim. et Cosmochim. Acta* **75**, 4340–4350.

Stoffers P. and Fischbeck R. (1974) Monohydrocalcite in the sediments of Lake Kivu (East Africa). *Sedimentology* **21**, 163–170.

Swainson I. P. (2008) The structure of monohydrocalcite and the phase composition of the beachrock deposits of Lake Butler and Lake Fellmongery, South Australia. *Amer. Mineral*. **93**, 1014–1018.

Tao J., Zhou D., Zhang Z., Xu X. and Tang R. (2009) Magnesium-aspartate-based crystallization switch inspired from shell molt of crustacean. *Proceed. Natl. Acad. Sci. U. S. A.* **106**, 22096–22101.

Taylor G. F. (1975) The occurrence of monohydrocalcite in two small lakes in the South-East of South Australia. *Amer. Mineral*. **60**, 690–697.

Vegard L. (1921) Die Konstitution der Mischkristalle und die Raumfüllung der Atome. *Zeitschrift für Physik,* **5**, 17.

Wang D., Hamm L. M., Giuffre A. J., Echigo T., Rimstidt J. D., De Yoreo J. J., Grotzinger J. and Dove P. M. (2012) Revisiting geochemical controls on patterns of carbonate deposition through the lens of multiple pathways to mineralization. *Faraday Discuss*. **159**, 1–16.

Wang D., Wallace A. F., De Yoreo J. J. and Dove P. M. (2009) Carboxylated molecules regulate magnesium content of amorphous calcium carbonates during calcification. *Proceed. Natl. Acad. Sci. U. S. A.* **106**, 21511–21516.

Weiss I. M., Tuross N., Addadi L. and Weiner S. (2002) Mollusc larval shell formation: amorphous calcium carbonate is a precursor phase for aragonite. *J. Experiment. Zoo*. **293**, 478–491.

Zhang Z., Xie Y., Xu X., Pan H. and Tang R. (2012) Transformation of amorphous calcium carbonate into aragonite. *J. Cryst. Growth* **343**, 62–67.

APPENDIX A. SUPPLEMENTARY INFORMATION FOR CHAPTER 2

A1. ADDITIONAL CHARACTERIZATION FIGURES

A.

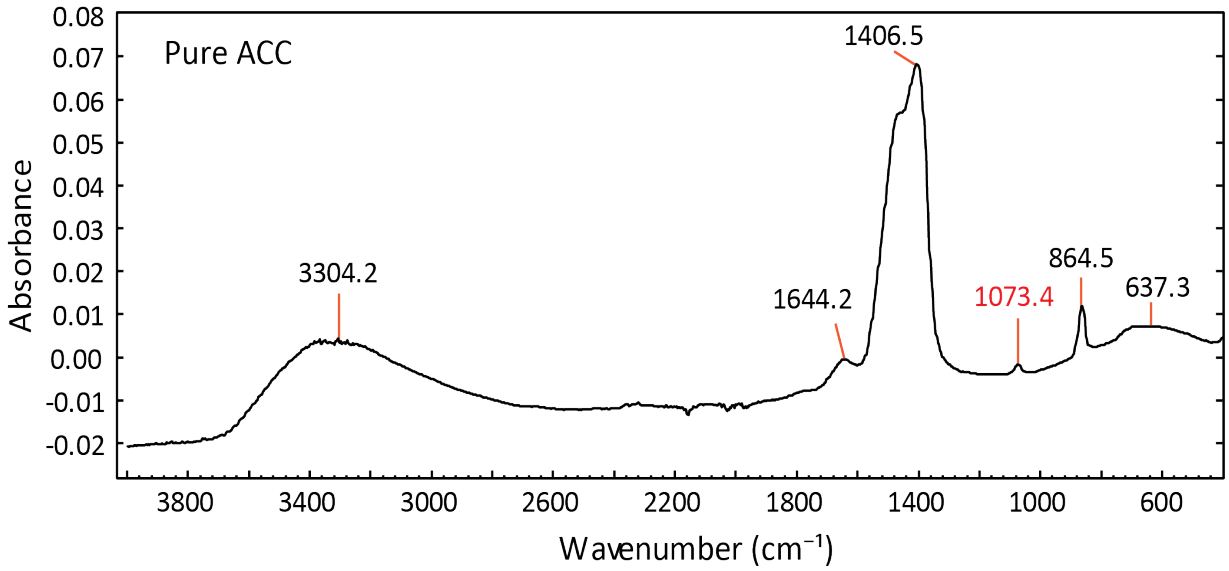

B.

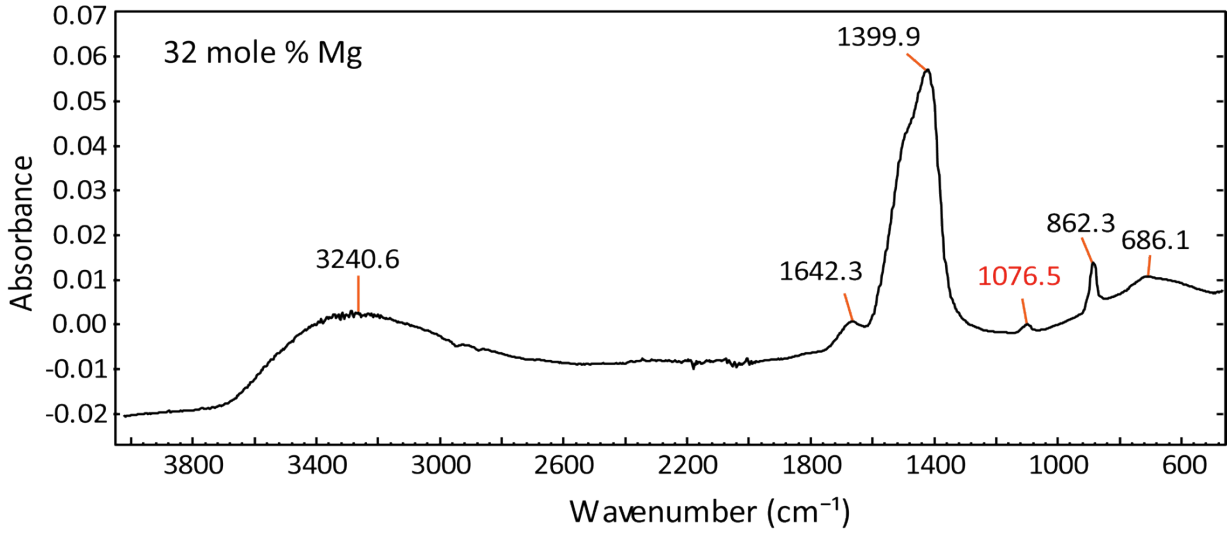

Figure A1. FTIR characterization of pure ACC and ACC with 32 mole % Mg. (A) FTIR characterization of pure ACC shows all carbonate vibrational modes exhibit broadened peaks. ν_3 (anti-symmetric stretch) occurs at 1406.5 cm^{-1}, ν_1 (symmetric stretch) occurs at 1073.4 cm^{-1}, and ν_2 (bend) occurs at 637.3 cm^{-1}. The broad hump around 3300 cm^{-1} and the peak at 1644.2 cm^{-1} are vibrational modes of water. The ν_1 peak (highlighted in red) is reported in Fig. A2. (B) FTIR characterization of ACC with 32 mole % Mg shows all carbonate vibrational modes have shifted with respect to pure ACC. ν_3 (anti-symmetric stretch) occurs at 1399.9 cm^{-1}, ν_1 (symmetric stretch) occurs at 1076.5 cm^{-1}, and ν_2 (bend) occurs at 686.1 cm^{-1}. The broad hump around 3200 cm^{-1} and the peak at 1642.3 cm^{-1} are vibrational modes of water. The ν_1 peak (highlighted in red) is reported in Fig. A2.

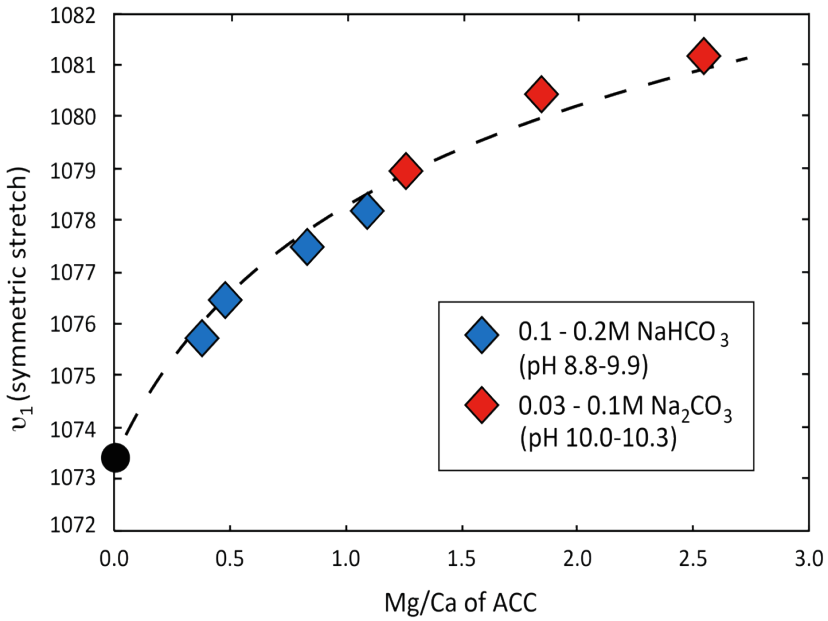

Figure A2. FTIR spectra of ACC synthesized from solutions with an initial Mg/Ca ratio of 5:1 shows a systematic shift to higher wavenumbers in the ν_1 (CO_3^{2-} symmetric stretch) peak with increasing Mg content. The relationship provides an additional, non-destructive means of calibrating the Mg/Ca ratio of ACC. The reactant solutions included both $NaHCO_3$ (blue diamonds) and Na_2CO_3 (red diamonds). The black circle represents the position of the ν_1 peak for the Mg-free control that was synthesized using 0.06 M Na_2CO_3 solution (pH 12).

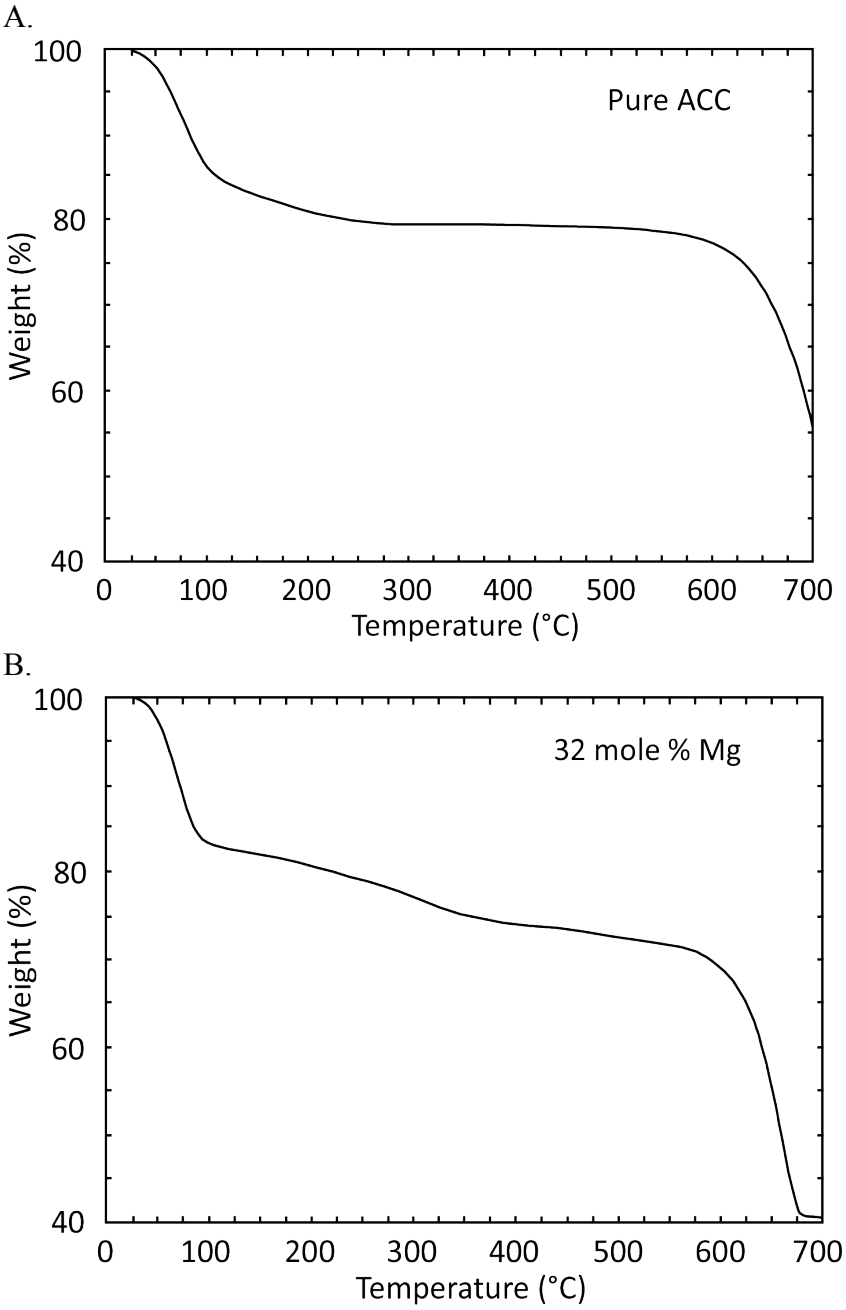

Figure A3. TGA weight loss curve of pure ACC and ACC with 32 mole % Mg. (A) TGA weight loss curve of an ACC sample synthesized without magnesium shows a weight loss of about 20% at 250°C, giving a stoichiometry of approximately 1.42 water molecules per calcium carbonate. (B) TGA weight loss curve of an ACC sample produced at a 5:1 Mg/Ca ratio and 100 mM $NaHCO_3$, resulting in 32 mole % Mg, shows a weight loss of about 21% at 250°C. The stoichiometry results in approximately 1.40 water molecules per magnesium, calcium carbonate ($Mg_{0.32}Ca_{0.68}CO_3 \bullet 1.40\ H_2O$). The presence of Mg in ACC does not significantly impact the amount of water in the structure.

A2. DISTRIBUTION COEFFICIENTS

A key feature of the mixed flow reactor design is that it allows precise control of the distribution of minor or trace elements between the solution and the ACC. The distribution of Mg between the ACC and the solution is expressed by a distribution coefficient:

$$K_D = \left(\frac{X_{\mathrm{Mg}}}{X_{\mathrm{Ca}}}\right) \Big/ \left(\frac{m_{\mathrm{Mg}}}{m_{\mathrm{Ca}}}\right) \tag{1}$$

In a mixed flow reactor operating at steady state, the concentrations of Mg and Ca in the reactor solution are constant. This means that the composition of the ACC remains constant over time and the $X_{\mathrm{Mg}}/X_{\mathrm{Ca}}$ depends upon the relative rates of removal of Mg and Ca from the solution. These rates are the difference between the concentration of each element in the feed and effluent solutions multiplied by the flow rate through the reactor:

$$\frac{X_{\mathrm{Mg}}}{X_{\mathrm{Ca}}} = \frac{R_{\mathrm{Mg}}}{R_{\mathrm{Ca}}} = \frac{\left(\left(m_{\mathrm{Mg}}\right)_{in} - \left(m_{\mathrm{Mg}}\right)_{out}\right)Q}{\left(\left(m_{\mathrm{Ca}}\right)_{in} - \left(m_{\mathrm{Ca}}\right)_{out}\right)Q} = \frac{\left(\left(m_{\mathrm{Mg}}\right)_{in} - \left(m_{\mathrm{Mg}}\right)_{out}\right)}{\left(\left(m_{\mathrm{Ca}}\right)_{in} - \left(m_{\mathrm{Ca}}\right)_{out}\right)} \tag{2}$$

Combining (1) and (2) and realizing that the effluent solution is a sample of the solution in the reactor leads to

$$K_D = \frac{\left(\left(m_{\mathrm{Mg}}\right)_{in} - \left(m_{\mathrm{Mg}}\right)_{out}\right)}{\left(\left(m_{\mathrm{Ca}}\right)_{in} - \left(m_{\mathrm{Ca}}\right)_{out}\right)} \Bigg/ \left(\frac{\left(m_{\mathrm{Mg}}\right)_{out}}{\left(m_{\mathrm{Ca}}\right)_{out}}\right) = \frac{\left(\left(m_{\mathrm{Mg}}\right)_{in} / \left(m_{\mathrm{Mg}}\right)_{out}\right) - 1}{\left(\left(m_{\mathrm{Ca}}\right)_{in} / \left(m_{\mathrm{Ca}}\right)_{out}\right) - 1} \tag{3}$$

This means that K_D can be computed from difference between the concentration of Mg and Ca in the feed and effluent solutions regardless of the flow or precipitation rate. These same data along with the flow rate can be used to find the precipitation rate of the major element so that a mixed flow reactor experiment is well suited to quantify the effect of precipitation rate on K_D.

APPENDIX B. SUPPLEMENTARY INFORMATION FOR CHAPTER 3

B1. ACC SYNTHESIS DATA

Table B1. Characterization of ACMC samples for all solution conditions. All values are an average of 3 experiments.

Mole % Mg	Carbonate Conc. (M)	Carbonate Source	Steady state pH	Mg/Ca (Effluent)	Raman ν_1 peak	FTIR ν_1 peak	FTIR ν_2 peak	FTIR ν_3 peak	# H_2O
0.0	0.06	Na_2CO_3	12.0	0.0	1080.1	1073.4	864.5	1406.5	1.42
24.8	0.10	$NaHCO_3$	9.10	6.95	1085.4	-			-
25.4	0.20	$NaHCO_3$	8.98	7.69	1085.8	-			-
25.9	0.06	$NaHCO_3$	9.39	7.19	1085.4	-			-
26.5	0.06	$NaHCO_3$	9.34	6.79	1086.1				-
27.5	0.20	$NaHCO_3$	9.12	8.65	1086.0	-			-
27.8	0.20	$NaHCO_3$	8.83	7.48	-	1075.8	862.2	1394.2	1.41
28.3	0.10	$NaHCO_3$	9.31	8.54	1086.0	-			-
28.6	0.20	$NaHCO_3$	9.14	8.80	1087.4	-			-
31.1	0.06	$NaHCO_3$	9.62	8.33	1086.6	-			-
31.3	0.10	$NaHCO_3$	9.49	9.20	1087.2	-			-
31.9	0.06	$NaHCO_3$	9.59	8.52	1087.4	-			-
32.1	0.20	$NaHCO_3$	9.33	9.95	1087.9	-			-
32.6	0.10	$NaHCO_3$	9.26	8.28	-	1076.5	862.3	1399.9	1.40
36.0	0.10	$NaHCO_3$	9.56	10.21	1088.5	-			-
36.3	0.60	$NaHCO_3$	9.75	9.09	-	-			-
37.9	0.60	$NaHCO_3$	9.80	10.22	1087.9	-			-
39.9	0.20	$NaHCO_3$	9.50	11.86	-	-			-
44.5	0.10	$NaHCO_3$	9.75	11.87	-	-			-
45.5	0.20	$NaHCO_3$	9.75	14.66	-	1077.5	863.4	1429.1	1.63
52.3	0.10	$NaHCO_3$	9.89	13.53	-	1078.2	862.2	1419.4	1.42
54.2	0.06	$NaHCO_3$	10.05	10.28	1090.0	-			-
64.8	0.06	Na_2CO_3	10.13	11.51	-	1080.4	861.2	1424.8	1.37
71.8	0.10	Na_2CO_3	10.34	14.33	-	1081.2	860.7	1434.7	1.60

B2. SUPPLEMENTARY FIGURES

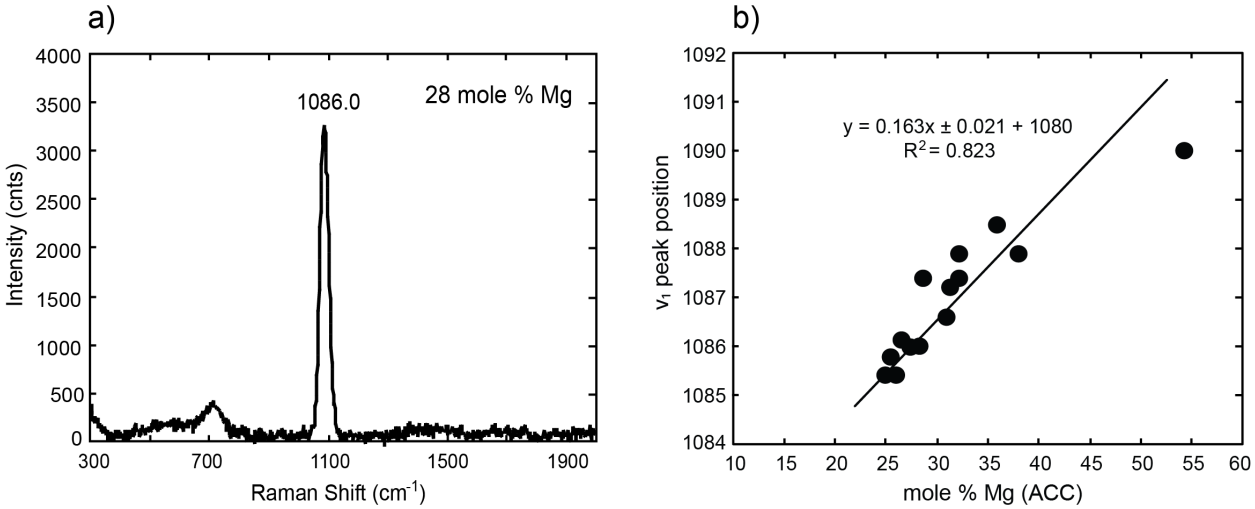

Figure B1. Analysis of ACMC products by Raman spectroscopy confirms an amorphous phase and shows a systematic relationship between ν_1 peak position and Mg content. (a) A representative Raman spectra for an ACMC sample with 28 mole % Mg displays only a broadened ν_1 peak (labeled) and a very broad peak around 700 cm^{-1} (ν_4), verifying an amorphous carbonate material. (b) A plot of the ν_1 peak positions for ACMC shows a systematic shift to higher wavenumbers with increasing Mg content.

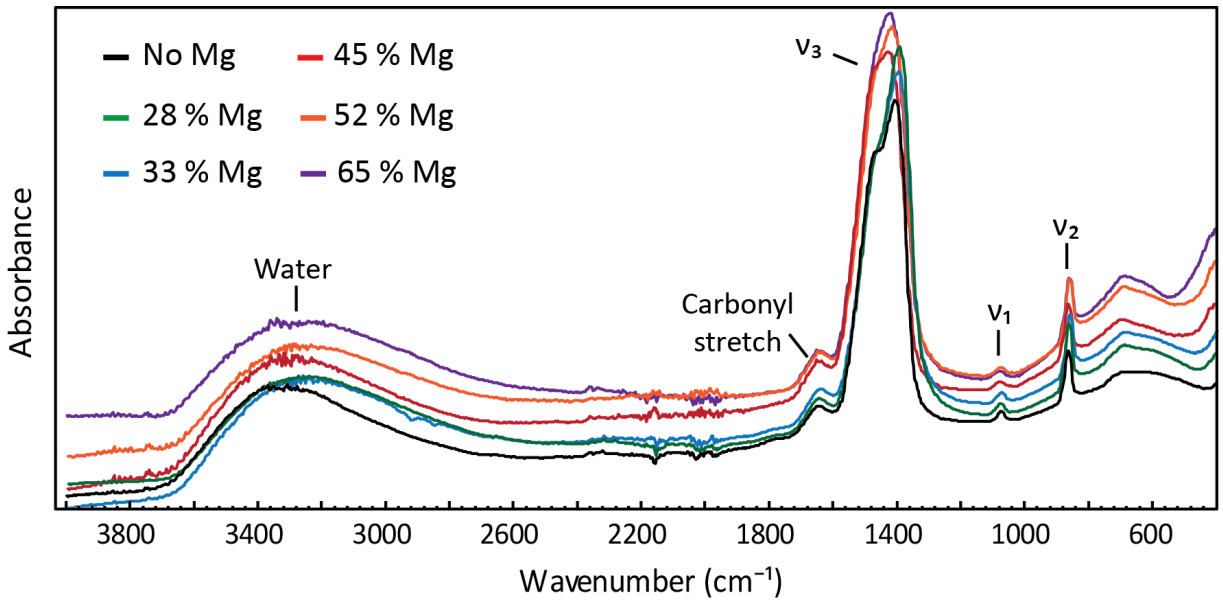

Figure B2. FTIR characterization of pure ACC (black line) and ACMC with variable amounts of Mg (colored lines) shows all carbonate vibrational modes exhibit broadened peaks. The carbonate vibrational modes of the samples containing Mg have shifted with respect to pure ACC (see Table A1 for individual values). The vibrational modes are as follows: ν_3 (anti-symmetric stretch), ν_1 (symmetric stretch), and ν_2 (out of plane bend). The broad peaks around 3300 cm^{-1} and the peaks around 1650 cm^{-1} are due to the vibrational modes of water.

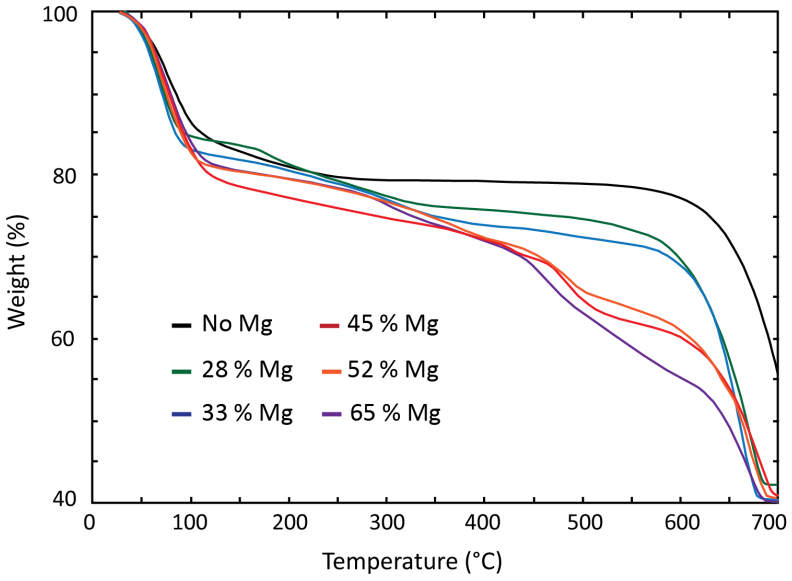

Figure B3. The TGA weight loss curves for six representative ACMC samples show the Mg content of ACMC does not significantly correlate with the amount of water. The weight loss curve of ACC synthesized without Mg (black line) shows a weight loss of about 20% at 250°C, giving a stoichiometry of approximately 1.42 water molecules per calcium carbonate. The weight loss curves of ACMC samples containing variable amounts of Mg (colored lines) show a weight loss of 22–24% at 250°C, resulting in 1.37–1.63 water molecules per calcium, magnesium carbonate (see Table A1). There is no correlation between the Mg concentration in an ACMC sample and the amount of water.

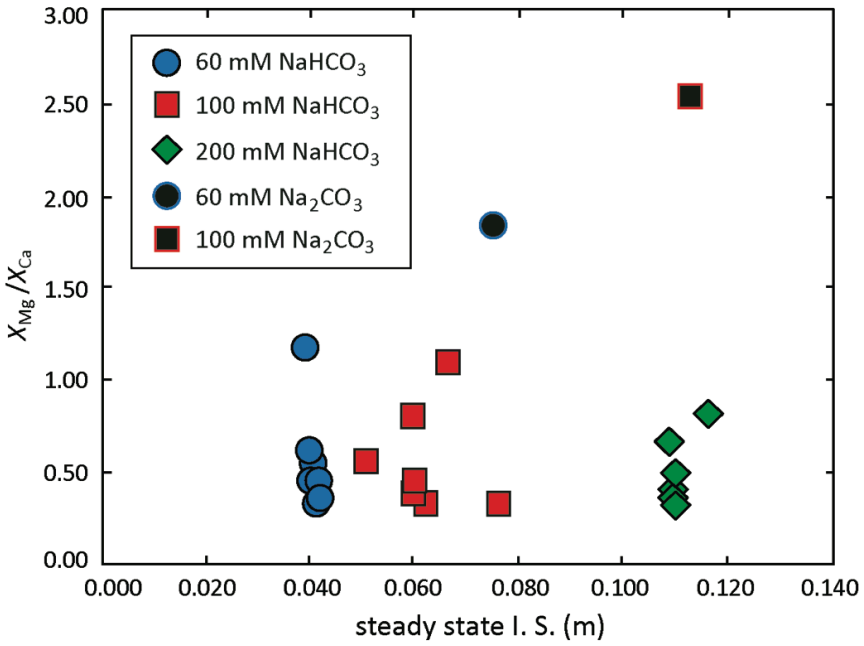

Figure B4. The ionic strength of the mineralizing solution has no effect on the Mg content of ACMC. All ionic strength values are significantly lower than seawater (~0.70 m).

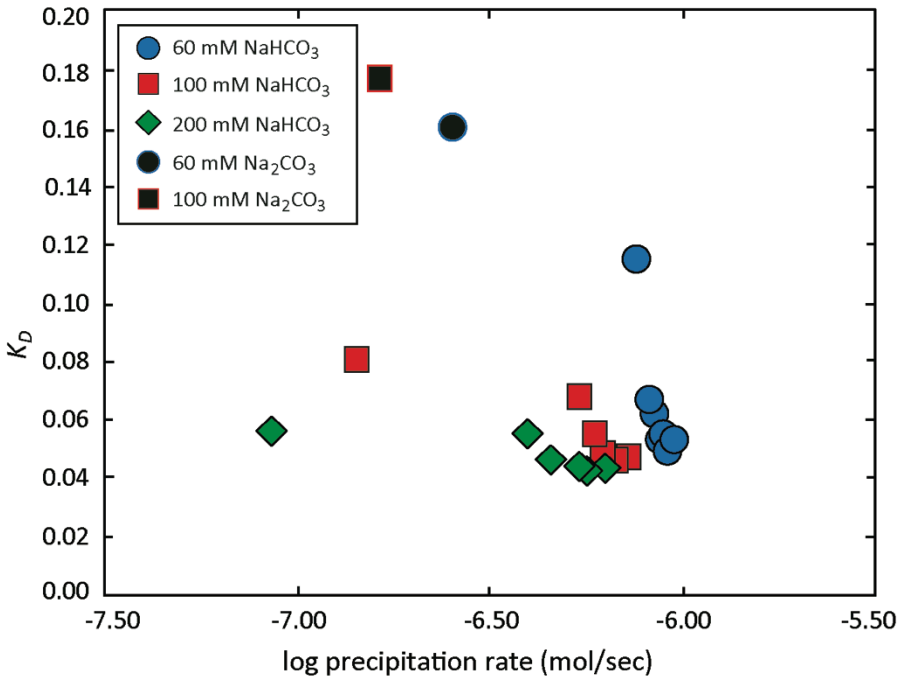

Figure. B5. For the conditions of this study, the dependence of ACMC composition upon the rate of precipitation is inconclusive. Experiments were not specifically designed to examine the control of kinetic effects on composition.

APPENDIX C. SUPPLEMENTARY INFORMATION FOR CHAPTER 4

C1. ACC TRANSFORMATION DATA (Table starts on next page)

Table C1.
Data for all ACC synthesis and ACC transformation experiments by time point

Exp. # 1		log activity (Geochemist's Workbench)					Calculated values			Measured values (pH, ICP-AES)					Mixed trans. (Y/N)
Initial concentration in 100 ml (mM)	Time (hr)[1]	Mg^{2+}	Ca^{2+}	CO_3^{2-}	Na^{+}	Cl^{-}	$\Omega_{calcite}$	I.S. (m)	Alk. (mg/kg)	pH	λ^2	Solution Mg/Ca	% Mg (solid)[3]	Solid phase (XRD)[4]	
$[MgCl_2]$: 50	0	-2.478	-3.323	-3.484	-1.600	-1.514	47.05	0.054	508.47	9.11	0.906	5.64	-	ACMC	Y
$[CaCl_2]$: 10	18	-	-	-	-	-	-	-	-	-	0.301	92.72	5	MHC	
$[NaHCO_3]$: 60	46	-	-	-	-	-	-	-	-	-	-	-	-	MHC	
[NaOH]: 2.0	72	-2.467	-4.665	-3.602	-1.599	-1.521	1.631	0.052	421.98	9.04	0.269	120.77	-	MHC	
pH: 9.70	168	-2.469	-4.754	-3.541	-1.599	-1.522	1.532	0.052	430.47	9.11	0.253	154.79	-	Arag	
Exp. # 2	0	-2.715	-3.848	-2.889	-1.388	-1.519	55.36	0.067	1288.94	9.36	0.678	9.48	-	ACMC	Y
$[MgCl_2]$: 50	6	-	-	-	-	-	-	-	-	-	0.563	11.67	-	ACMC	
$[CaCl_2]$: 10	12	-	-	-	-	-	-	-	-	-	0.575	11.56	-	ACMC	
$[NaHCO_3]$: 100	18	-	-	-	-	-	-	-	-	-	0.554	11.96	-	ACMC	
[NaOH]: 4.0	24	-	-	-	-	-	-	-	-	-	0.604	11.83	-	ACMC	
pH: 9.80	30	-	-	-	-	-	-	-	-	-	0.548	14.93	-	ACMC	
	36	-	-	-	-	-	-	-	-	-	0.261	143.70	23	MHC	
	42	-2.577	-4.875	-3.173	-1.386	-1.397	2.71	0.070	721.12	9.33	0.258	162.12	-	MHC	
	168	-2668	-4.781	-3.576	-1.382	-1.382	1.33	0.066	470.12	9.01	0.344	100.62	-	MHC	
Exp. # 3	0	-2.186	-3.016	-3.771	-1.614	-1.356	49.33	0.081	494.71	8.83	0.941	5.38	28	ACMC	Y
$[MgCl_2]$: 100	6	-	-	-	-	-	-	-	-	-	0.846	6.18	-	ACMC	
$[CaCl_2]$: 20	12	-	-	-	-	-	-	-	-	-	0.322	57.06	-	Arag	
$[NaHCO_3]$: 60	18	-2.196	-4.196	-4.558	-1.609	-1.389	0.53	0.072	358.91	8.08	0.309	82.05	-	Arag	
[NaOH]: 2.0	24	-2.164	-4.290	-4.427	-1.611	-1.376	0.58	0.075	393.49	8.18	0.274	109.80	-	Arag	
pH: 9.70	48	-2.200	-4.428	-4.417	-1.609	-1.392	0.43	0.071	357.04	8.23	0.275	140.25	-	Arag	
Exp. # 4	0	-2.227	-3.291	-3.475	-1.397	-1.277	51.70	0.097	802.97	8.94	0.649	9.23	27	ACMC	Y
$[MgCl_2]$: 100	6	-	-	-	-	-	-	-	-	-	0.599	11.44	-	ACMC	
$[CaCl_2]$: 20	12	-2.245	-3.416	-3.512	-1.396	-1.283	35.64	0.094	738.37	8.93	0.586	11.56	-	ACMC	
$[NaHCO_3]$: 100	18	-2.220	-3.401	-3.469	-1.397	-1.278	40.71	0.097	797.78	8.95	0.564	11.79	-	ACMC	
[NaOH]: 4.0	24	-2.231	-3.417	-3.517	-1.397	-1.280	35.11	0.096	760.25	8.91	0.570	11.95	-	ACMC	
pH: 9.80	48	-2.235	-4.625	-3.544	-1.395	-1.288	2.05	0.092	688.00	8.92	0.242	198.45	-	MHC	
Exp. # 5	0	-2.182	-3.089	-3.913	-1.330	-1.166	30.01	0.114	379.56	8.82	0.946	6.33	29	ACMC	Y
$[MgCl_2]$: 140	6	-2.112	-3.058	-3.929	-1.614	-1.308	31.11	0.090	410.17	8.75	0.865	7.16	-	ACMC	
$[CaCl_2]$: 24	12	-2.048	-3.748	-4.460	-1.616	-1.298	1.87	0.093	399.12	8.16	0.379	40.93	-	MHC	
$[NaHCO_3]$: 60	18	-2.063	-3.826	-4.447	-1.615	-1.307	1.61	0.090	382.83	8.19	0.370	47.27	-	MHC, Arag	
[NaOH]: 2.4	24	-2.075	-3.912	-4.481	-1.614	-1.314	1.22	0.088	367.89	8.17	0.357	56.97	-	Arag	
pH: 9.87															
Exp. # 6	0	-2.287	-3.061	-3.791	-1.214	-1.129	42.47	0.126	646.65	8.68	0.986	4.57	28	ACMC	Y
$[MgCl_2]$: 90	6	-2.266	-3.677	-4.672	-1.492	-1.352	1.35	0.077	463.03	7.85	0.452	21.35	-	Arag, Calc	
$[CaCl_2]$: 20	12	-2.271	-4.136	-4.681	-1.492	-1.357	0.46	0.076	440.86	7.86	0.332	62.51	-	Arag, Calc	
$[NaHCO_3]$: 80	18	-2.296	-4.319	-4.628	-1.490	-1.364	0.34	0.073	413.78	7.94	0.316	86.98	-	Arag, Calc	
[NaOH]: 1.8	24	-2.241	-4.370	-4.341	-1.493	-1.351	0.59	0.078	488.46	8.17	0.275	110.37	-	Arag, Calc	
pH: 9.49															

Exp. # 7		log activity (Geochemist's Workbench)					Calculated values			Measured values (pH, ICP-AES)					Mixed trans. (Y/N)
Initial concentration in 100 ml (mM)	Time (hr)[1]	Mg^{2+}	Ca^{2+}	CO_3^{2-}	Na^{+}	Cl^{-}	$\Omega_{calcite}$	I.S. (m)	Alk. (mg/kg)	pH	λ^2	Solution Mg/Ca	% Mg (solid)[3]	Solid phase (XRD)[4]	
$[MgCl_2]$: 68	0	-2.356	-3.008	-3.926	-1.331	-1.231	35.17	0.098	509.77	8.62	1.056	3.56	-	ACMC	Y
$[CaCl_2]$: 18	4	-2.317	-3.573	-5.256	-1.618	-1.450	0.45	0.061	354.75	7.36	0.457	15.50	-	ACMC, Arag	
$[NaHCO_3]$: 60	8	-2.351	-3.758	-5.216	-1.616	-1.464	0.32	0.058	322.00	7.44	0.422	21.95	-	ACMC, Arag	
[NaOH]: 1.1	12	-2.336	-3.889	-5.048	-1.616	-1.462	0.35	0.059	337.57	7.59	0.374	30.32	-	Arag, Calc	
pH: 9.41	16	-2.340	-4.014	-4.860	-1.616	-1.465	0.40	0.058	337.99	7.78	0.344	41.26	-	Arag, Calc	
	24	-2.341	-4.165	-4.742	-1.616	-1.467	0.37	0.058	338.10	7.90	0.317	56.48	-	Arag, Calc	
Exp. # 8	0	-2.736	-3.454	-3.383	-1.257	-1.263	43.90	0.086	575.69	9.18	0.840	4.00	16	ACMC	Y
$[MgCl_2]$: 32	4	-2.691	-3.483	-3.371	-1.534	-1.537	42.25	0.051	549.70	9.18	0.737	4.87	-	ACMc	
$[CaCl_2]$: 10	8	-2.719	-4.654	-3.623	-1.531	-1.528	1.59	0.048	386.33	9.03	0.296	74.78	-	MHC	
$[NaHCO_3]$: 70	12	-2.692	-4.743	-3.576	-1.531	-1.529	1.45	0.048	417.91	9.05	0.276	84.77	-	MHC	
[NaOH]: 2.1	20	-2.679	-4.746	-3.562	-1.532	-1.529	1.48	0.049	432.54	9.05	0.268	88.48	-	MHC	
pH: 9.70	24	-2.710	-4.734	-3.625	-1.531	-1.528	1.32	0.048	392.72	9.02	0.280	91.13	-	MHC	
	48	-2.714	-4.842	-3.553	-1.531	-1.530	1.22	0.048	400.24	9.10	0.274	100.24	-	MHC, Arag	
	168	-2.741	-5.449	-3.509	-1.530	-1.531	0.33	0.047	382.03	9.18	0.231	286.25	-	Arag	
Exp. # 9	0	-2.324	-3.006	-3.763	-1.548	-1.395	51.46	0.074	580.03	8.73	0.909	3.91	18	ACMC	Y
$[MgCl_2]$: 70	4	-2.316	-3.596	-4.651	-1.544	-1.409	1.71	0.068	435.43	7.89	0.436	16.10	-	Arag, Calc	
$[CaCl_2]$: 20	8	-2.354	-4.011	-4.922	-1.542	-1.421	0.35	0.064	370.18	7.68	0.350	38.32	-	Arag, Calc	
$[NaHCO_3]$: 70	12	-2.316	-4.162	-4.713	-1.543	-1.413	0.40	0.067	411.70	7.85	0.298	57.70	-	Arag, Calc	
[NaOH]: 1.8	24	-2.349	-4.334	-4.566	-1.542	-1.423	0.38	0.064	382.48	8.03	0.289	80.36	-	Arag, Calc	
pH: 9.59															
Exp. # 10	0	-2.189	-2.842	-3.949	-1.555	-1.313	48.86	0.091	560.93	8.56	0.929	3.64	18	ACMC	Y
$[MgCl_2]$: 100	4	-2.213	-3.420	-5.457	-1.549	-1.346	0.40	0.78	355.82	7.17	0.480	13.40	-	Arag, Calc	
$[CaCl_2]$: 30	8	-2.190	-3.529	-5.331	-1.550	-1.341	0.42	0.80	380.69	7.27	0.418	18.29	-	Arag, Calc	
$[NaHCO_3]$: 70	24	-2.300	-3.779	-5.296	-1.544	-1.383	0.25	0.68	286.12	7.42	0.427	25.57	-	Arag, Calc	
[NaOH]: 1.8	48	-2.173	-3.808	-4.935	-1.550	-1.341	0.55	0.81	410.12	7.64	0.330	36.09	-	Arag, Calc	
pH: 9.58															
Exp. # 11	0	-2.498	-3.039	-3.751	-1.594	-1.496	48.98	0.057	507.95	8.78	1.001	2.87	27	ACMC	Y
$[MgCl_2]$: 46	2	-2.550	-3.461	-4.357	-1.589	-1.512	4.60	0.050	336.92	8.29	0.605	7.00	-	Calc	
$[CaCl_2]$: 16	4	-2.560	-3.937	-4.961	-1.587	-1.516	0.38	0.048	284.42	7.74	0.417	20.68	-	Calc, Arag	
$[NaHCO_3]$: 62	6	-2.521	-4.119	-4.775	-1.589	-1.513	0.39	0.050	312.29	7.89	0.346	34.39	-	Calc, Arag	
[NaOH]: 1.3	8	-2.492	-4.235	-4.596	-1.589	-1.509	0.45	0.051	337.59	8.04	0.305	47.91	-	Calc, Arag	
pH: 9.47	12	-2.502	-4.383	-4.439	-1.589	-1.512	0.46	0.050	331.40	8.21	0.285	67.89	-	Calc, Arag	
	30	-2.516	-4.605	-4.337	-1.588	-1.515	0.35	0.050	321.59	8.33	0.264	104.35	-	Calc, Arag	
Exp. # 12	0	-2.544	-3.162	-3.619	-1.398	-1.390	50.10	0.074	805.69	8.71	0.859	3.31	13	ACMC	Y
$[MgCl_2]$: 44	1	-2.629	-3.284	-3.741	-1.395	-1.388	28.49	0.069	618.10	8.69	0.828	3.65	-	ACMC, MHC	
$[CaCl_2]$: 16	3	-2.591	-3.443	-3.787	-1.395	-1.387	17.81	0.070	615.78	8.64	0.632	5.79	-	ACMC, Calc	
$[NaHCO_3]$: 100	6	-2.590	-4.586	-4.332	-1.393	-1.383	0.36	0.067	486.94	8.16	0.286	77.54	-	Calc, Arag	
[NaOH]: 1.7	24	-2.538	-4.745	-4.148	-1.395	-1.383	0.39	0.069	561.95	8.29	0.239	124.03	-	Calc, Arag	
pH: 9.35															

Exp. # 13		log activity (Geochemist's Workbench)					Calculated values			Measured values (pH, ICP-AES)					Mixed trans. (Y/N)
Initial concentration in 100 ml (mM)		Time (hr)[1]	Mg^{2+}	Ca^{2+}	CO_3^{2-}	Na^{+}	Cl^{-}	$\Omega_{calcite}$	I.S. (m)	Alk. (mg/kg)	pH	λ^2	Solution Mg/Ca	% Mg (solid)[3]	Solid phase (XRD)[4]	
$[MgCl_2]$:	50	0	-2.422	-2.892	-3.914	-1.671	-1.495	47.22	0.058	453.15	8.66	1.012	2.47	-	ACMC	Y
$[CaCl_2]$:	20	1	-2.420	-2.899	-3.876	-1.671	-1.495	50.71	0.058	456.90	8.70	0.993	2.52	-	ACMC	
$[NaHCO_3]$:	52	2	-2.410	-3.209	-5.010	-1.668	-1.509	1.83	0.054	341.53	7.62	0.592	5.44	-	Calc, Arag	
[NaOH]:	1.0	6	-2.572	-3.599	-5.465	-1.660	-1.556	0.26	0.043	200.01	7.38	0.543	9.30	-	Calc, Arag	
pH:	9.47	14	-2.440	-3.677	-5.215	-1.664	-1.529	0.39	0.049	275.14	7.50	0.404	15.15	-	Calc, Arag	
		24	-2.437	-3.862	-5.004	-1.664	-1.532	0.41	0.049	277.41	7.71	0.353	23.26	-	Calc, Arag	
Exp. # 14		0	-2.192	-2.820	-3.938	-1.335	-1.200	52.63	0.120	975.62	8.32	0.788	3.32	13	ACMC	Y
$[MgCl_2]$:	100	2	-2.265	-3.465	-5.273	-1.327	-1.227	0.55	0.101	546.14	7.18	0.448	12.80	-	Calc, Arag	
$[CaCl_2]$:	40	4	-2.257	-3.741	-5.203	-1.327	-1.229	0.34	0.100	546.55	7.25	0.363	24.74	-	Calc, Arag	
$[NaHCO_3]$:	120	8	-2.222	-3.970	-4.887	-1.328	-1.226	0.42	0.103	616.94	7.52	0.296	44.46	-	Calc, Arag	
[NaOH]:	2.5	24	-2.256	-4.280	-4.650	-1.327	-1.235	0.36	0.099	574.57	7.79	0.269	85.31	-	Calc, Arag	
pH:	9.40															
Exp. # 15		0	-2.533	-3.043	-3.784	-1.542	-1.470	44.99	0.060	541.22	8.71	0.827	2.66	12	ACMC	Y
$[MgCl_2]$:	42	1	-2.551	-3.299	-4.134	-1.539	-1.476	11.15	0.056	422.40	8.43	0.603	4.74	-	Calc	
$[CaCl_2]$:	20	2	-2.606	-3.899	-5.029	-1.535	-1.485	0.36	0.051	292.85	7.66	0.402	17.22	8	Calc, Arag	
$[NaHCO_3]$:	70	4	-2.579	-4.150	-4.837	-1.536	-1.484	0.31	0.052	309.94	7.83	0.331	32.23	-	Calc, Arag	
[NaOH]:	1.6	24	-2.568	-4.429	-4.620	-1.536	-1.484	0.27	0.052	318.76	8.04	0.277	65.39	-	Calc, Arag	
pH:	9.50															
Exp. # 16		0	-2.330	-2.817	-4.010	-1.053	-1.007	44.92	0.171	1062.57	8.22	0.748	2.28	10	ACMC	Y
$[MgCl_2]$:	70	0.2	-2.307	-2.796	-4.067	-1.333	-1.240	41.40	0.109	973.42	8.17	0.724	2.44	-	ACMC	
$[CaCl_2]$:	42	0.5	-2.344	-3.152	-5.090	-1.327	-1.251	1.73	0.097	644.99	7.29	0.503	5.20	6.5	Calc	
$[NaHCO_3]$:	120	1	-2.424	-3.359	-5.228	-1.323	-1.263	0.78	0.089	494.90	7.26	0.487	7.05	-	Calc, Arag	
[NaOH]:	2.2	3	-2.420	-3.682	-5.072	-1.323	-1.268	0.53	0.088	479.61	7.43	0.383	14.95	-	Calc, Arag	
pH:	9.80	24	-2.419	-4.204	-4.953	-1.322	-1.271	0.21	0.087	467.17	7.56	0.285	50.38	-	Calc, Arag	
Exp. # 17		0	-2.717	-3.067	-3.743	-1.527	-1.505	46.74	0.054	520.62	8.76	0.808	1.85	9	ACC	Y
$[MgCl_2]$:	28	0.2	-2.763	-3.137	-3.842	-1.525	-1.505	31.73	0.052	443.31	8.72	0.791	1.98	-	ACC	
$[CaCl_2]$:	20	0.5	-2.748	-3.609	-4.875	-1.522	-1.501	0.99	0.049	308.44	7.79	0.471	6.34	6	Calc	
$[NaHCO_3]$:	72	1	-2.815	-3.871	-5.071	-1.520	-1.504	0.35	0.046	244.48	7.69	0.435	10.00	-	Calc	
[NaOH]:	1.5	3	-2.755	-4.046	-4.902	-1.521	-1.503	0.34	0.047	275.31	7.81	0.354	16.99	-	Calc, Arag	
pH:	9.44	24	-2.723	-4.416	-4.793	-1.522	-1.502	0.19	0.048	289.40	7.90	0.271	44.95	-	Calc, Arag	
Exp. #18		0	-3.036	-3.400	-3.766	-1.535	-1.581	20.64	0.043	454.30	8.77	0.798	1.93	8.5	Calc	Y
$[MgCl_2]$:	14	0.1	-3.013	-3.922	-4.202	-1.564	-1.533	2.27	0.042	331.13	8.44	0.442	6.96	-	Calc, Arag	
$[CaCl_2]$:	10	0.5	-3.032	-4.454	-4.445	-1.532	-1.558	0.38	0.041	280.55	8.26	0.319	24.27	-	Calc, Arag	
$[NaHCO_3]$:	70	1	-3.082	-4.654	-4.462	-1.531	-1.554	0.23	0.040	246.03	8.30	0.314	33.98	5	Calc, Arag	
[NaOH]:	1.0	3	-3.068	-4.754	-4.371	-1.531	-1.555	0.23	0.040	254.23	8.38	0.286	48.10	5	Calc, Arag	
pH:	9.27	24	-2.746	-4.450	-3.937	-1.538	-1.591	1.24	0.046	582.51	8.47	0.243	70.43	-	Calc, Arag	

Exp. # 19		log activity (Geochemist's Workbench)					Calculated values			Measured values (pH, ICP-AES)					Mixed trans. (Y/N)
Initial concentration in 100 ml (mM)	Time (hr)[1]	Mg^{2+}	Ca^{2+}	CO_3^{2-}	Na^{+}	Cl^{-}	$\Omega_{calcite}$	I.S. (m)	Alk. (mg/kg)	pH	λ^2	Solution Mg/Ca	% Mg (solid)[3]	Solid phase (XRD)[4]	
[$MgCl_2$]: 30	0	-2.681	-2.869	-4.001	-1.566	-1.497	40.75	0.055	469.12	8.53	0.862	1.30	7	ACC	Y
[$CaCl_2$]: 28	0.1	-2.781	-3.182	-4.290	-1.560	-1.516	10.18	0.047	286.53	8.43	0.678	2.17	-	Calc	
[$NaHCO_3$]: 66	0.5	-2.707	-3.177	-5.284	-1.561	-1.505	1.04	0.049	293.70	7.40	0.603	2.56	4	Calc	
[NaOH]: 1.25	1	-2.707	-3.247	-5.272	-1.561	-1.507	0.91	0.049	281.58	7.43	0.561	3.02	-	Calc	
pH: 9.39	3	-2.702	-3.410	-5.304	-1.560	-1.510	0.58	0.048	260.56	7.43	0.482	4.45	-	Calc	
	24	-2.657	-3.751	-5.265	-1.560	-1.510	0.29	0.047	259.80	7.47	0.346	10.73	-	Calc, Arag	
Exp. # 20	0	-2.849	-2.983	-3.927	-1.536	-1.515	37.17	0.051	449.10	8.62	0.747	1.15	5	ACC	Y
[$MgCl_2$]: 20	0.1	-2.975	-3.411	-5.148	-1.530	-1.516	0.84	0.044	218.26	7.66	0.580	2.38	4	Calc	
[$CaCl_2$]: 26	0.5	-2.923	-3.475	-5.263	-1.530	-1.514	0.55	0.045	225.44	7.53	0.506	3.14	4	Calc	
[$NaHCO_3$]: 70	1	-2.913	-3.556	-5.231	-1.530	-1.515	0.49	0.044	221.33	7.57	0.470	3.82	4	Calc	
[NaOH]: 1.7	3	-2.891	-3.775	-5.209	-1.530	-1.515	0.31	0.044	212.32	7.61	0.390	6.59	4	Calc, Arag	
pH: 9.46	24	-2.877	-4.207	-5.077	-1.529	-1.516	0.16	0.044	203.80	7.76	0.294	19.12	-	Calc, Arag	
Exp. # 21	0	-2.988	-2.788	-4.089	-1.601	-1.556	40.10	0.047	406.55	8.49	0.851	0.54	3	ACC, Vat	Y
[$MgCl_2$]: 14	0.1	-3.119	-3.073	-5.355	-1.594	-1.565	1.13	0.040	203.16	7.48	0.724	0.79	2	Vat	
[$CaCl_2$]: 32	0.5	-3.032	-3.048	-5.435	-1.596	-1.560	0.99	0.041	227.86	7.35	0.648	0.91	2	Vat, Calc	
[$NaHCO_3$]: 60	1	-3.024	-3.088	-5.486	-1.595	-1.561	0.81	0.041	216.92	7.32	0.612	1.02	2	Vat, Calc	
[NaOH]: 1.3	3	-3.013	-3.201	-5.566	-1.594	-1.564	0.52	0.040	192.37	7.29	0.537	1.37	2	Calc, Arag	
pH: 9.49	24	-2.959	-3.350	-5.576	-1.594	-1.565	0.36	0.039	183.19	7.30	0.428	2.18	-	Calc, Arag	
Exp. # 22	0	-3.357	-3.258	-3.674	-1.541	-1.588	35.34	0.041	387.96	8.95	0.671	0.66	3.5	ACC	Y
[$MgCl_2$]: 6	0.1	-3.428	-3.739	-4.210	-1.538	-1.559	3.39	0.038	182.66	8.70	0.477	1.77	4	Calc	
[$CaCl_2$]: 16	0.5	-3.441	-4.254	-4.723	-1.536	-1.551	0.32	0.037	127.72	8.33	0.648	5.94	4	Calc, Arag	
[$NaHCO_3$]: 68	1	-3.422	-4.334	-4.694	-1.536	-1.551	0.28	0.037	127.38	8.35	0.322	7.94	4	Calc, Arag	
[NaOH]: 1.6	3	-3.395	-4.491	-4.582	-1.537	-1.552	0.25	0.037	132.20	8.45	0.289	10.58	3	Calc, Arag	
pH: 9.49	24	-3.349	-5.038	-4.483	-1.537	-1.553	0.09	0.037	139.51	8.53	0.211	38.97	2	Calc, Arag	
Exp. # 23	0	-3.436	-3.473	-3.462	-1.425	-1.478	35.07	0.051	417.34	9.18	0.599	0.87	4	ACC	Y
[$MgCl_2$]: 6	0.1	-3.501	-4.174	-3.861	-1.422	-1.447	2.78	0.049	186.80	9.10	0.390	3.93	6	Calc	
[$CaCl_2$]: 16	0.5	-3.506	-4.692	-4.021	-1.422	-1.442	0.58	0.048	152.87	9.01	0.304	12.59	6	Calc	
[$NaHCO_3$]: 90	1	-3.498	-4.913	-4.032	-1.422	-1.442	0.34	0.048	152.09	9.00	0.269	22.42	6	Calc	
[NaOH]: 2.4	24	-3.452	-5.396	-3.967	-1.422	-1.444	0.13	0.048	166.81	9.03	0.219	53.77	6	Calc	
pH: 9.52	72	-3.431	-5.397	-3.947	-1.422	-1.445	0.14	0.048	174.88	9.03	0.214	53.31	6	Calc	
	168	-3.497	-5.398	-3.913	-1.422	-1.443	0.15	0.048	153.07	9.14	0.226	63.06	-	Calc	
Exp. # 24	0	-1.898	-3.023	-3.906	-1.133	-0.958	35.55	0.217	1483.68	8.22	0.630	9.71	36	ACMC	Y
[$MgCl_2$]: 250	3	-1.949	-3.129	-4.003	-1.129	-0.976	22.25	0.201	1256.95	8.18	0.615	11.14	-	ACMC	
[$CaCl_2$]: 50	6	-1.935	-4.217	-4.141	-1.128	-0.981	1.33	0.197	1171.39	8.06	0.274	143.39	4	MHC	
[$NaHCO_3$]: 200	10	-1.911	-4.260	-4.087	-1.130	-0.974	1.36	0.203	1256.25	8.09	0.255	164.65	5	MHC	
[NaOH]: 6.2	24	-1.926	-4.319	-4.033	-1.129	-0.979	1.34	0.199	1216.15	8.16	0.256	180.77	4	MHC	
pH: 9.50	48	-1.963	-4.381	-4.033	-1.127	-0.990	1.16	0.190	1100.15	8.20	0.268	193.13	9	MHC	
	144	-1.933	-4.258	-4.011	-1.128	-0.981	1.63	0.197	1197.58	8.19	0.266	157.46	17	MHC, Nesq	

Exp. # 25		log activity (Geochemist's Workbench)					Calculated values			Measured values (pH, ICP-AES)					Mixed trans. (Y/N)
Initial concentration in 100 ml (mM)	Time (hr)[1]	Mg^{2+}	Ca^{2+}	CO_3^{2-}	Na^{+}	Cl^{-}	$\Omega_{calcite}$	I.S. (m)	Alk. (mg/kg)	pH	λ^2	Solution Mg/Ca	% Mg (solid)[3]	Solid phase (XRD)[4]	
[$MgCl_2$]: 250	0	-1.920	-3.050	-3.871	-1.132	-0.966	36.24	0.210	1405.10	8.28	0.637	9.84	35	ACMC	Y
[$CaCl_2$]: 50	3	-1.947	-3.134	-4.011	-1.129	-0.976	21.64	0.201	1260.62	8.17	0.311	11.27	26	ACMC	
[$NaHCO_3$]: 200	6	-1.902	-4.210	-4.067	-1.130	-0.971	1.60	0.205	1293.18	8.10	0.256	149.48	8	MHC	
[NaOH]: 6.2	18	-1.926	-4.298	-4.043	-1.129	-0.979	1.38	0.199	1213.38	8.15	0.259	172.32	7	MHC	
pH: 9.49	24	-1.970	-4.352	-4.090	-1.126	-0.992	1.09	0.188	1072.28	8.15	0.275	180.57	4	MHC	
(Repeat of exp. # 24)	48	-1.963	-4.381	-4.023	-1.127	-0.990	1.19	0.190	1102.86	8.21	0.266	198.62	6	MHC	
	144	-1.943	-4.390	-3.915	-1.128	-0.984	1.50	0.195	1181.32	8.30	0.255	204.68	5	MHC	
Exp. # 26	0	-1.975	-3.105	-3.928	-1.128	-0.983	27.98	0.196	1199.65	8.28	0.661	9.95	-	ACMC	N
[$MgCl_2$]: 250	3	-1.953	-3.122	-3.996	-1.129	-0.977	23.01	0.200	1249.30	8.19	0.624	10.86	28	ACMC	
[$CaCl_2$]: 50	6	-1.967	-3.134	-4.040	-1.128	-0.982	20.23	0.197	1195.19	8.16	0.633	10.83	28	ACMC	
[$NaHCO_3$]: 200	24	-1.931	-3.193	-3.942	-1.130	-0.973	22.16	0.204	1310.01	8.23	0.555	13.39	28	ACMC	
[NaOH]: 6.2	34	-1.915	-3.268	-4.009	-1.131	-0.969	15.99	0.207	1334.99	8.15	0.499	16.52	27	Calc, MHC	
pH: 9.53	48	-1.899	-3.597	-4.115	-1.131	-0.968	5.86	0.208	1323.70	8.04	0.369	36.59	28	Calc, MHC	
	120	-1.823	-3.950	-4.052	-1.136	-0.943	3.01	0.230	1611.32	8.03	0.242	97.67	21	Calc, MHC	
Exp. # 27	0	-1.970	-3.108	-3.895	-1.128	-0.982	30.02	0.197	1219.73	8.31	0.655	10.08	-	ACMC	N
[$MgCl_2$]: 250	3	-1.983	-3.156	-3.998	-1.127	-0.986	21.16	0.193	1151.43	8.22	0.636	10.98	27	ACMC	
[$CaCl_2$]: 50	6	-1.970	-3.149	-3.966	-1.128	-0.983	23.21	0.196	1195.94	8.24	0.626	11.11	27	ACMC	
[$NaHCO_3$]: 200	24	-1.930	-3.143	-3.937	-1.130	-0.971	25.10	0.206	1326.98	8.23	0.584	11.95	27	ACMC	
[NaOH]: 6.2	34	-1.946	-3.239	-3.989	-1.129	-0.978	17.87	0.200	1241.66	8.20	0.547	14.40	26	Calc	
pH: 9.52	48	-1.924	-3.520	-4.128	-1.130	-0.975	6.79	0.202	1245.13	8.05	0.412	28.91	28	Calc	
(Repeat of exp. # 26)	120	-1.844	-3.915	-4.153	-1.134	-0.950	2.58	0.223	1504.46	7.95	0.262	0.262	27	Calc, MHC	
Exp. # 28	12	-1.859	-3.040	-3.888	-1.126	-0.945	35.65	0.228	1638.54	8.20	0.564	10.99	26	ACMC	N
[$MgCl_2$]: 250	28	-1.891	-3.199	-3.922	-1.133	-0.969	22.85	0.215	1454.34	8.21	0.506	14.85	24	ACMC, Calc	
[$CaCl_2$]: 50	50	-1.838	-3.663	-4.063	-1.135	-0.947	5.68	0.226	1563.58	8.03	0.302	48.74	22	Calc, MHC	
[$NaHCO_3$]: 200															
[NaOH]: 6.1															
pH: 9.49															
(Repeat of exp. # 27)															
Exp. # 29	0	-2.241	-3.130	-3.670	-1.121	-1.084	47.90	0.153	1373.13	8.46	0.500	5.78	23	ACMC	Y
[$MgCl_2$]: 100	0.5	-2.312	-3.247	-3.853	-1.117	-1.088	23.99	0.144	1085.06	8.36	0.519	6.52	18	ACMC	
[$CaCl_2$]: 50	1	-2.302	-3.248	-3.834	-1.117	-1.087	25.05	0.145	1114.09	8.37	0.509	6.65	17	ACMC	
[$NaHCO_3$]: 200	2	-2.276	-4.249	-3.962	-1.116	-1.087	1.86	0.142	1016.92	8.27	0.252	71.80	6	MHC	
[NaOH]: 6.0	24	-2.276	-4.460	-3.896	-1.116	-1.088	1.33	0.142	1019.65	8.34	0.229	114.52	6	MHC	
pH: 9.52															

Exp. # 30		log activity (Geochemist's Workbench)					Calculated values			Measured values (pH, ICP-AES)					Mixed trans. (Y/N)
Initial concentration in 100 ml (mM)	Time (hr)[1]	Mg^{2+}	Ca^{2+}	CO_3^{2-}	Na^{+}	Cl^{-}	$\Omega_{calcite}$	I.S. (m)	Alk. (mg/kg)	pH	λ^2	Solution Mg/Ca	% Mg (solid)[3]	Solid phase (XRD)[4]	
[$MgCl_2$]: 100	0	-2.260	-3.164	-3.782	-1.120	-1.085	34.20	0.150	1269.01	8.37	0.506	6.01	17	ACMC	N
[$CaCl_2$]: 50	1	-2.271	-3.210	-3.759	-1.119	-1.086	32.44	0.148	1227.16	8.41	0.494	6.53	17	ACMC	
[$NaHCO_3$]: 200	3	-2.303	-3.255	-3.785	-1.118	-1.088	27.55	0.144	1120.17	8.42	0.506	6.74	17	ACMC	
[NaOH]: 5.9	6.5	-2.314	-3.230	-3.833	-1.117	-1.088	26.12	0.144	1090.63	8.38	0.529	6.24	19	Calc	
pH: 9.50	28	-2.246	-3.792	-4.161	-1.118	-1.084	3.37	0.146	1096.10	8.03	0.305	23.66	19	Calc	
Exp. # 31	0	-2.766	-3.322	-3.553	-1.257	-1.306	40.27	0.086	930.68	8.71	0.621	2.79	11	ACMC	Y
[$MgCl_2$]: 28	0.1	-2.781	-3.370	-3.580	-1.257	-1.302	33.88	0.085	870.99	8.71	0.603	3.03	10	ACMC	
[$CaCl_2$]: 20	0.5	-2.772	-3.386	-3.576	-1.257	-1.303	32.91	0.086	878.78	8.71	0.581	3.21	10	ACMC	
[$NaHCO_3$]: 140	1	-2.905	-3.985	-3.923	-1.252	-1.279	3.73	0.080	494.37	8.59	0.442	9.81	13	Calc	
[NaOH]: 2.7	48	-2.789	-5.005	-3.930	-1.254	-1.284	0.35	0.082	592.72	8.50	0.215	140.81	14	Calc, Arag	
pH: 9.29															
Exp. # 32	0	-2.766	-3.317	-3.511	-1.258	-1.308	44.87	0.086	947.20	8.75	0.623	2.76	11.5	ACMC	Y
[$MgCl_2$]: 28	0.1	-2.915	-3.478	-3.712	-1.254	-1.288	19.53	0.082	619.90	8.72	0.677	2.90	10	ACMC	
[$CaCl_2$]: 20	0.5	-2.899	-3.487	-3.671	-1.254	-1.289	20.99	0.082	641.19	8.75	0.655	3.06	10	ACMC	
[$NaHCO_3$]: 140	1	-2.892	-3.632	-3.809	-1.253	-1.285	10.94	0.081	582.09	8.64	0.568	4.35	13	Calc	
[NaOH]:	96	-3.801	-3.102	-4.126	-1.251	-1.274	17.87	0.078	391.96	8.48	0.213	139.16	14	Calc, Arag	
pH: 9.32															
(Repeat of exp. # 31)															
Exp. # 33	0	-2.615	-3.523	-3.222	-1.159	-1.224	54.34	0.112	1414.53	8.91	0.581	5.92	21	ACMC	Y
[$MgCl_2$]: 44	1	-2.680	-3.649	-3.289	-1.156	-1.210	34.85	0.109	1150.70	8.93	0.576	6.92	19	ACMC	
[$CaCl_2$]: 16	3	-2.695	-3.672	-3.339	-1.156	-1.206	29.46	0.108	1082.54	8.90	0.581	7.07	19	ACMC	
[$NaHCO_3$]: 180	6	-2.675	-3.672	-3.297	-1.156	-1.210	32.45	0.109	1152.11	8.92	0.559	7.35	20	ACMC	
[NaOH]: 3.9	26	-2.618	-4.910	-3.290	-1.157	-1.210	1.91	0.109	1167.68	8.92	0.222	136.76	2	MHC	
pH: 9.38	48	-2.638	-4.914	-3.261	-1.156	-1.209	2.02	0.108	1133.50	8.97	0.225	142.96	3	MHC	
Exp. # 34	0	-2.887	-3.845	-2.868	-1.107	-1.185	58.48	0.116	1281.47	9.45	0.502	6.17	21	ACMC	Y
[$MgCl_2$]: 30	6	-2.881	-5.000	-2.960	-1.106	-1.169	3.31	0.115	1049.31	9.43	0.233	100.58	3.5	MHC	
[$CaCl_2$]: 15	18	-2.871	-5.106	-2.937	-1.106	-1.172	2.73	0.115	1092.66	9.44	0.218	122.77	3	MHC	
[$NaHCO_3$]: 200	46	-2.901	-5.083	-2.997	-1.105	-1.164	2.51	0.011	971.97	9.42	0.239	111.66	21	MHC, Nesq	
[NaOH]: 7.0															
pH: 9.60															
Exp. # 35	0	-2.421	-3.394	-3.452	-1.232	-1.227	43.05	0.107	1052.74	8.80	0.637	7.16	24	ACMC	Y
[$MgCl_2$]: 72	6	-2.485	-3.548	-3.534	-1.229	-1.226	25.05	0.102	853.44	8.80	0.608	8.83	22	ACMC	
[$CaCl_2$]: 20	18	-2.417	-4.649	-3.863	-1.230	-1.224	1.85	0.104	899.09	8.74	0.254	135.11	4	MHC	
[$NaHCO_3$]: 150	46	-2.382	-4.719	-3.505	-1.232	-1.225	1.80	0.106	997.97	8.76	0.229	160.07	4	MHC	
[NaOH]: 4.0															
pH: 9.47															

Exp. # 36		log activity (Geochemist's Workbench)					Calculated values			Measured values (pH, ICP-AES)					Mixed trans. (Y/N)
Initial concentration in 100 ml (mM)		Time (hr)[1]	Mg^{2+}	Ca^{2+}	CO_3^{2-}	Na^{+}	Cl^{-}	$\Omega_{calcite}$	I.S. (m)	Alk. (mg/kg)	pH	λ^2	Solution Mg/Ca	% Mg (solid)[3]	Solid phase (XRD)[4]	
$[MgCl_2]$:	20	0	-2.906	-3.501	-3.205	-1.228	-1.319	59.38	0.088	1142.81	9.01	0.562	2.91	12	ACMC	Y
$[CaCl_2]$:	15	0.5	-3.011	-3.648	-3.315	-1.226	-1.291	32.89	0.085	824.32	9.04	0.594	3.25	10	ACMC	
$[NaHCO_3]$:	150	1	-3.002	-3.643	-3.317	-1.226	-1.292	33.15	0.085	837.50	9.03	0.585	3.31	10	ACMC	
[NaOH]:	3.1	2	-2.965	-3.786	-3.334	-1.226	-1.291	22.91	0.085	834.05	9.01	0.475	5.03	8	ACMC	
pH:	9.35	24	-2.939	-4.952	-3.369	-1.225	-1.282	1.44	0.085	736.63	9.03	0.223	75.97	5	MHC, Arag	
Exp. # 37		0	-2.710	-3.059	-3.783	-1.511	-1.492	43.42	0.056	549.19	8.69	0.807	1.84	8	ACC	Y
$[MgCl_2]$:	28	0.5	-2.767	-3.635	-4.864	-1.505	-1.489	0.96	0.050	309.18	7.80	0.477	6.36	6	Calc	
$[CaCl_2]$:	20	1	-2.803	-3.838	-5.036	-1.504	-1.489	0.40	0.048	266.19	7.69	0.438	9.35	6	Calc	
$[NaHCO_3]$:	75															
[NaOH]:	1.6															
pH:	9.46															
Exp. # 38		0	-2.748	-3.353	-3.443	-1.257	-1.310	48.35	0.087	984.35	8.81	0.570	3.10	11	ACMC	Y
$[MgCl_2]$:	28	0.5	-2.853	-3.499	-3.595	-1.254	-1.293	24.35	0.083	708.02	8.79	0.601	3.45	11	ACMC	
$[CaCl_2]$:	20	1	-2.842	-3.502	-3.545	-1.254	-1.295	27.11	0.083	734.65	8.83	0.587	3.55	11	ACMC	
$[NaHCO_3]$:	140	2.5	-2.839	-4.638	-3.868	-1.252	-1.281	0.94	0.081	539.43	8.61	0.276	52.12	15	Calc	
[NaOH]:	3.0															
pH:	9.37															
Exp. # 39		0	-2.748	-3.027	-3.957	-1.511	-1.491	31.36	0.056	511.39	8.53	0.909	1.59	8	ACC	Y
$[MgCl_2]$:	28	0.1	-2.896	-3.193	-4.014	-1.507	-1.495	18.73	0.050	345.96	8.64	0.900	1.68	6	ACC	
$[CaCl_2]$:	20	0.5	-2.841	-3.628	-5.064	-1.505	-1.491	0.61	0.048	260.85	7.67	0.540	5.32	5	Calc	
$[NaHCO_3]$:	75	24	-2.719	-4.073	-5.044	-1.506	-1.488	0.23	0.050	307.39	7.62	0.326	19.46	4	Calc, Arag	
[NaOH]:	1.4															
pH:	9.40															
Exp. # 40		0	-2.748	-3.280	-3.557	-1.259	-1.311	43.96	0.087	984.76	8.68	0.629	2.65	10	ACC	Y
$[MgCl_2]$:	28	0.5	-2.843	-3.432	-3.681	-1.256	-1.295	23.32	0.083	728.11	8.68	0.632	3.07	9	ACC	
$[CaCl_2]$:	20	1	-2.840	-4.356	-4.092	-1.254	-1.281	1.08	0.081	527.18	8.38	0.321	27.07	11.5	Calc	
$[NaHCO_3]$:	140															
[NaOH]:	2.3															
pH:	9.22															
Exp. # 41		0	-2.746	-3.270	-3.614	-1.503	-1.493	39.45	0.053	467.99	8.96	0.648	2.73	10.5	ACC	Y
$[MgCl_2]$:	28	0.1	-2.946	-3.494	-3.808	-1.498	-1.494	15.07	0.048	270.56	8.99	0.704	2.93	10	ACC	
$[CaCl_2]$:	20	0.5	-2.867	-3.434	-3.737	-1.500	-1.494	20.36	0.049	329.02	8.98	0.664	3.07	10	ACC	
$[NaHCO_3]$:	75	1	-2.866	-3.486	-3.779	-1.500	-1.493	16.40	0.049	315.34	8.95	0.632	3.47	10	ACC	
[NaOH]:	2.5															
pH:	9.69															

Exp. # 42		log activity (Geochemist's Workbench)					Calculated values			Measured values (pH, ICP-AES)					Mixed trans. (Y/N)
Initial concentration in 100 ml (mM)	Time (hr)[1]	Mg^{2+}	Ca^{2+}	CO_3^{2-}	Na^{+}	Cl^{-}	$\Omega_{calcite}$	I.S. (m)	Alk. (mg/kg)	pH	λ^2	Solution Mg/Ca	% Mg (solid)[3]	Solid phase (XRD)[4]	
$[MgCl_2]$: 28	0	-2.751	-3.341	-3.483	-1.501	-1.496	45.25	0.053	471.85	9.12	0.698	3.12	12	ACMC	Y
$[CaCl_2]$: 20	1	-2.857	-3.488	-3.609	-1.498	-1.494	24.13	0.049	341.76	9.12	0.703	3.48	11	ACMC	
$[NaHCO_3]$: 75	2	-2.824	-3.604	-3.670	-1.498	-1.493	16.11	0.050	337.02	9.05	0.606	4.92	11.5	ACMC, MHC	
[NaOH]: 2.8	2.5	-2.834	-4.400	-3.911	-1.497	-1.490	1.48	0.048	262.84	8.88	0.368	31.48	10	MHC, Calc	
pH: 9.82															
(Repeat of exp. # 41)															
Exp. # 43	0	-2.823	-3.593	-3.181	-1.251	-1.306	50.81	0.085	882.40	9.19	0.589	4.36	15	ACC	Y
$[MgCl_2]$: 28	1	-2.906	-3.745	-3.285	-1.249	-1.291	28.16	0.082	667.98	9.20	0.588	5.23	15	ACC	
$[CaCl_2]$: 20	2	-2.906	-3.756	-3.296	-1.249	-1.290	26.75	0.082	661.98	9.19	0.583	5.34	14	ACC	
$[NaHCO_3]$: 140															
[NaOH]: 4.4															
pH: 9.65															
Exp. # 44	0	-2.799	-3.567	-3.245	-1.496	-1.503	46.49	0.051	458.72	9.48	0.517	4.50	17	ACMC	Y
$[MgCl_2]$: 28	2	-2.900	-3.739	-3.302	-1.494	-1.501	27.50	0.049	347.97	9.56	0.530	5.39	16	ACMC	
$[CaCl_2]$: 20	3	-2.885	-3.738	-3.280	-1.494	-1.502	29.00	0.049	363.33	9.57	0.517	5.55	16	ACMC	
$[NaHCO_3]$: 75	3.5	-2.951	-3.952	-3.448	-1.492	-1.496	12.02	0.047	269.09	9.48	0.492	8.04	16	ACMC	
[NaOH]: 3.5	4	-2.891	-3.926	-3.301	-1.494	-1.501	17.91	0.048	337.30	9.58	0.456	8.35	10	MHC	
pH: 10.1	5	-2.840	-4.801	-3.281	-1.494	-1.501	2.50	0.049	347.79	9.59	0.258	72.18	3	MHC	
	22	-2.814	-4.902	-3.271	-1.494	-1.502	2.03	0.049	368.32	9.57	0.231	107.67	2	MHC	
Exp. # 45	0	-2.773	-3.713	-3.161	-1.253	-1.311	40.41	0.086	941.99	9.18	0.404	6.39	16	ACMC	Y
$[MgCl_2]$: 28	1	-2.888	-3.722	-3.282	-1.250	-1.294	29.93	0.083	697.94	9.18	0.510	5.16	15	ACMC	
$[CaCl_2]$: 20	2	-2.865	-3.718	-3.249	-1.251	-1.297	32.55	0.083	743.25	9.19	0.491	5.35	15	ACMC	
$[NaHCO_3]$: 140	3	-2.993	-3.928	-3.429	-1.248	-1.280	13.28	0.080	495.54	9.17	0.516	6.65	15	ACMC	
[NaOH]: 4.0	4	-3.001	-4.918	-3.469	-1.247	-1.275	1.24	0.080	424.79	9.20	0.310	61.62	4	MHC	
pH: 9.65	22	-2.835	-4.966	-3.274	-1.250	-1.292	1.74	0.082	671.80	9.21	0.223	105.30	2	MHC	
(Repeat of exp. # 43)															
Exp. # 46	0	-2.718	-3.054	-3.877	-1.511	-1.491	35.39	0.056	531.07	8.60	0.824	1.80	9	ACC	N
$[MgCl_2]$: 28	1	-2.747	-3.171	-4.018	-1.509	-1.491	19.53	0.053	448.31	8.52	0.732	2.24	7	ACC, Calc	
$[CaCl_2]$: 20	2	-2.749	-3.220	-4.006	-1.508	-1.492	17.95	0.053	431.40	8.55	0.689	2.50	7	Calc	
$[NaHCO_3]$: 75	48	-2.716	-3.996	-4.964	-1.506	-1.488	0.33	0.050	315.39	7.69	0.339	16.44	5	Calc, Arag	
[NaOH]: 1.5															
pH: 9.39															
Exp. # 47	0	-2.728	-3.133	-3.635	-1.262	-1.318	51.42	0.089	1108.46	8.54	0.749	1.98	11	ACMC	N
$[MgCl_2]$: 28	1	-2.822	-3.278	-3.769	-1.259	-1.301	27.07	0.085	818.65	8.53	0.730	2.27	7	ACC	
$[CaCl_2]$: 20	2	-2.746	-3.242	-3.738	-1.261	-1.309	31.64	0.087	965.77	8.49	0.660	2.47	7	ACC	
$[NaHCO_3]$: 140	2.5	-2.785	-3.331	-3.818	-1.259	-1.301	21.44	0.085	831.22	8.47	0.640	2.78	8	Calc	
[NaOH]: 1.8	24	-2.892	-4.498	-4.534	-1.254	-1.277	0.28	0.079	441.23	8.00	0.328	33.33	8	Calc, Arag	
pH: 9.10															

Exp. # 48		log activity (Geochemist's Workbench)					Calculated values			Measured values (pH, ICP-AES)					Mixed trans. (Y/N)
Initial concentration in 100 ml (mM)	Time (hr)[1]	Mg^{2+}	Ca^{2+}	CO_3^{2-}	Na^{+}	Cl^{-}	$\Omega_{calcite}$	I.S. (m)	Alk. (mg/kg)	pH	λ^2	Solution Mg/Ca	% Mg (solid)[3]	Solid phase (XRD)[4]	
[$MgCl_2$]: 28	0	-2.717	-3.125	-3.712	-1.508	-1.492	43.98	0.055	526.01	8.79	0.740	2.11	10	ACC	N
[$CaCl_2$]: 20	1	-2.811	-3.270	-3.851	-1.504	-1.493	22.87	0.051	388.25	8.77	0.725	2.40	8	ACC, Calc	
[$NaHCO_3$]: 75	2	-2.766	-3.344	-3.924	-1.505	-1.491	16.29	0.052	393.67	8.68	0.619	3.17	8	Calc	
[NaOH]: 2.0	168	-2.711	-4.377	-4.789	-1.503	-1.487	0.21	0.050	313.76	7.87	0.275	38.25	7	Calc, Arag	
pH: 9.55															
Exp. # 49	0	-2.679	-3.254	-3.310	-1.260	-1.330	82.38	0.090	1257.10	8.85	0.543	2.84	12	ACMC	N
[$MgCl_2$]: 28	1	-2.781	-3.403	-3.424	-1.256	-1.306	45.07	0.086	908.92	8.87	0.578	3.21	10	ACMC	
[$CaCl_2$]: 20	2	-2.740	-3.375	-3.357	-1.257	-1.315	56.06	0.087	1027.18	8.89	0.545	3.27	11	ACMC, Calc	
[$NaHCO_3$]: 140	3	-2.729	-3.403	-3.428	-1.257	-1.311	44.57	0.087	997.68	8.82	0.515	3.63	13	Calc	
[NaOH]: 3.0	24	-2.663	-4.513	-3.697	-1.256	-1.299	1.86	0.086	849.95	8.59	0.199	56.08	13	Calc, Arag	
pH: 9.36															
Exp. # 50	0	-2.754	-3.307	-3.534	-1.502	-1.495	43.48	0.053	466.77	9.06	0.628	2.89	11	ACMC	N
[$MgCl_2$]: 28	1	-2.826	-3.426	-3.654	-1.500	-1.493	25.13	0.050	365.59	9.03	0.630	3.62	10	ACMC	
[$CaCl_2$]: 20	2	-2.826	-3.429	-3.693	-1.500	-1.493	22.81	0.050	360.09	8.99	0.625	3.33	11	ACMC	
[$NaHCO_3$]: 75	3	-2.820	-3.441	-3.670	-1.500	-1.493	23.38	0.050	365.50	9.01	0.613	3.44	12	Calc	
[NaOH]: 2.7	24	-2.752	-4.557	-3.954	-1.499	-1.489	0.93	0.049	312.08	8.75	0.268	50.63	11	Calc, Arag	
pH: 9.80															
Exp. # 51	0	-2.758	-3.526	-3.089	-1.254	-1.322	73.38	0.087	1090.89	9.20	0.461	4.26	15	ACMC	N
[$MgCl_2$]: 28	1	-2.817	-3.642	-3.185	-1.251	-1.306	45.03	0.085	872.85	9.19	0.476	4.96	15	ACMC	
[$CaCl_2$]: 20	2	-2.806	-3.641	-3.173	-1.252	-1.308	46.38	0.085	899.79	9.19	0.464	5.06	15	ACMC	
[$NaHCO_3$]: 140	3	-2.803	-3.638	-3.169	-1.252	-1.308	47.10	0.085	907.08	9.19	0.463	5.05	15	ACMC	
[NaOH]: 4.2	6.5	-2.779	-3.678	-3.151	-1.252	-1.311	44.76	0.086	949.19	9.19	0.421	5.82	13	ACMC	
pH: 9.58	24	-2.726	-4.057	-3.136	-1.253	-1.313	19.38	0.086	982.37	9.19	0.272	15.90	3	MHC	

[1]Time 0 is ACC precipitation at steady state in the mixed flow reactor

[2]λ described in Eq. 4.4

[3]% $Mg_{(solid)}$ = 100 x ([$MgCO_3$] / [$CaCO_3$] + [$MgCO_3$]). Calculated from ICP-AES data from precipitates.

[4]ACC= Amorphous Calcium Carbonate; ACMC = Amorphous Calcium, Magnesium Carbonate; MHC = Monohydrocalcite; Calc = Calcite; Arag = Aragonite; Vat = Vaterite; Nesq = Nesquehonite

C2. SUPPLEMENTARY FIGURES

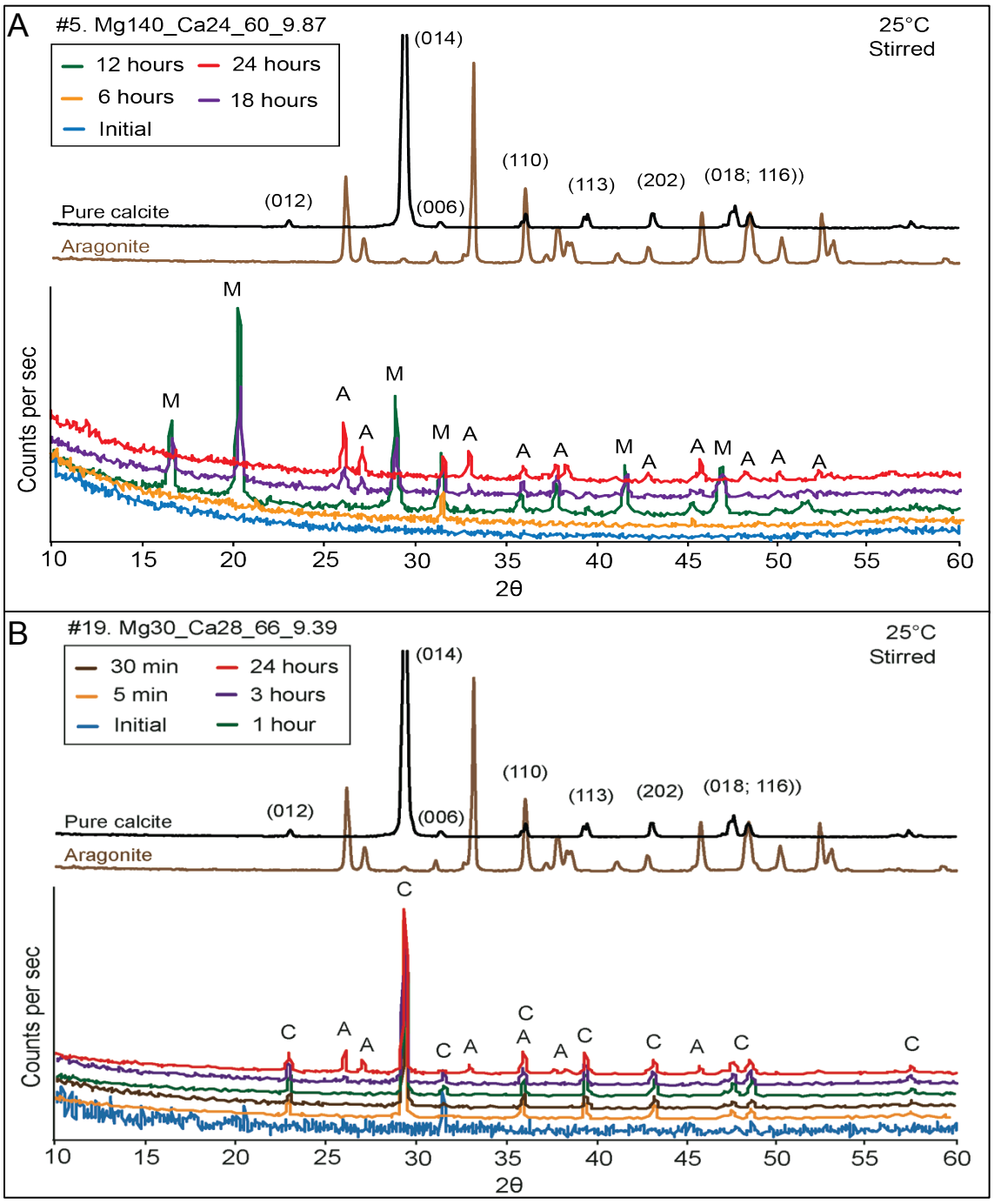

Figure C1. XRD analysis shows the evolution of polymorph stability over time. Calcite and aragonite standards are shown for reference above the time-stacked XRD patterns. (A) ACC transforms to monohydrocalcite (labeled "M") after 12 hours, a mixture of monohydrocalcite and aragonite (labeled "A") occur after 18 hours, and only aragonite remains after 24 hours. (B) ACC transforms to calcite (labeled "C") within 5 minutes, and a mixture of calcite and aragonite appear within 24 hours.

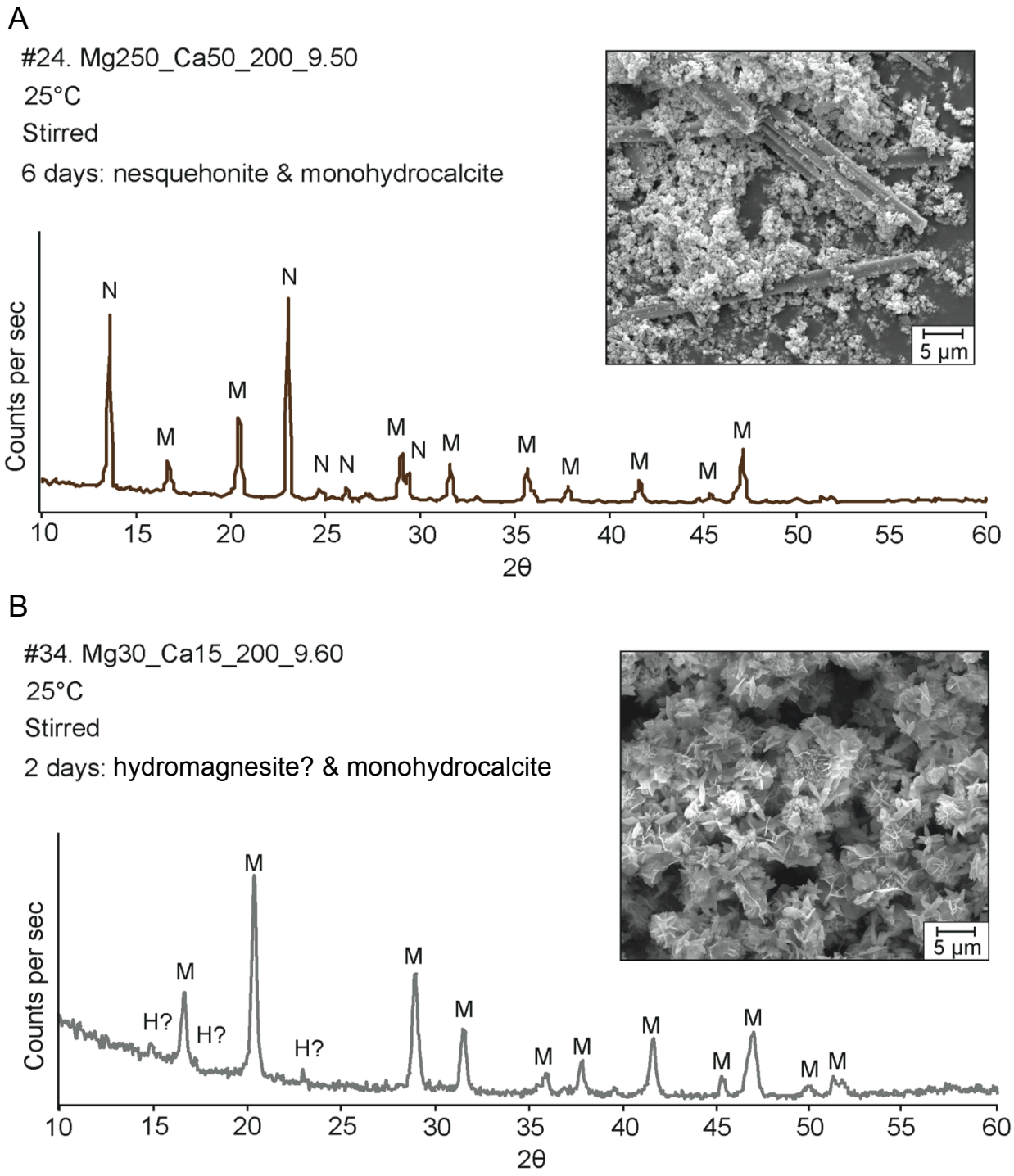

Figure C2. XRD and SEM characterization of other phases formed in transformation experiments. Nesquehonite occurred in one experiment after 6 days, and hydromagnesite (?) occurred in association with monohydrocalcite in one experiment after 2 days.

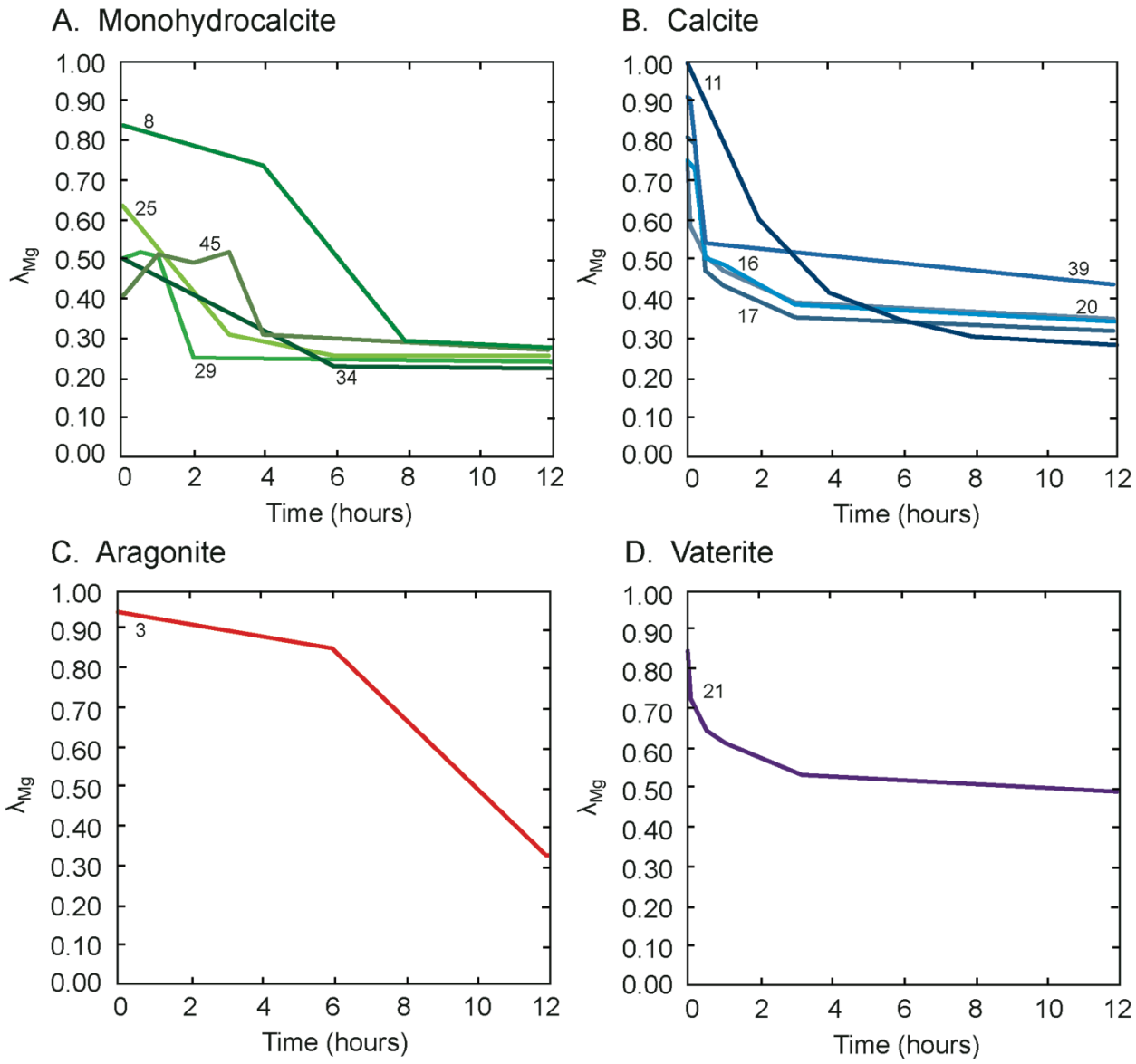

Figure C3. Partition coefficient values for Mg (λ_{Mg}) drop over time for all experimental conditions. The sharpest drop in λ_{Mg} coincides with initial crystallization of the polymorph. Over time λ_{Mg} continues to drop as a result of Ostwald ripening. (A) λ_{Mg} values over time for monohydrocalcite. (B) λ_{Mg} values over time for calcite. (C) λ_{Mg} values over time for aragonite. (D) λ_{Mg} values over time for vaterite. The numbers next to the lines correspond to the experiment number in **Table C1**. The colors and experiment numbers in (A) correspond to **Fig. 4.4B**, and the colors and experiment numbers in (B) correspond to **Fig. 4.4A**.